Investigating the Function of Secreted EspD from *Mycobacterium tuberculosis*

A Thesis Submitted to the
College of Graduate and Postdoctoral Studies
In Partial Fulfillment of the Requirements
For the Degree of Master of Science
In the Department of Biochemistry, Microbiology and Immunology
University of Saskatchewan
Saskatoon

By

Zoe Sereggela

Permission to Use

In presenting this thesis in partial fulfilment of the requirements for a Postgraduate degree from the University of Saskatchewan, I agree that the Libraries of this University may make it freely available for inspection. I further agree that permission for copying of this thesis in any manner, in whole or in part, for scholarly purposes may be granted by the professor Dr. Jeffrey Chen, PhD at the Vaccine and Infectious Disease Organization, who supervised my thesis work or, in his absence, by the Head of the Department or the Dean of the College in which my thesis work was done. It is understood that any copying or publication or use of this thesis or parts thereof for financial gain shall not be allowed without my written permission. It is also understood that due recognition shall be given to me and to the University of Saskatchewan in any scholarly use which may be made of any material in my thesis.

Requests for permission to copy or to make other use of material in this thesis in whole or part should be addressed to:

Head of the Department of Biochemistry, Microbiology and Immunology
GA20, Health Sciences
107 Wiggins Road
University of Saskatchewan
Saskatoon, Saskatchewan, S7N 5E5
Canada

OR

Dean
College of Graduate and Postdoctoral Studies
University of Saskatchewan
116 Thorvaldson Building, 110 Science Place
Saskatoon, Saskatchewan S7N 5C9
Canada

Abstract

Mycobacterium tuberculosis (*M. tb*) is able to persist within macrophages by utilizing its type VII ESX-1 protein secretion system to subvert host-defense mechanisms. ESX-1 is encoded by genes in two separate loci, the *esx-1* locus and the *espACD* operon. EspD, encoded by the third gene on the *espACD* operon, had previously been found to be necessary within the mycobacterial cell for the stability and secretion of several ESX-1 proteins. However, the function of secreted EspD within the host-cell remains unknown. This question was addressed here through studies using *M. tb* strains expressing variant EspD proteins and through the characterization of recombinant EspD protein expressed and purified from *Escherichia coli* (*E. coli)*. To generate these *M. tb* strains, an *espA* transposon insertion mutant (*M. tb espA*::Tn), which is unable to express the entire *espACD* operon, was used. *M. tb espA*::Tn was transformed with an empty plasmid vector (*M. tb espA*::Tn pMD31) or plasmid vectors encoding the *espACD* genes containing either wild-type *espD* (*M. tb espA*::Tn pMD*espACD*^{WT}), *espD* containing a premature stop codon (*M. tb espA*::Tn pMD*espACD*^{STOP}), or *espD* containing single point mutations. While all strains exhibited similar growth rates, *M. tb espA*::Tn pMD31 and *M. tb espA*::Tn pMD*espACD*^{STOP} were deficient in both EsxA and EspD secretion. *M. tb espA*::Tn pMD*espACD*^{W19R} was capable of secreting EsxA, but not EspD. All other strains expressing variants of EspD were able to secrete both EspD and EsxA to some level. During infections of THP-1 human macrophages, *M. tb espA*::Tn pMD*espACD*^{W19R} appeared less cytotoxic and induced reduced production of the pro-inflammatory cytokines IL1β and TNFα. These results strongly suggest that secreted EspD is involved in the induction of pro-inflammatory response. *M. tb espA*::Tn pMD*espACD*^{STOP} also appeared less cytotoxic to THP-1 cells, but in contrast induced an increased production of IL1β and TNFα. This is a novel observation indicating that ESX-1 mediated cell death in macrophages does not necessarily correspond to an increased pro-inflammatory response. Additionally, purified recombinant EspD appears to be capable of forming a large oligomeric structure and appears to bind specifically to several eukaryotic phospholipids, including PI4P. It is unknown if this binding occurs *in vivo* or if this binding underlies the inflammatory response induced by secreted EspD during macrophage infections.

Acknowledgements

I would like to acknowledge that the work performed in this thesis took place on Treaty 6 territory, the traditional territory of Cree Peoples, and on the homeland of the Métis Nation. To my supervisor, Dr. Jeffrey Chen, and to my committee members, Dr. Aaron White, Dr. Miroslaw Cygler, and Dr. Linda Chelico, thank you for your advice and support throughout my program, I have learned a lot from being able to speak with you all about this work. I am grateful to everyone at VIDO who aided me throughout my training, especially members of the Chen Lab and White Lab. I would also like to acknowledge the help I received from LaRhonda Sobchishin with TEM imaging at the WCVM and the help from Will Deck with SEC at VIDO. This work is supported by a grant from the National Sanitarium Association and through Devolved Graduate Scholarships from the Department of Biochemistry, Microbiology and Immunology, College of Medicine, and the College of Graduate and Postdoctoral Studies.

Permission to Reproduce

Previously published figures used in this document have been reproduced with permissions from the publishing journals.

Figure 1: adapted from Poirier, V., and Av-Gay, Y. (2012). Mycobacterium tuberculosis modulators of the macrophage's cellular events. Microbes Infect. *14*, 1211–1219.

Figure 2: adapted from Schroder, K., and Tschopp, J. (2010). The Inflammasomes. Cell *140*, 821–832.

Figure 3: adapted from Chen, K.W., Boucher, D., and Broz, P. (2019). Divide to conquer: NLRP3 is activated on dispersed trans-Golgi network. Cell Res. *29*, 181–182.

Figure 4: adapted from Gröschel, M.I., Sayes, F., Simeone, R., Majlessi, L., and Brosch, R. (2016). ESX secretion systems: Mycobacterial evolution to counter host immunity. Nat. Rev. Microbiol. *14*, 677–691.

Figure 33: adapted from Rathinam, V.A.K., and Fitzgerald, K.A. (2016). Inflammasome Complexes: Emerging Mechanisms and Effector Functions. Cell *165*, 792–800.

Table of Contents **Page**

List of Tables

List of Figures

List of Abbreviations

AEC	anion exchange chromatography
Ag85	Antigen 85
AIM2	absent in melanoma 2
ASC	apoptosis-associated speck-like containing a CARD
ATCC	American Type Culture Collection
BCA	bicinchoninic acid
BCG	bacillus Calmette Guérin
BSA	bovine serum albumin
BSL	biosafety level
CD	circular dichroism
CF	culture filtrate
CFP-10	10 kDa culture filtrate protein
CL	cell lysate
CV	column volumes
DLS	dynamic light scattering
DMEM	Dulbecco's Modified Eagle Medium
E. coli	*Escherichia coli*
ecc	*esx*-conserved components
EDTA	ethylenediaminetetraacetic acid
EEA1	early endosomal markers such as early endosome antigen-1
ESAT-6	6 kDa early secretory antigenic target
espACD	*esx-1* secretion-associated proteins ACD
ESX-1	ESAT-6 secretion system
FBS	fetal bovine serum
FT	flow through
GFP	green fluorescent protein
HIV	human immunodeficiency virus
Hrs	hepatocyte growth factor–regulated tyrosine kinase substrate
IL1β	interleukin-1 β
IPTG	isopropyl β-d-1-thiogalactopyranoside

LB	Luria Broth
LDH	Lactate Dehydrogenase
LDS	lithium dodecyl sulfate
LEW	lysis/equilibrium/wash
LPA	lysophosphatidic acid
LPC	lysophosphocholine
M. bovis	*Mycobacterium bovis*
M. tb	*Mycobacterium tuberculosis*
MHC	major histocompatibility complex
MOI	multiplicity of infection
MTBC	*Mycobacterium tuberculosis* complex
MWCO	molecular weight cut off
NF-κB	nuclear factor kappa-light-chain-enhancer of activated B cells
Ni-IDA	Nickel-iminoacetic acid
NLRP3	NOD-, LRR, and pyrin domain-containing protein 3
OADC	oleic acid-albumin-dextrose-catalase
OD	optical density
PA	phosphatidic acid
PAGE	polyacrylamide gel electrophoresis
PAMPs	pathogen-associated molecular patterns
PBS	phosphate buffered saline
PBST	phosphate buffered saline + 0.01% Tween-20
PC	phosphatidylcholine
PE	Proline-Glutamate
PEA	phosphatidylethanolamine
PI	phosphatidylinositol
PI3P	phosphatidylinositol 3-phosphate
PI4P	phosphatidylinositol 4-phosphate
PI5P	phosphatidylinositol 5-phosphate
PIP	phosphorylated phosphatidylinositol species
PMA	phorbol 12-myristate-13-acetate

pNF-κB	phosphorylated NF-κB
PPE	Proline-Proline-Glutamate
PS	phosphatidylserine
RFP	red fluorescent protein
RFUs	relative fluorescence units
RIPA	radioimmunoprecipitation
ROS	reactive oxygen species
RPMI	Roswell Park Memorial Institute Medium
RT	room temperature
S1P	sphingosine 1-phosphate
SEC	size exclusion chromatography
TAT	twin-arginine translocation
TB	Tuberculosis
TBST	Tris-buffered saline + 0.05% Tween-20
TEM	transmission electron microscopy
TNFα	tumor necrosis factor α
WXG	Tryptophan-X-Glycine

1. Introduction

1.1. Tuberculosis

Tuberculosis (TB) is a severe chronic infection that has plagued the human population for millennia and is currently estimated to affect one quarter of the world's population (World Health Organization, 2019). In 2019, 1.4 million lives were claimed by this disease with over 200,000 deaths as a result of co-infections with human immunodeficiency virus (HIV) (World Health Organization, 2019). TB is the number one cause of death due to a single bacterial pathogen, the bacillus *Mycobacterium tuberculosis* (*M. tb*) (Philips and Ernst, 2012). Infections with *M. tb* most commonly affect the lungs (pulmonary TB), but can impact other organs as well (extrapulmonary TB) if dissemination has occurred (Pai *et al.*, 2016). In Canada, overall case numbers of TB have been declining since the middle of the 20th century, but the remaining cases disproportionately affect Aboriginal and foreign-born Canadians (Public Health Agency of Canada, 2014). TB remains a major global and local health problem and further research and innovation are critical to further understand, prevent, and treat TB in order to end this epidemic.

There are three potential outcomes of an exposure to *M. tb*. Firstly, the host may be able to successfully eliminate the bacteria (Ernst, 2012). This can occur due to acquired T-cell immunity or due to an effective innate immune response that clears the pathogen from the body entirely (Pai *et al.*, 2016). In the second possible outcome of an *M. tb* exposure, the host will not eliminate the pathogen, but instead remain latently infected (World Health Organization, 2019). The individual will exhibit a persistent immune response to *M. tb* to control the infection, but will remain asymptomatic (World Health Organization, 2019). Around 10% of latently infected people are likely to reactivate and progress into active disease in their lifetime, which is the third possible outcome of *M. tb* exposure (Pai *et al.*, 2016). Symptoms of Active TB include coughing, fever, weight loss, hemoptysis, and could result in death if the disease goes untreated (Public Health Agency of Canada, 2014). Those infected with HIV are much more likely to develop TB disease (Pai *et al.*, 2016). Similarly, individuals experiencing undernutrition, diabetes, alcoholism, or those who smoke have a higher probability for progression to active disease following an exposure to *M. tb* (Pai *et al.*, 2016).

1.1.1 *Mycobacterium tuberculosis* complex

M. tb is the primary causative agent of TB and has no reservoir in the environment outside of humans (Pai *et al.*, 2016). In addition to *M. tb* there are several other pathogenic mycobacteria that are capable of causing TB disease across several species, these mycobacteria are collectively named the *Mycobacterium tuberculosis* complex (MTBC) (Forrellad *et al.*, 2013). The MTBC includes *M. tb*, *Mycobacterium africanum*, *Mycobacterium bovis* (*M. bovis*), *Mycobacterium caprae, Mycobacterium canettii*, *Mycobacterium microti*, and *Mycobacterium pinnipedii*. These species are genetically very similar and taken together can infect a wide range of animals (Forrellad *et al.*, 2013). A very small fraction of human TB cases are known to be caused by infections with *Mycobacterium africanum*, *M. bovis*, or *Mycobacterium caprae* (Pai *et al.*, 2016). *M. bovis* is also capable of infecting animals associated with agriculture, like cattle. The resulting bovine TB disease leads to significant economic loss around the world (Ejeh *et al.*, 2014; Pérez-Morote *et al.*, 2020).

1.1.2. Treatment and prevention of TB

Recommended treatment of TB involves a six-to-nine-month chemotherapy regimen involving a combination of several anti-microbial drugs (Pai *et al.*, 2016). The first-line drugs used to treat TB are isoniazid, rifampin, ethambutol, and pyrazinamide (World Health Organization, 2019). A typical drug regimen would include taking all four first-line drugs daily for two months followed by an additional four months taking just isoniazid and rifampin (Pai *et al.*, 2016). Treatment can be very difficult to complete as it requires vigilance from the patient and can cause several uncomfortable side-effects (World Health Organization, 2019). These challenges contribute to the increasing number of drug-resistant TB cases. Globally, more than 3% of new TB cases and around 18% of previously treated cases were found to be multidrug-resistant (World Health Organization, 2019). Success in treating these cases is becoming increasingly more difficult to achieve and indicates the necessity for more effective treatments and vaccines to prevent infection.

The only vaccine currently available against TB is a live-attenuated strain of *M. bovis* called bacillus Calmette Guérin (BCG) (Philips and Ernst, 2012). Routine vaccination with BCG is widely performed around the world and has been very successful in preventing severe forms of TB in young children (World Health Organization, 2019). BCG was developed through serial

passaging of *M. bovis* over the course of 13 years, from 1908-1921, now making it 100 years old (Tran *et al*., 2014). Passaging allowed for spontaneous genetic deletions to occur, leading to the attenuation observed in BCG (Tran *et al.*, 2014). Despite being very safe and effective in infants, the vaccine is considered controversial as its efficacy is highly variable (0-80%) (Anderson and Doherty, 2005). In Canada, BCG vaccination is only recommended for some travellers and young children in settings with high-incidences of TB (Public Health Agency of Canada, 2014). Efficacy of the BCG vaccine often wanes once the individual reaches adolescence (Pai *et al.*, 2016). To this point, there is no reliable vaccine against TB for adults.

1.2. *M. tb* pathogenesis

M. tb is a slow-growing, facultative intracellular pathogen with a low infective dose (<10 bacilli) and is easily spread through aerosol droplets (Pai *et al.*, 2016). After being breathed in by the host, the bacterium enters the lower respiratory tract and eventually reaches the lung alveoli (Lerner *et al*., 2015). Resident phagocytes including alveolar macrophages, dendritic cells, and neutrophils make up the innate defense against *M. tb* in this region (Lerner *et al.*, 2015). Macrophages are the first host-cell to encounter and phagocytose *M. tb* after an exposure (Liu et al., 2017a). Cells that effectively neutralize and eliminate the bacteria will prevent an infection from being established (Pai *et al.*, 2016). Macrophages have several methods of defense including phagosome acidification, autophagy, nitrosative and oxidative stresses, cytokine production, and more (Sia and Rengarajan, 2019). If macrophages are unable to eliminate *M. tb*, they become the primary niche for the bacteria to replicate and survive (Sia and Rengarajan, 2019). *M. tb* has developed strategies to hijack key host-cell defense mechanisms allowing it to persist within the host for long periods of time, often in a state of latency (Stutz *et al*., 2018). *M. tb* is able to evade the acidification of the phagosome and can adapt to the immunological pressures of the intracellular environment using highly specialized virulence factors (Sia and Rengarajan, 2019).

1.2.1. Phagosomal maturation

Macrophages express pattern recognition receptors on their surface that recognize invading microorganisms through the pathogen-associated molecular patterns (PAMPs) on the bacterial surface (Xu *et al.*, 2014). This recognition begins a signalling cascade that readies the macrophage's host-cell defence mechanisms (Xu *et al.*, 2014). Phagocytosed material is then

contained within the host-cell in a membrane-bound structure called a phagosome (Stutz *et al.*, 2018). The phagosome then proceeds through a process called phagosomal maturation wherein the engulfed material is inactivated after stepwise fusion processes with endosomes and lysosomes (Figure 1) (Poirier and Av-Gay, 2012). The final fusion step with the lysosome gives rise to the phagolysosome. This compartment will have a lower internal pH, and reactive oxygen species (ROS), and degradative enzymes that will lyse internalized contents (Poirier and Av-Gay, 2012).

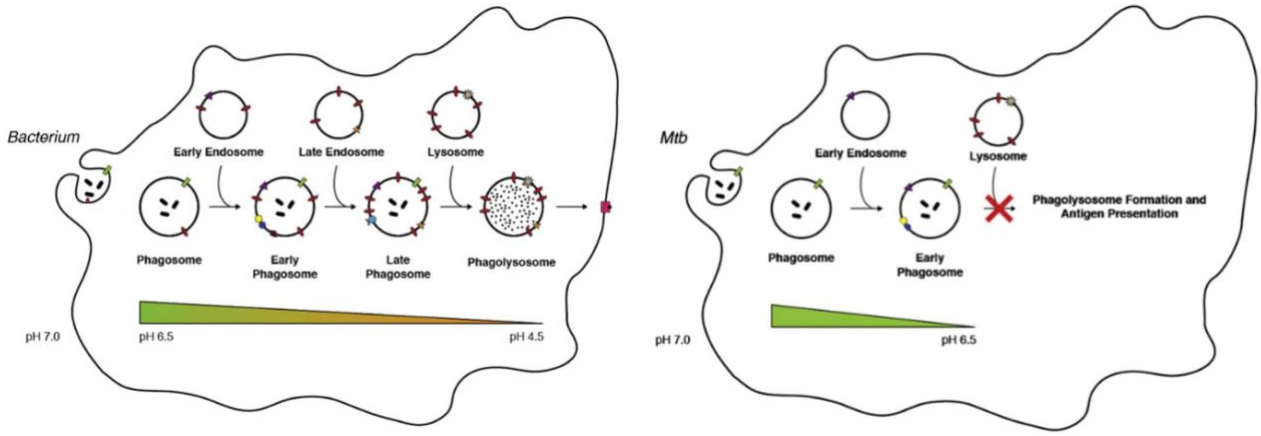

Figure 1: Phagosomal maturation is the process by which a phagosome containing engulfed foreign material is fused with endosomes and lysosomes in order to inactivate the internalized material. *M. tb* is able to inhibit phagosomal maturation. Figure is adapted from Poirier and Av-Gay, 2012.

M. tb is an ancient bacterium that has been co-evolving alongside its human host for a very long time (Zhang *et al.*, 2021). This has allowed *M. tb* to develop successful strategies to avoid being killed within the host macrophage in several ways (Liu et al., 2017a). *M. tb* can inhibit phagosomal maturation, hijack the phagosome to be an intracellular habitat, and cause damage to the phagosomal membrane to allow for escape into the cytosol (Stutz *et al.*, 2018). There are several *M. tb* virulence factors that have been demonstrated to be involved in these processes. For example, SapM is a secreted 3-phosphatase that functions on phosphatidylinositol 3-phosphate (PI3P) to produce phosphatidylinositol (PI), ultimately inhibiting phagosomal maturation by blocking the fusion between the lysosome and the phagosome (Puri *et al.*, 2013). The presence of PI3P on phagosomes is linked to maturation of the phagosome and can be observed in higher concentrations when macrophages are infected with attenuated mycobacteria as opposed to virulent strains (Vergne *et al.*, 2005). Lower levels of PI3P on the phagosome are

proposed to stop the binding of early endosomal markers such as early endosome antigen-1 (EEA1) and hepatocyte growth factor–regulated tyrosine kinase substrate (Hrs), which possess PI3P binding domains (Hu *et al.*, 2015; Vieira *et al.*, 2001).

M. tb has also demonstrated the ability to escape from the phagosome entirely and enter the cytosol of the host-cell (Zhai *et al.*, 2019). This process is dependent on one of *M. tb*'s Type VII secretion systems, ESX-1 (Sia and Rengarajan, 2019). It was originally proposed that a prominent secreted effector of this system, the 6 kDa early secretory antigen target (ESAT-6), also called EsxA, may be capable of lysing membranes and destabilizing the phagosome by creating pores (De Jonge *et al.*, 2007). Recent work has demonstrated that the ESX-1 dependent lysis may be due to direct contact between the bacterium and the eukaryotic membrane, which leads to tearing of the phagosome (Conrad *et al.*, 2017).

1.2.2. Autophagy

Autophagy is a programmed pathway in eukaryotic cells that allows for the turnover of degraded material in the cytoplasm (Deretic, 2008). These turnover processes can also be involved in the innate and adaptive immune responses necessary to control intracellular pathogens (Gutierrez *et al.*, 2004). Autophagy is important for regulating the major histocompatibility complex (MHC) class II presentation of antigens from these internalized pathogens (Romao *et al.*, 2013). *M. tb* has demonstrated an ability to suppress antigen presentation during infections (Saini *et al.*, 2016). The virulence protein PE_PGRS47 was found to be critical in the inhibition of autophagy and antigen presentation that occurs during *M. tb* infections of macrophages (Saini *et al.*, 2016).

The foreign material destined for degradation through autophagy is surrounded by a double membrane and contained within a structure called the autophagosome (Romao *et al.*, 2013). Similar to phagosomal maturation, this structure requires maturation and acidification through fusion with the lysosome (Harris *et al.*, 2017). The autophagosomal membrane becomes decorated with PI3P, which recruits EEA1 and Hrs to perform organelle tethering and membrane sorting functions required for lysosomal fusion (Deretic, 2008). Virulent *M. tb* strains have demonstrated an ability to avoid being killed through this autophagic process, by inhibiting the late stage of autophagy in an ESX-1-dependent manner (Romagnoli *et al.*, 2012). The inhibition of these bacteriolytic processes in the host cell facilitate the opportunity for *M. tb* to escape into

the cytosol and replicate (Pai *et al.*, 2016). Ultimately, the macrophage will be killed, enabling the bacteria to infect other cells (Di Russo Case and Samuel, 2016).

1.2.3. TB induced host-cell death pathways

The death of macrophages and subsequent release of the infecting *M. tb* bacteria is an important step in the pathogenesis of TB disease (Pai *et al.*, 2016). Despite that there is little known about the mechanism of how *M. tb* infected macrophages decide to perform programmed cell death, this death has been demonstrated to involve rupture of cell membranes, permeability of the mitochondria and lysosome, and the production of ROS (Lee *et al.*, 2011; Zhao *et al.*, 2017). There are several identified pathways of programmed cell death that have been identified during *M. tb*'s killing of macrophages. These include apoptosis, which is the most well described method of programmed cell death, as well as necroptosis and pyroptosis, which are programmed forms of necrosis (Zhang *et al.*, 2021).

Apoptosis is a form of cell death that is necessary for normal development in host organisms, but it can also be involved in the immune response against infecting pathogens (Zhang *et al.*, 2021). Several hallmarks of apoptotic cell death include shrinking of the cell, membrane blebbing, exposure of phosphatidylserine (PS) on the outer surface of the cell, and the formation of apoptotic bodies (Nagata, 2018). In the case of *M. tb* infected macrophages, apoptosis has been reportedly induced in association with either autocrine or paracrine signaling of a key pro-inflammatory cytokine, tumor necrosis factor α (TNFα) (Keane *et al.*, 1997). Notably, virulent strains of *M. tb* lead to less apoptosis of infected cells than is observed with avirulent strains (Keane *et al.*, 2000). Extending the life of an infected host-cell can be beneficial to the pathogen as it can continue to replicate within the intracellular environment, therefore *M. tb*'s ability to suppress apoptosis in macrophages contributes to its ability to persist within the host (Di Russo Case and Samuel, 2016).

While macrophages infected with attenuated strains of *M. tb* predominantly die through apoptosis, virulent strains of *M. tb* induce macrophage necrosis (Divangahi *et al.*, 2009). However, it is not fully clear how much of this *M. tb* induced necrosis is 'accidental' and how much is specifically driven by the macrophage. Necroptosis is defined as an inflammatory cell death that is a type of programmed necrosis (Berghe *et al.*, 2014). Similarly to apoptosis, necroptosis is associated with the stimulation of TNFα production, which at high levels can lead to

mitochondrial ROS production (Xu *et al.*, 2014). There is still much to be understood about how necroptosis is involved in *M. tb* induced cell death, but it appears to be favoured by virulent *M. tb* strains as it allows for survival and spread of the bacteria (Zhang *et al.*, 2021).

Another form of programmed necrosis is pyroptosis, which has been demonstrated to involve the activation of inflammasome complexes (Zhang *et al.*, 2021). Inflammasomes are eukaryotic protein complexes that function to activate caspases that directly contribute to the inflammatory response (Broz and Dixit, 2016). Inflammasome complexes are formed as a host-defense response when pathogens are detected within immune cells (Rathinam and Fitzgerald, 2016). *M. tb* has been implicated in manipulating both the absent in melanoma 2 (AIM2) and NOD-, LRR-, and pyrin domain-containing protein 3 (NLRP3) inflammasome complexes in infected macrophages (Mishra *et al.*, 2010; Shah *et al.*, 2013). The AIM2 inflammasome is constructed when the inflammatory ligand AIM2 binds to the adapter protein apoptosis-associated speck-like protein containing a CARD domain (ASC) which further binds the inflammatory caspase, caspase-1 (Figure 2a) (Schroder and Tschopp, 2010). Oligomerization of these components then forms the AIM2 inflammasome which auto-processes caspase-1 into the active form of cleaved caspase-1 which can then cleave Pro-interleukin-1 ß (IL1ß) into IL1ß (Broz and Dixit, 2016). It has been proposed that virulent *M. tb* is able to inhibit the AIM2 inflammasome, which allows the bacterium to control IL1ß production (Shah *et al.*, 2013). However, details of how this inhibition occurs are yet to be understood.

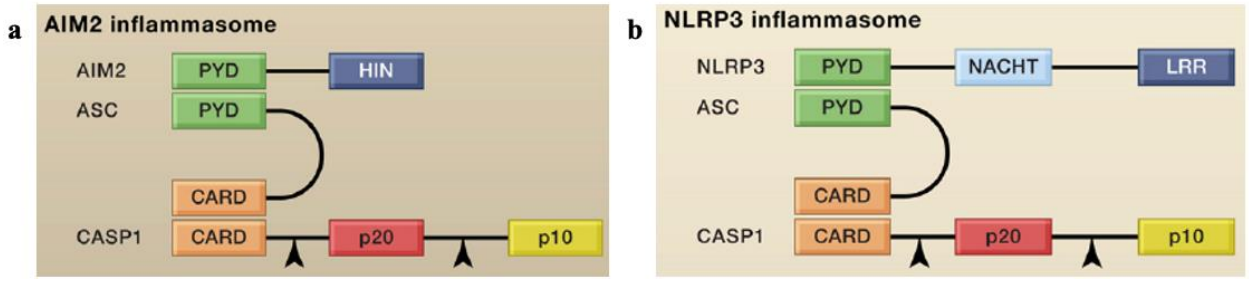

Figure 2: Unoligomerized inflammasome complexes for the (a) AIM2 and (b) NLRP3 inflammasomes. Figure adapted from Schroder and Tschopp, 2010.

Similarly to the AIM2 inflammasome, the NLRP3 inflammasome involves complexing of ASC and caspase-1 (Swanson *et al.*, 2019). This inflammasome is constructed on the Golgi apparatus after NLRP3 is recruited and scaffolded to phosphatidylinositol 4-phosphate (PI4P), which makes up a significant portion of the Golgi apparatus (Chen *et al.*, 2019). NLRP3 is then

able to bind ASC and caspase-1, oligomerize, and form the NLRP3 inflammasome complex (Figure 3) (Chen *et al.*, 2019). Cleaved caspase-1 can then cleave pro-IL1ß into IL1ß, contributing to the pro-inflammatory response (Yang *et al.*, 2019). *M. tb* has been shown to induce IL1ß production through activation of the NLRP3 inflammasome in macrophages in an ESX-1 dependent fashion (Dorhoi *et al.*, 2012). The secreted effector EsxA has been proposed to be responsible for this NLRP3 activation, as *M. tb* Δ*esxA* was only capable of low levels of IL1ß production in macrophages (Mishra *et al.*, 2010).

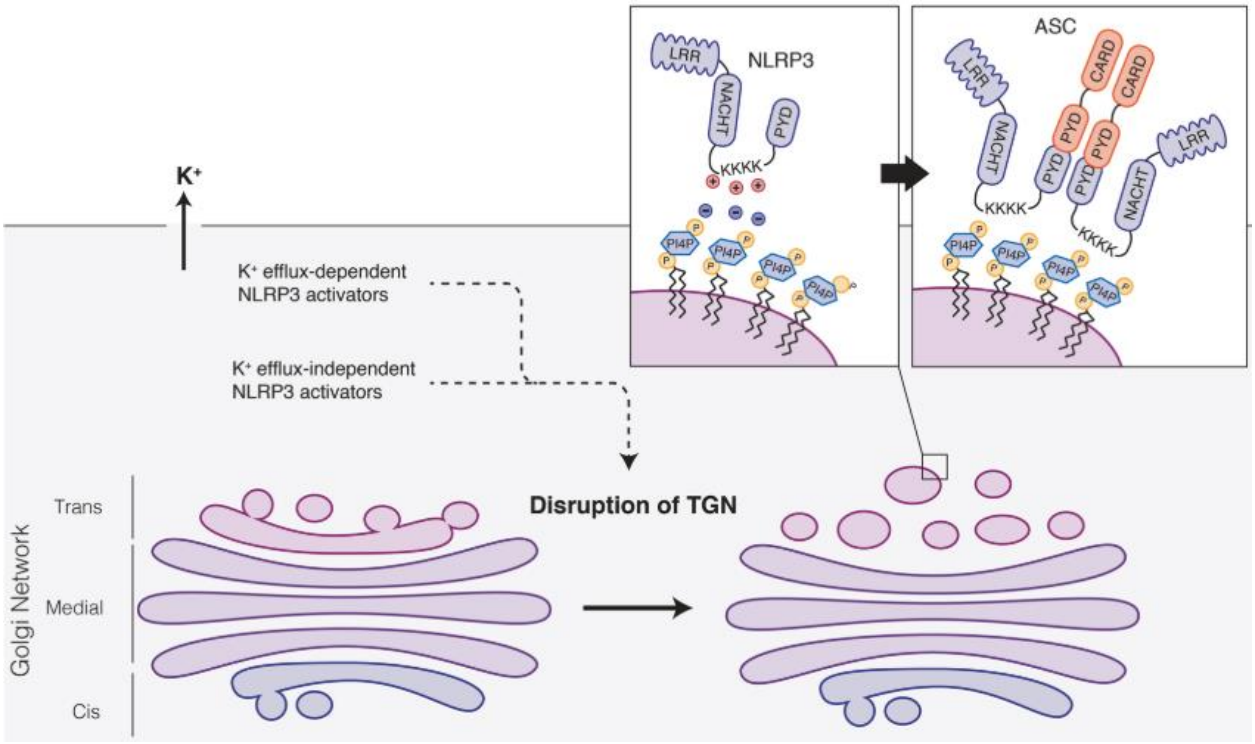

Figure 3: Negatively charged PI4P on the dispersed trans-golgi network recruits NLRP3 through ionic bonding with its poly-lysine motif. NLRP3 aggregates and further binds to ASC for formation of the inflammasome. Figure adapted from Chen *et al.*, 2019.

1.3. Type VII secretion systems

M. tb possesses five distinct ESX secretion systems, at least three of which (ESX-1, ESX-3, and ESX-5), appear to be necessary for the bacteria's viability or virulence (Figure 4) (Bottai *et al.*, 2017). These specialized Type VII secretion systems are required to transport substrates across the thick and mycolic acid-rich cell envelope, which provides protection to the bacterium when exposed to harsh environmental conditions (Gröschel *et al.*, 2016). The five ESX systems of *M. tb* differ in their genetic size and complexity, but they all share several core features. Firstly,

each of the ESX loci contain a pair of *esx* genes (*esxA* and *esxB* in ESX-1), which encode for small proteins with a Tryptophan-X-Glycine (WXG) motif (Gröschel *et al.*, 2016). Secondly, these systems encode esx conserved component (*ecc*) genes, which express the proteins important for the mechanistic components of a secretion system (Bottai *et al.*, 2017). These proteins contain ATP-binding and transmembrane domains (Bottai *et al.*, 2017). Next, all systems contain a *mycP* gene, which encodes a subtilisin-like serine protease (Chen, 2016). Lastly, all systems excluding ESX-4 contain *pe* and *ppe* genes, which encode proteins with Proline-Glutamate (PE) and Proline-Proline-Glutamate (PPE) motifs their N-terminal regions (Bottai *et al.*, 2017). These proteins represent two mycobacteria-specific classes of proteins, members of which have been implicated in variety of functions including intracellular growth, phagocytosis, phagosomal maturation, and more (Bottai *et al.*, 2017). Otherwise, these protein classes remain largely understudied.

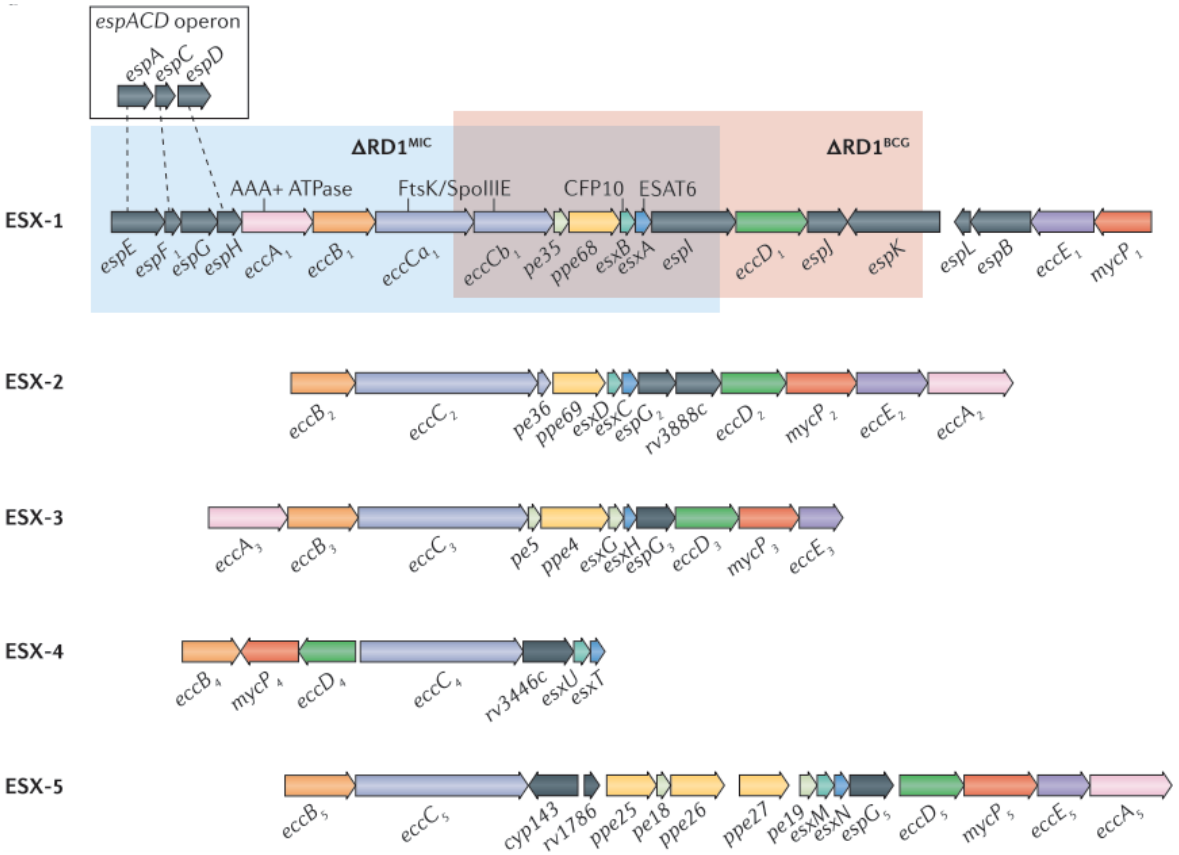

Figure 4: Genetic organization of the ESX secretion systems of *M. tb*. The *espACD* operon is located 300 kb upstream of the *esx-1* locus. The region identified as the ΔRD1 region indicates the genes lost in the *M. bovis* BCG vaccine strain that interrupts the ESX-1 system, contributing to its attenuation. The absent RD1 region includes the gene for EsxA, the most highly characterized ESX effector. Image adapted from Groschel *et al.*, 2016.

Of the *M. tb* Type VII secretion systems, ESX-4 is the simplest. It is composed of the least number of genes and is thought to be an ancestral system through which the other ESX systems may have evolved (Bottai *et al.*, 2017). ESX-4, along with ESX-2, appears to be a non-essential system that is uninvolved in *M. tb*'s intracellular survival or virulence (Gröschel *et al.*, 2016). The functions of both ESX-4 and ESX-2 are entirely unknown (Bunduc *et al.*, 2020).

ESX-3 is highly conserved across different mycobacterial species and is predominantly established to be involved in metal acquisition and homeostasis (Gröschel *et al.*, 2016). A pair of secreted proteins, the EsxG-EsxH heterodimer of the ESX-3 system, are implicated as regulators for the secretion of several proteins of the PE and PPE protein families (Tufariello *et al.*, 2016). This system has also been found to be involved in *M. tb* virulence, as depending on the genotype of the host, the ESX-3 system is capable of counteracting a restricted iron availability (Bottai *et al.*, 2017). Additionally, the EsxG-EsxH complex is known to impair phagosomal maturation in *M. tb* infected macrophages through EsxH interaction with the host's Hrs protein (Mehra *et al.*, 2013). Hrs is a eukaryotic protein that contributes to sorting processes directing material for lysosomal degradation (Mehra *et al.*, 2013).

ESX-5 is evolutionarily the most recently emerged of the ESX systems (Bunduc *et al.*, 2020). Unlike ESX-3, ESX-5 is only present in slow-growing species of mycobacteria (Bottai *et al.*, 2017). This system is proposed to be necessary for bacterial viability due to its role in nutrient uptake (Bunduc *et al.*, 2020). Additionally, ESX-5 exports many PE and PPE proteins, which are largely encoded on entirely distinct loci from the genes encoding the ESX-5 system itself (Gröschel *et al.*, 2016). Loss of ESX-5 secretion leads to considerable damage to the cell envelope of the mycobacteria (Bottai *et al.*, 2012).

1.3.1. The ESX-1 system

Much of *M. tb*'s ability to survive within macrophages is due to the ESX-1 system. As mentioned, this system is involved in avoiding phagosomal maturation (Stutz *et al.*, 2018) and autophagy (Romagnoli *et al.*, 2012), preventing apoptosis (Keane *et al.*, 2000) and inducing necrosis (Wong and Jacobs, 2011) as well as activating the NLRP3 inflammasome (Dorhoi *et al.*, 2012). Yet, much is still to be elucidated about this system. Very few structures have been obtained for the mechanistic components of ESX-1 and the actual mechanism of secretion is still largely unknown (Figure 5) (Bottai *et al.*, 2017). Type I, Type III, and Type VI secretion occur

through a channel that spans both membranes of a Gram-negative bacterium, allowing substrates to be secreted in a single step. Type II and Type IV secretion systems work together with the SecA-dependent or Twin-arginine translocation (TAT) cytoplasmic membrane transport systems to secrete substrates (Beeckman and Vanrompay, 2010). With Type VII, the Ecc core components contain transmembrane domains, which could span across the mycomembrane, and the ESX substrates do not encode for Sec or TAT signal sequences, therefore it has been hypothesized that this secretion could also occur in a single step (Houben *et al.*, 2012).

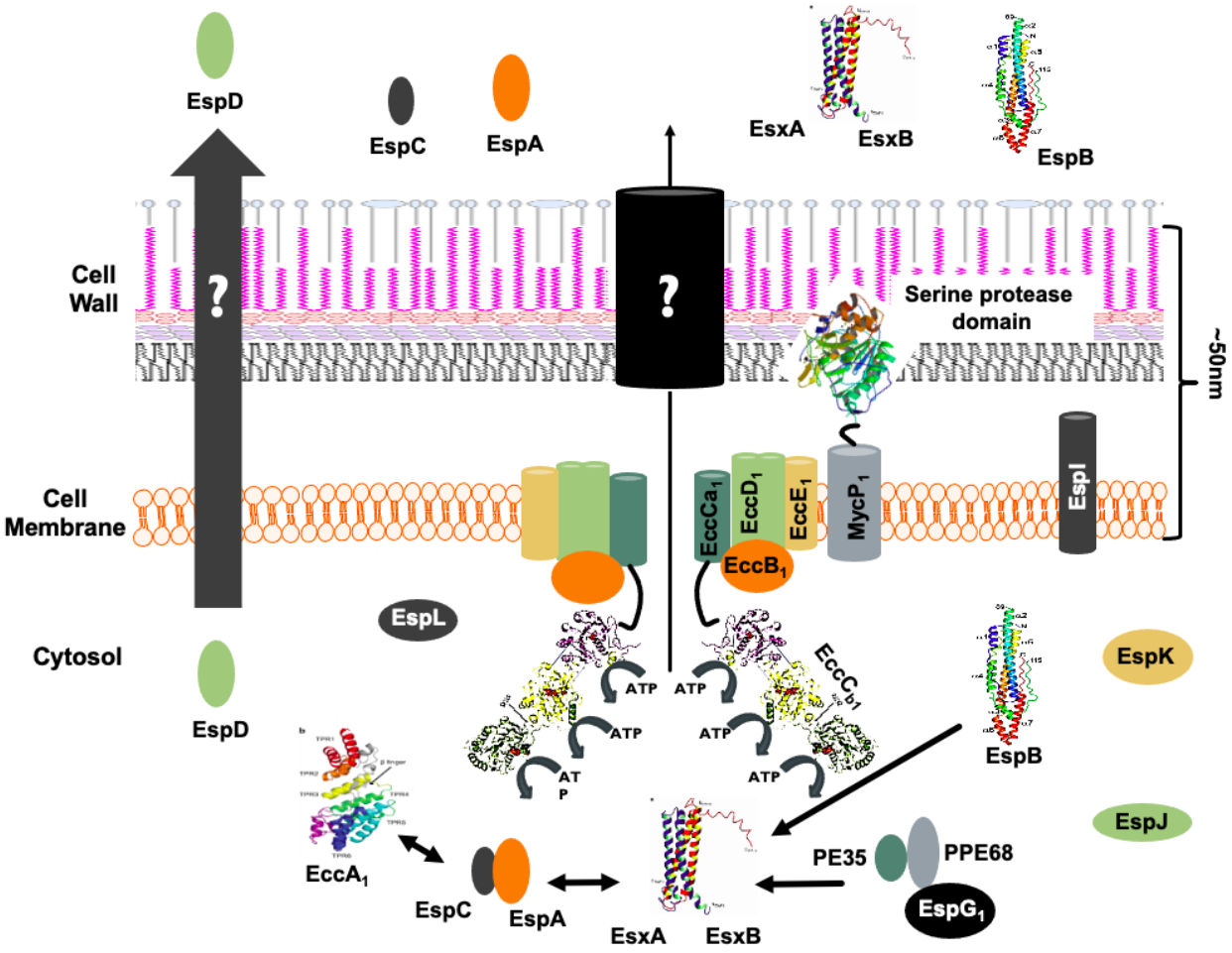

Figure 5: Organization of the components of the ESX-1 Type VII secretion system of *M. tb*.

1.3.2. ESX-1 secreted proteins

M. tb's ESX-1 system is encoded by 23 genes spanning two separate loci on the bacterial chromosome, the *esx-1* locus and the *esx-1* secretion-associated proteins ACD (*espACD*) operon (Figure 4) (Gröschel *et al.*, 2016). Several of these genes, namely those called *esp* or *esx* genes, encode for proteins thought to be secreted themselves or somehow involved in secretion

modulation (Gröschel *et al.*, 2016). Secreted proteins are some of the main tools *M. tb* uses during infection to survive intracellularly and hijack host-cell defence mechanisms. EsxA, EsxB, EspA, EspB, EspC, and EspD have all been identified as secreted proteins of the ESX-1 system (Bottai *et al.*, 2017).

The most well characterized member of the ESX-1 system is EsxA, which is a 6 kDa secreted effector known to be a potent T-cell antigen (Aguiló *et al.*, 2013). EsxA is co-secreted as a heterodimer with another effector, EsxB, also called 10 kDa culture filtrate protein, (CFP-10) (Fortune *et al.*, 2005). EsxA is linked to *M. tb*'s ability to disrupt the phagosome during macrophage infections (De Jonge *et al.*, 2007). The ability of EsxA to form pores in the phagosomal membrane through lytic activity is controversial, however EsxA remains an essential component of *M. tb*'s virulence. EsxA is also thought to induce NLRP3 inflammasome activation in macrophages contributing to the pro-inflammatory response (Mishra *et al.*, 2010).

Another core member of the ESX-1 system that is necessary for the full virulence of *M. tb* is EspB. EspB is expressed as a 60 kDa protein, processed by the MycP1 protease, and secreted as a 50 kDa substrate (Ohol *et al.*, 2010). The secretion of EspB does not require co-secretion with EsxA or EsxB and does not require the expression of the products of the *espACD* operon (Chen *et al.*, 2013a). Recombinant EspB purified from *Escherichia coli* (*E. coli)* has been shown to inhibit IFN-γ-induced autophagy in murine macrophages (Huang and Bao, 2016). Additionally, EspB may contribute to *M. tb*'s virulence through binding of the eukaryotic phospholipids phosphatidic acid (PA) and PS (Chen *et al.*, 2013a).

1.3.3. The *espACD* operon

The *espACD* operon is located around 300 kb upstream of the *esx-1* locus in the genomes of pathogenic mycobacteria (Bottai *et al.*, 2017). The genes of this operon are all co-transcribed and are regulated by the DNA-binding protein EspR (Blasco *et al.*, 2012; Chen *et al.*, 2012). The EspA, EspC, and EspD proteins are homologous to the core *esx-1* proteins EspE, EspF, and EspH, respectively (Gröschel *et al.*, 2016). EspA and EspC are also co-secreted with EsxA and EsxB through the ESX-1 system (Fortune *et al.*, 2005). EspA requires both EspC and EspD to be expressed in order to maintain normal protein levels within the mycobacterial cell. Similarly, for EspC to remain stable and for EspA and EspC to be secreted, EspD needs to be present within the mycobacterium (Chen *et al.*, 2012). Despite being critical for the secretion of EsxA and EsxB,

EspA's function as a secreted protein has yet to be fully understood (Chen *et al*., 2013b). EspC has been found to be able to form long filamentous oligomers and recently has been implicated in the induction of endoplasmic reticulum stress-mediated apoptosis (Guo *et al.*, 2021; Lou *et al.*, 2017).

1.3.4. Published data on EspD

To date, the work done to establish the function of EspD has taken a genetic approach, using mutated *M. tb* strains and determining the impact of these mutations on the function of the mycobacteria. A transposon insertion into the *espA* gene stops the expression of EspA, EspC, and EspD and therefore creates a strain missing the entire *espACD* operon, called *M. tb espA*::Tn. This disruption attenuates the bacteria and is known to significantly decrease its relative cytotoxicity during infections (Chen *et al.*, 2013). However, this strain can further be complemented with a plasmid encoding the entire *espACD* operon or a plasmid encoding the *espACD* operon containing targeted truncations, single point mutations, or early stop codons in order to express variants of EspD within *M. tb*. These strains are called *M. tb espA*::Tn pMD31 (empty vector, missing the *espACD* operon), *M. tb espA*::Tn pMDespACD^{WT} (fully complemented wildtype strain), and *M. tb espA*::Tn pMDespACD^{STOP} (early stop codon in *espD* prevents expression of EspD alone). Using these strains, as well as strains encoding single point mutations on EspD, the functions of EspD within the mycobacterial cell were defined. EspD maintains the stability of EspA and EspC and facilitates the secretion of EspA, EspC, EsxA, and EsxB (Chen *et al.*, 2012). EspD itself however, was found to still be capable of secretion when all other ESX-1 secretion is shut down (Chen *et al.*, 2012). Additionally, EspD has been identified as a binding partner to another ESX-1 component, EspL, but little is known about the consequences of this interaction (Sala *et al.*, 2018). There is no published work on the function of secreted EspD protein. It is currently unknown what impact EspD secretion has on the eukaryotic host-cell during *M. tb* infection.

1.3.5. Unpublished work on EspD characterization

Previous work established the secretion profile for an *M. tb* strain expressing EspD with a Tryptophan to Arginine mutation on position 19 (W19R), *M. tb espA*::Tn pMDespACD^{W19R}. This strain is deficient in EspD^{W19R} secretion alone and is still capable of secreting other ESX-1

members (Chen *et al.*, 2012). *M. tb espA*::Tn pMDespACD^{W19R} was tested alongside *M. tb espA*::Tn pMDespACD^{WT} and *M. tb espA*::Tn pMDespACD^{STOP} to observe any differences in the bacterial load present in the lungs and spleen of infected mice after 14-days (Figure 6). This experiment indicated a significant reduction in the bacterial load in mice infected with *M. tb espA*::Tn pMDespACD^{W19R} compared to *M. tb espA*::Tn pMDespACD^{WT}. This data appears to indicate that secreted EspD protein contributes to *M. tb* virulence.

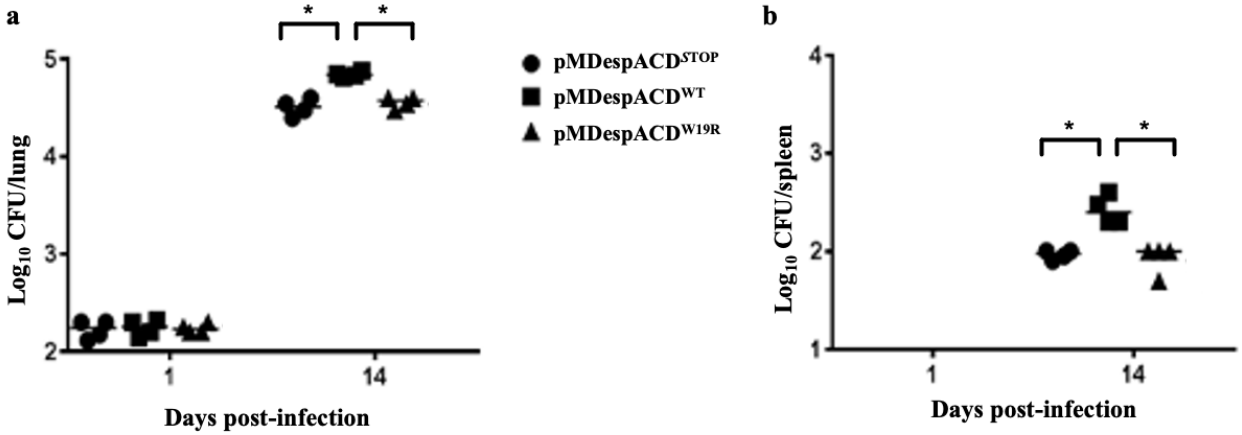

Figure 6: Bacterial load measured in (a) lung and (b) spleen of mice infected with *M. tb espA*::Tn pMDespACD^{STOP}, *M. tb espA*::Tn pMDespACD^{WT} and *M. tb espA*::Tn pMDespACD^{W19R} for 14 days. (*) indicates a statistically significant difference with $p < 0.05$.

To begin investigating the role of secreted EspD, attempts were made to express the protein in *E. coli* for purification. Gene products from *M. tb* are notoriously difficult to express and purify from *E. coli* due to a lack of necessary chaperones and the high GC content of mycobacterial genes (Miyoshi-Akiyam *et al.*, 2012). Due to these challenges, the attempt to express and purify EspD resulted in only very limited amounts of the protein. Nevertheless, some analyses of EspD protein's structure and function were conducted.

Recombinant EspD protein was subjected to size exclusion chromatography (SEC) and transmission electron microscopy (TEM) to analyze any quaternary structure of the protein. EspD's size was observed through SEC on an S-400 sephacryl column by monitoring the A280 nm as protein was eluted. EspD appeared to demonstrate structures upwards of 400 kDa in size across various salt concentrations, with a slight increase in oligomer size in higher salt concentrations (Figure 7a). This oligomerization was further investigated with TEM at 100k magnification of the recombinant protein sample. The EspD protein appeared to be forming oligomers representative of a ball-on-chain structure, which appeared to be of various sizes

(Figure 7b). Taken together, this data appears to indicate that EspD binds to itself to form large scale oligomers.

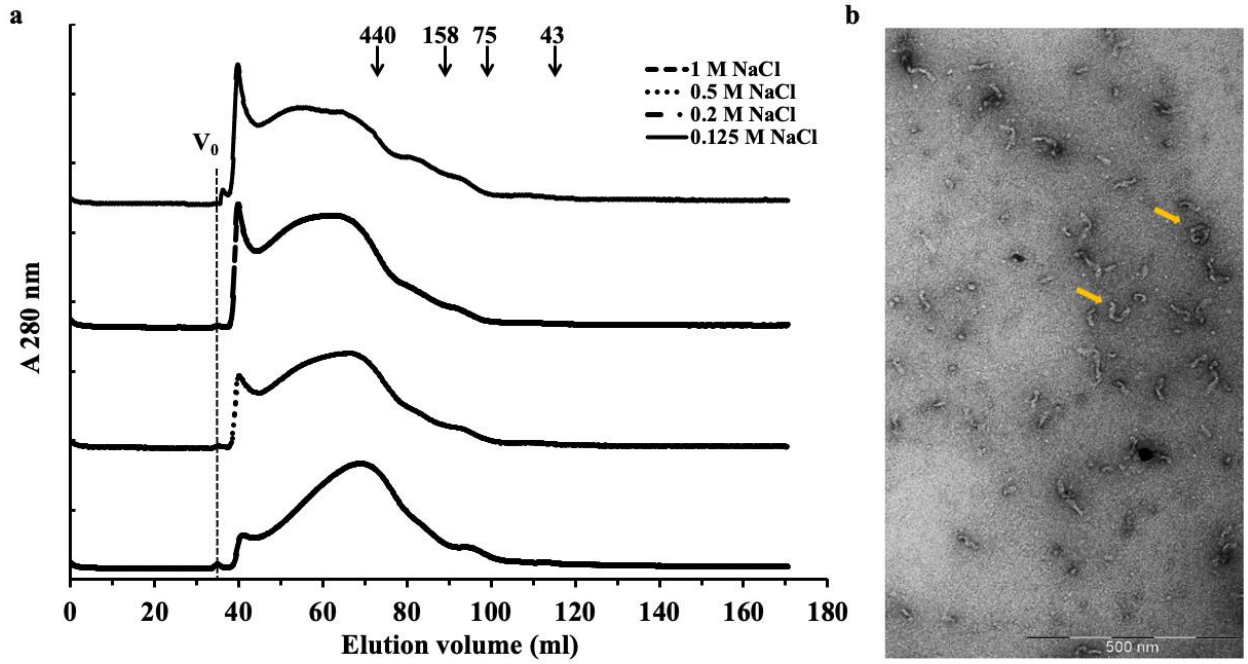

Figure 7: (a) SEC performed on S-400 sephacryl column using natively purified EspD in a series of buffers containing a variety of salt concentrations. (b) TEM image of recombinant EspD sample taken at 100k magnification. Yellow arrows indicate some of the protein appearing to form oligomeric structures.

Attempts to determine a biochemical function for EspD were additionally explored. Purified recombinant EspD protein did not appear to be toxic to cells in culture and was not found to exhibit any enzymatic function (data not shown). Another *M. tb* secreted protein, EspB, is known to interact with the eukaryotic phospholipids, PA and PS (Chen *et al.*, 2013a). Therefore, EspD was examined for a similar ability using membranes embedded with a variety of eukaryotic phospholipids. Binding was observed through immunoblot. EspD appeared to bind specifically to several phospholipids, namely, the phosphatidylinositol monophosphates, PA, and PS (Figure 8). These molecules are involved in a variety of key processes within the cell and are commonly targeted by effectors of bacterial pathogens to promote bacterial survival during infections (Ham *et al.*, 2011; Walpole *et al.*, 2018; Yeung *et al.*, 2009). EspD-phospholipid binding could aid *M. tb* during infection in its ability to survive and persist within a host by disrupting normal host-cell defense mechanisms.

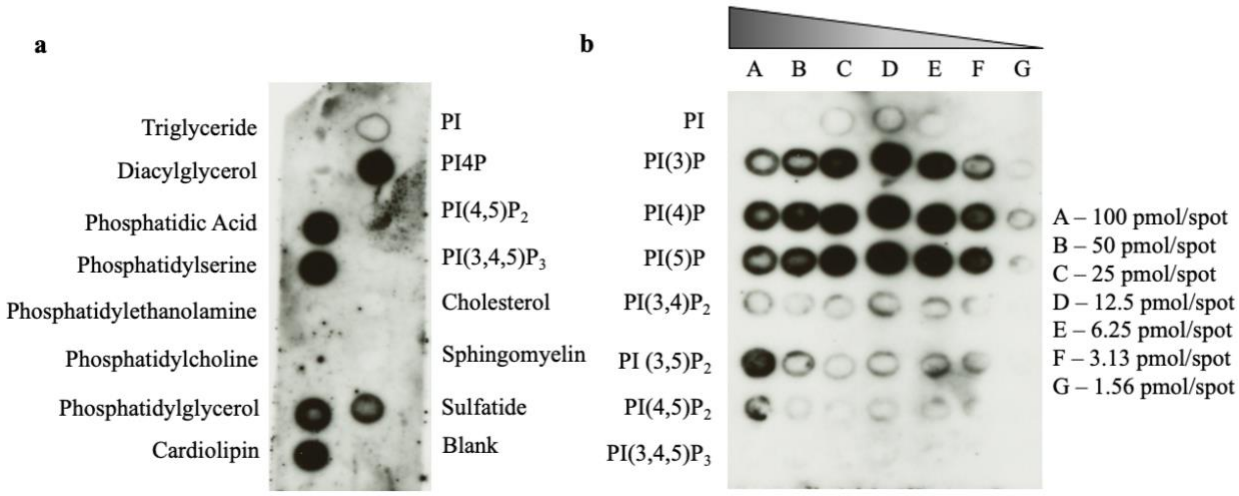

Figure 8: Phospholipid embedded (a) Membrane Lipid Strip and (b) PIP Array were incubated with the sample of recombinant EspD protein. Signal was detected through immunoblot with α-EspD primary antibody.

2. Rationale, Hypothesis, and Objectives

2.1. Rationale

The *M. tb* secreted protein EspD has demonstrated its importance within the mycobacterial cell to facilitate the secretion and maintain the stability of several ESX-1 members (Chen *et al.*, 2012). EspD was also shown to be secreted when all other ESX-1 secretion appears to have been shut down (Chen *et al.*, 2012). This result implies that EspD secretion may be a priority to the bacteria. Therefore, the role of secreted EspD is of interest for investigation. Unpublished work on purified recombinant EspD has demonstrated that the protein may be involved in binding eukaryotic phospholipids. Bacterial effectors capable of binding host-cell phospholipids can disrupt normal microbicidal functions such as phagosomal maturation and autophagy, ultimately contributing to bacterial survival and virulence (Ham *et al.*, 2011; Walpole *et al.*, 2018; Yeung *et al.*, 2009). Using a combination of genetic and biochemical approaches, we seek to understand the role of secreted EspD during *M. tb* infections of macrophages.

2.2. Hypothesis

Secreted EspD interacts with eukaryotic phospholipids and disrupts host-cell processes to potentiate ESX-1 mediated *M. tb* virulence.

2.3. Objectives

To investigate this hypothesis, three main objectives were established:

1. Characterization of *M. tb* strains that express variants of EspD. The construction and characterization of these *M. tb* strains allows us to observe phenotypic differences caused by these point mutations through comparison with *M. tb* expressing wild-type EspD. Strains will be monitored for their relative growth rates, secretion profiles, and cytotoxicity in macrophages.

2. Analysis of the impact of secreted EspD during *M. tb* infections of human macrophages. Macrophages infected with *M. tb* strains that express variants of EspD will be examined for the impact of secreted EspD on cytokine production, inflammatory pathway activation, and phospholipid organization.

3. Purification of recombinant EspD protein from *E. coli* to investigate the structure and function of secreted EspD. Recombinant protein will be evaluated for its ability to form oligomers and bind phospholipids.

3. Materials and Methods

All chemicals were reagent grade and obtained from Sigma-Aldrich (St. Louis, MO) unless otherwise noted. All experiments involving *M. tb* bacteria were performed in a biosafety level (BSL) 3 laboratory. Samples transferred from BSL-3 to BSL-2 were filtered to remove bacteria.

3.1. *M. tb espA*::Tn variant strain construction

3.1.1. pMD*espACD* plasmid collection

Previous lab members cloned the entire *espACD* operon sequence from *M. tb* into the episomal *E.coli*-mycobacteria shuttle vector, pMD31 (sourced from the Liu lab at University of Toronto), containing a kanamycin resistance cassette. This construct was named pMDespACD. Several single point mutations were performed to the *espD* gene region of pMDespACD and the resultant plasmids were inherited for this thesis and are detailed below.

3.1.2. Transformations into *M. tb espA*::Tn

M. tb espA::Tn strain was sourced from the Stewart Cole lab at École polytechnique fédérale de Lausanne (Lausanne, Switzerland). Middlebrook 7H11 Agar Base, Middlebrook oleic acid-albumin-dextrose-catalase (OADC) Growth Supplement, and Middlebrook 7H9 Broth Base were purchased from Becton, Dickinson and Company (Franklin Lakes, NJ) and prepared according to manufacturer's instructions. *M. tb espA*::Tn cultures were grown in Middlebrook 7H9 liquid media to mid-late log phase of growth. Bacteria was pelleted by centrifugation at 3000 x g for 5 min. Supernatants were discarded and the volume was replaced with 10% glycerol to resuspended the bacterial pellet, followed by pelleting at 3000 x g for 5 mins. This was repeated three additional times, decreasing the volume of 10% glycerol solution by half each time. The final pellet was resuspended in $1/10^{th}$ the original volume of culture in 10% glycerol. Competent *M. tb espA*::Tn cells were combined with purified pMD31, pMDespACD, or a mutated pMDespACD plasmid sample in an electroporation cuvette and allowed to incubate at room temperature (RT) for 10 min prior to electroporating at 2.5 kV using the Bio-Rad Gene Pulser Xcell Microbial System. Gene Pulser electroporation cuvettes (0.2 cm gap) were purchased from Bio-Rad Laboratories (Hercules, CA). Cells were added to Middlebrook 7H9 media and allowed

to recover at 37°C with 100 rpm shaking for 24 h. Recovered bacteria was plated on Middlebrook 7H11 agar and allowed to incubate at 37°C until colonies appear.

Table 1: List of all *M. tb espA*::Tn strains transformed with variants of pMD31 or pMDespACD vectors.

Strain name	Variation
M. tb espA::Tn pMD31	Missing the genes that encode for EspA, EspC, and EspD
M. tb espA::Tn pMDespACD^{WT}	Fully complemented, wild-type strain
M. tb espA::Tn pMDespACD^{STOP}	Gene that encodes for EspD has a premature stop codon, resulting in lack of EspD protein
M. tb espA::Tn pMDespACD^{W19R}	Expresses EspD with W19R mutation, EspD^{W19R}
M. tb espA::Tn pMDespACD^{W27R}	Expresses EspD with W27R mutation, EspD^{W27R}
M. tb espA::Tn pMDespACD^{P31A}	Expresses EspD with P31A mutation, EspD^{P31A}
M. tb espA::Tn pMDespACD^{R83A}	Expresses EspD with R83A mutation, EspD^{R83A}
M. tb espA::Tn pMDespACD^{R92A}	Expresses EspD with R92A mutation, EspD^{R92A}
M. tb espA::Tn pMDespACD^{R113A}	Expresses EspD with R113A mutation, EspD^{R113A}
M. tb espA::Tn pMDespACD^{K115A}	Expresses EspD with K115A mutation, EspD^{K115A}
M. tb espA::Tn pMDespACD^{R169A}	Expresses EspD with R169A mutation, EspD^{R169A}

3.2. *M. tb espA*::Tn strain tests

All *M. tb espA*::Tn strains containing pMD vectors (Table 1) were streaked onto Middlebrook 7H11 + 10% Middlebrook OADC + 30 /mL kanamycin selective agar and grown at 37°C for several weeks until colonies form. Single colonies were resuspended in 7H9 complete media (Middlebrook 7H9 + 10% ADC broth + 0.05% Tween-80 + 30 μg/mL kanamycin) and grown for several days to the desired optical density (OD_{600}) at 37°C with 100 rpm shaking. These cultures grown in 7H9 complete media inoculated with colonies from 7H11 agar are hereby called starter cultures.

3.2.1. Growth curves

Starter cultures were shifted into either 7H9 complete media or Sautons media (0.06% glycerol, 4 g/L L-Asparagine, 2 g/L Citric Acid, 0.5 g/L KH_2PO_4, 0.5 g/L $MgSO_4 \cdot 7H_2O$, 0.05 g/L Ammonium iron (III) citrate, 0.1 mL/L $ZnSO_4 \cdot H_2O$, pH 7.4) + 0.05% Tween-80 at a starting OD_{600} of 0.1. Cultures were grown for 48 h intervals at 37°C with 100 rpm shaking undisturbed.

At each interval, OD_{600} was measured after thorough culture resuspension and centrifugation at 300 x g for 2 min. Cultures were diluted in inactivating diluent of phosphate buffered saline (PBS) + 5% formaldehyde + 0.05% Tween-20 to measure the OD_{600} in biological duplicates using SpectraMax i3x with SoftMax Pro version 7.0.3 Data Acquisition and Analysis software. The measure of a blank (media diluted in inactivating diluent) was subtracted from measurements of the diluted cultures. Final values were calculated from averaging duplicates, after adjusting for dilution. Growth curves were compiled over the course of several days and conclusions were made about the relative strain growth across several repeated growth curves.

3.2.2. Culture filtrate and cell lysate analysis

7H9 starter cultures were prepared as previously stated and grown to mid-late log phase of growth. Starter cultures were inoculated into Sautons + 0.05% Tween-20 to an OD_{600} of 0.1 and grown at 37°C with 100 rpm shaking until cultures reached an OD_{600} of 0.6-0.8. Sautons + 0.05% Tween-20 cultures were measured for their OD_{600} values. The volumes necessary to inoculate new cultures at a starting OD_{600} of 0.3 were centrifuged at 3500 x g for 15 mins. Supernatants were discarded and the pellets were resuspended gently in fresh Sautons alone. Sautons cultures were grown in non-treated plug-seal tissue culture flasks at 37°C with 100 rpm shaking for 3 days. Cultures were then centrifuged at 3500 x g for 15 mins. Supernatants were filtered through 0.45 um and 0.2 um filters and transferred from BSL-3 to BSL-2. These samples are hereby called culture filtrates. Culture filtrates were concentrated using 5 kDa molecular weight cut off (MWCO) Sartorius Vivaspin 20 Centrifugal Concentrators (Sigma).

Cell pellets were resuspended in ice-cold PBS containing cOmplete, ethylenediamine-tetraacetic acid (EDTA)-Free Protease Inhibitor. Cells were lysed using a Mini-Beadbeater-24 with 0.25 g of Zirconia beads for each mL of cell pellet resuspension. Zirconia beads (0.1 mm) were sourced from BioSpec Products (Bartlesville, OK). Bead beating was performed at 1 min intervals of beating followed by 1 min rest on ice, repeated 7-8 times. Cell lysates were filtered through 0.45 um and 0.2 um filters and transferred from BSL-3 to BSL-2. Protein concentrations of all culture filtrates and cell lysates were determined using Pierce Bicinchoninic Acid (BCA) Protein Assay Kit (Thermo) according to manufacturer's instructions. Samples were analyzed through Western blotting using α-EspD, α-EsxA, α-GroEL2, and α-Antigen 85 (Ag85) primary antibodies for all samples.

3.3. *M. tb* THP-1 infections

3.3.1. Bacterial culture preparation

7H9 starter cultures were grown to late log phase of growth as previously described. 24 h before *M. tb* infections of THP-1 cells were performed, starter cultures were resuspended and centrifuged at 300 x g for 2 min. The OD_{600} of the starter cultures was measured as described for growth curves. OD_{600} values were used to calculate the necessary volume of culture required to inoculate fresh 7H9 media at a starting OD_{600} of 0.1 to create the working culture. Working cultures were incubated at 37°C with 100 rpm shaking until the following day when infections were performed.

3.3.2. THP-1 seeding and differentiation

THP-1 human monocyte cell line was purchased from American Type Culture Collection (ATCC) (Manassas, VA). THP-1 cells were revived from $3x10^6$ cells/stocks in liquid nitrogen through rapid thawing and addition to Roswell Park Memorial Institute Medium (RPMI) 1640 media + 10% previously heat-denatured fetal bovine serum (FBS). Cells were allowed to expand at 37°C + 5% CO_2. Media was added to the THP-1 cultures as needed to maintain cell density between $3x10^5$ cells/mL – $8x10^5$ cells/mL. Once an appropriate volume of cells was achieved, THP-1s were centrifuged at 125 x g until pelleted and resuspended in RPMI + 10% FBS + 100 ng/mL phorbol 12-myristate-13-acetate (PMA). Cells were immediately seeded at concentrations respective of the plate format used (Table 2). 24-well plates were seeded with $2x10^5$ cells/well and 48-well plates were seeded with $1x10^5$ cells/well. Cells were incubated at 37°C + 5% CO_2 for 3 days in media containing PMA, with differentiation monitored through microscopy daily. After 72 h, media containing PMA was replaced with RPMI + 10% FBS to allow cells to recover for 48 h at 37°C + 5% CO_2 before infections were performed.

Table 2: Seeding density values for THP-1 cell infections in 24-well and 48-well plates.

Cell number	Well volume	Plate format
$1x10^5$ cells/mL	2 mL	24-well plate
$1x10^5$ cells/mL	1 mL	48-well plate

3.3.3. Performing infections

The OD_{600} of the *M. tb* working cultures were measured as previously described for growth curves. The volume of *M. tb* culture needed for the appropriate multiplicity of infection (MOI) was calculated according to Formula 1. This volume was then prepared in the necessary volume of RPMI + 10% FBS to make infection solutions.

$$\frac{(\text{volume of infection solution})(\text{MOI})\left(\text{number of THP-1}\,\frac{\text{cells}}{\text{well}}\right)}{(\text{OD}_{600}\text{ of } M.\ tb \text{ working culture})\left(3\text{x}10^{8}\,\frac{\text{cfu}}{\text{mL}}\right)} = \text{volume of } M.\ tb \text{ working culture needed in infection solution (mLs)}$$

Formula 1: Calculation to determine the volume of *M. tb* culture needed to be added to the infection solution.

Infections performed for the production of cytokines were executed in a 24-well plate format with $2x10^5$ THP-1 cells/well at an MOI of 10 for 24 h. Media on THP-1 cells was replaced with the prepared infection solutions and cells were allowed to incubate at 37°C + 5% CO_2. After 24 h, supernatants from each well were saved and cells were lysed in radioimmunoprecipitation (RIPA) buffer (0.05 M Tris pH 8.0, 0.15 M NaCl, 0.1% SDS, 1% NP-40, 1% Deoxycholic acid) for 10 min at 37°C. Lysate samples were then physically disrupted and individually passed through 0.2 um filters and transferred from BSL-3 to BSL-2 for analysis through Western blotting.

Infections performed for cytotoxicity tests were performed in a 48-well plate format with $1x10^5$ THP-1 cells/well at an MOI of 5 for 3 days. Infection solutions were prepared by diluting the required volume of *M. tb* working cultures in RPMI media + 10% FBS. Media on the THP-1 cells was replaced with the infection solutions and cells were allowed to incubate at 37°C + 5% CO_2. After 3 days, cytotoxicity was measured through PrestoBlue or Lactate Dehydrogenase (LDH) Assay analysis.

3.4. Cytotoxicity assays

3.4.1. PrestoBlue

Cell viability was measured through the addition of PrestoBlue Cell Viability Reagent (Thermo). This resazurin-based solution is converted into a fluorescent product by the reducing power of viable cells. The relative fluorescence output can be quantified and compared between infected and uninfected groups of cells. These measurements can then be converted into values

of percent cytotoxicity. PrestoBlue was diluted 1:10 in RPMI media + 10% FBS and allowed to incubate with cells for 15 min at 37°C. Fluorescence was read using a SpectraMax i3x with SoftMax Pro version 7.0.3 Data Acquisition and Analysis software (excitation at 560 nm and emission at 590 nm). The value for each well was calculated from the average of nine measurements from different areas within the well. The mean of all well values in each replicate group was then calculated and represents the average relative fluorescence units (RFUs) emitted for each treatment group. To calculate percent relative cytotoxicity, RFUs of the treatment group were compared to the RFUs of the uninfected group according to Formula 2. All statistical analysis was performed using GraphPad Prism Version 8.4.3.

$$\frac{\text{Uninfected - Treatment}}{\text{Uninfected}} \text{ x } 100\% \ = \ \% \text{ Relative Cytotoxicity}$$

Formula 2: Percent relative cytotoxicity from mean relative fluorescence units.

3.4.2. LDH

LDH is a cytosolic enzyme released from cells when the plasma membrane is damaged. To perform the LDH Assay, the CyQUANT LDH Cytotoxicity Assay Kit (Thermo) was used. A set of uninfected cells were lysed according to the manufacturer's instructions prior to transferring the infection supernatants to a clean 48-well plate. LDH assay was performed, and measurements were acquired with the SpectraMax i3x with SoftMax Pro version 7.0.3 Data Acquisition and Analysis software. A single independent experiment was performed and graphed using GraphPad without statistical analyses.

3.5. ELISA

Enzyme-linked immunosorbent assays (ELISA) were performed to detect IL1β and TNFα using the kits: Human IL-1 beta Uncoated ELISA and Human TNF alpha Uncoated ELISA (Thermo). ELISAs were performed according to manufacturer's instructions. Samples were prepared neat and in several dilutions (1:2 through 1:40, as necessary) for evaluation. Samples were incubated in the IL1β ELISA plates for 3 h at RT or incubated in the TNFα ELISA plates for 2 h at RT. All incubation steps for the TNFα ELISAs were performed with 500 rpm shaking. Multi-well plates were read at 450 nm and 570 nm (background) using a the SpectraMax i3x with

SoftMax Pro version 7.0.3 Data Acquisition and Analysis software. Statistical analysis was performed with GraphPad Prism Version 8.4.3.

3.6. Western blotting

Samples were prepared with Nu-Polyacrylamide gel electrophoresis (PAGE) lithium dodecyl sulfate (LDS) buffer (Thermo) (1x final concentration with 2% beta-mercaptoethanol) and boiled for 10 min prior to being electrophoresed using NuPAGE 4-12%, Bis-Tris, 1.5 mm, protein gels (Thermo). Samples were electrophoresed at 200 V for 25 min. BLUelf Prestained Protein Ladder (3.5 kDa to 250 kDa) was purchased from FroggaBio Inc. (Concord, ON) and was used on each blot to track the mass of proteins in the sample. Protein was transferred to nitrocellulose membranes using the iBlot 2 Dry Blotting System (Thermo) according to manufacturer's instructions. Membranes were blocked with 3% bovine serum albumin (BSA) in Tris-buffered saline + 0.05% Tween-20 (TBST) for 1 h at RT with gentle shaking. Primary antibodies were prepared in TBST + 1% BSA with the dilutions defined in Table 3 and incubated with membranes overnight at 4°C with gentle shaking. Appropriate fluorescent secondary antibodies were prepared at 1:10,000 dilutions in TBST + 1% BSA and incubated with membranes for 1 h at RT to allow for visualization on Li-Cor Odyssey CLx using Image Studio Version 5.2 software.

Table 3: Primary antibodies were prepared in TBST + 1% BSA at the listed dilutions for Western blotting analysis. Fluorescent secondary antibodies against the appropriate animal source of the primary antibody were then used for imaging.

Primary Antibody	Dilution used	Animal Source
α-NLRP3	1:1000	Rabbit
α-cleaved caspase-1	1:1000	Rabbit
α-NF-κB	1:1000	Mouse
α-pNF-κB	1:1000	Rabbit
α-β-actin	1:1000	Mouse
α-EspD	1:200	Rat
α-EsxA	1:1000	Mouse
α-Ag85	1:3000	Rabbit
α-GroEL2	1:1000	Mouse

Antibodies against NLRP3, cleaved caspase-1, total nuclear factor kappa-light-chain-enhancer of activated B cells (NF-κB), and phosphophorylated NF-κB (pNF-κB) were purchased

from Cell Signaling Technology (Danvers, MA). Antibody against β-actin was purchased from Abcam (Cambridge, UK).

3.7. Recombinant EspD production

3.7.1. Expression in *E. coli*

The gene for EspD was encoded on pET28a vector with an N-terminal 6xHis-tag containing a kanamycin resistance cassette. This vector was named pJMC19 and was transformed into BL21(DE3) pLysS competent *E. coli* cells purchased from Agilent Technologies (Santa Clara, CA) through heat shock for 45 sec at 42°C and recovered in Luria Broth (LB) for 1 h at 37°C before plating on LB agar and incubating overnight at 37°C. Recovered transformant colonies were inoculated into 10 mL of LB media and grown at 37°C overnight. Overnight cultures were added to 1 L of broth to a starting OD of 0.1 and grown at 37°C with 200 rpm shaking until reaching an OD of 0.5 at which point vector protein expression was induced using 100 mM Isopropyl β-d-1-thiogalacto-pyranoside (IPTG) (final concentration). Induction was allowed to proceed for 18 h at 16°C with 200 rpm shaking.

3.7.2. EspD protein purification under denaturing conditions

Three liters of induced *E. coli* pJMC19 culture were combined and cells were pelleted at 10,000 x g for 30 min. Cell pellets were resuspended in lysis/equilibrium/wash (LEW) buffer (50 mM NaH_2PO_4, 300 mM NaCl, pH 8.0) and lysed using an Avestin french press achieving 15,000 psi for two full passages. Lysate was clarified at 10,000 x g for 30 min and inclusion bodies were collected and solubilized in Denaturing Buffer (8M Urea, 50 mM NaH_2PO_4, 300 mM NaCl, pH 8.0). Sample was added to Macherey-Nagel Protino Nickel-iminodiacetic acid (Ni-IDA) dry silica resin purchased from D-Mark Biosciences (Toronto, ON) in a gravity column. Resin with bound protein was washed with a series of Denaturing Buffers containing low concentrations (10 mM, 20 mM, and 30 mM) of imidazole (IM). Protein was eluted with Denaturing Buffer + 300 mM IM. LDS-PAGE electrophoresis was performed on samples taken over the course of the column purification. Elution samples determined to contain the most EspD protein were combined and promoted to refold through stepwise dialysis, slowing removing urea over 6-8 full buffer exchanges. Purified EspD samples prepared in this manner with all denaturing agents removed are hereby called refolded EspD. Protein samples were then concentrated with 30 kDa

MWCO Sartorius Vivaspin 20 Centrifugal Concentrators (Sigma) at 1000 x g. Final protein concentration was then determined with the Pierce BCA Protein Assay Kit (Thermo) according to manufacturer's instructions.

3.8. Recombinant EspD assays

3.8.1. Native PAGE

Native PAGE analysis of purified EspD protein is performed for varying concentrations (5 μg, 2.5 μg, and 1.25 μg per well) of protein. Samples were prepared in 1x final concentration NativePAGE Sample Buffer (Thermo). Electrophoresis was performed at 150 V for 90 min using the NativePAGE Novex Bis-Tris Gels (Thermo) with NativeMark Unstained Protein Standard (Thermo). Protein was transferred to nitrocellulose membranes as described above and Western blotting was performed with α-EspD primary antibody.

3.8.2. TEM

Purified EspD protein was diluted to a 1000 nM concentration in LEW buffer. 400 mesh Formvar/Carbon coated copper grids were glow discharged with Quorum Q150T ES. Protein samples were absorbed to the grid for 1 min, washed with water, and stained with 2% Uranyl Acetate for 1 min. The preparation was dried prior to imaging at 50k magnification using the Hitachi HT7700 microscope. TEM was performed at the Western College of Veterinary Medicine Imaging Centre.

3.8.3. PIP strips and arrays

PIP strips and PIP Arrays were purchased from Echelon Biosciences (Salt Lake City, UT). PIP Strip or PIP Array membranes were blocked in PBS + 0.01% Tween-20 (PBST) + 3% BSA for 1 h at RT with gentle shaking prior to incubation with purified EspD protein of interest at a concentration of 0.5 μg/mL in PBST + 3% BSA for 1 h at RT with shaking. Protein sample is removed, and membranes were washed with PBST alone followed by incubation with 1:200 α-EspD primary antibody in PBST + 3% BSA overnight at 4°C with gentle shaking. Membranes were washed with PBST and incubated with 1:10,000 α-rat secondary antibody diluted in PBST + 3% BSA for 1 hr at RT with shaking. Detection was performed using the Li-Cor Odyssey CLx using Image Studio Version 5.2 software.

3.8.4. Phospholipid-coated bead pull-downs

50 µL slurries of each Lipid Coated Bead (Echelon) type, including PI3P, PI4P, PI5P, PA, PS, and control beads, were incubated with either 5 µg of purified EspD or 30 µg of culture filtrate/cell lysate sample. Beads were incubated with the protein sample overnight at 4°C while rotating. Mixtures were centrifuged at 800 x g and supernatants were removed. Beads were washed with 5 x sample volume of wash buffer (10 mM HEPES pH 7.4, 150 mM NaCl, 0.25% Igepal) and centrifuged at 800 x g prior to removal of the supernatant. Wash steps were repeated 4-5 times. Protein was eluted off the beads through the addition of LDS sample buffer and boiling. Western blotting using α-EspD antibody was performed as previously described.

3.9. Phospholipid biosensors

3.9.1. Maintaining COS-7 cells

COS-7 fibroblast-like monkey kidney cells (ATCC) were rapidly thawed from liquid nitrogen and resuspended in complete Dulbecco's Modified Eagle Medium (DMEM) (DMEM + 10% FBS, 1mM sodium pyruvate, 0.05 mg/mL gentamycin) and maintained in a treated tissue culture flask incubated at 37°C + 5% CO_2. Cells were kept between 30-90% confluency and lifted with Trypsinization. Media was removed and cells were washed with PBS prior to the addition of trypsin for 3-5 min at 37°C to dissociate adherent cells from the flask. Complete DMEM was then added to neutralize the trypsin and cells were pelleted at 800 rpm for 8 min. Cells were resuspended in complete DMEM and counted on a hemocytometer using a trypan blue exclusion method with dilutions in 0.4% trypan blue dye. To expand, the appropriate volume of cells was aliquoted into a new flask with fresh complete DMEM and returned to 37°C + 5% CO_2 incubation. For transfections, the volume of cells needed to seed $2.5x10^5$ cells was resuspended in 2 mLs of complete DMEM in a 35 mm petri dish containing a non-treated coverslip. Cells were allowed to settle for 15 min and then were incubated overnight at 37°C + 5 % CO_2.

3.9.2. Maintaining RAW 264.7 cells

RAW 264.7 murine macrophage cells (ATCC) were rapidly thawed from liquid nitrogen and resuspended in complete DMEM. Cells were incubated at 37°C + 5% CO_2 in a treated tissue culture flask and maintained below 90% confluency. To count, cells were lifted with the addition of versene (0.5 mM $EDTA.Na_2.2H_2O$, 140 mM NaCl, 2.5 mM KCl, 9.5 mM Na_2HPO_4 1.5 mM

KH_2PO_4, 1 mM $C_6H_{12}O_6$) and mixing before pelleting at 1200 x g for 5 min. Cells were resuspended in complete DMEM and counted using the trypan blue exclusion method on a hemocytometer with dilutions in 0.4% trypan blue dye. An appropriate volume of cells was returned to a treated tissue culture flask for expansion and incubated 37°C + 5% CO_2. For transfections, the volume of cells needed to seed $2.5x10^5$ cells was resuspended in 2 mLs of complete DMEM in a 35 mm petri dish containing a non-treated coverslip. Cells were allowed to settle for 15 min and then were incubated overnight at 37°C + 5 % CO_2.

3.9.3. Preparation of plasmids for transfection

A library of fluorescent biosensors was established by sourcing previously constructed biosensor plasmids. Fluorescent biosensor plasmids pGFP-LactC2, pEGFP-2FYVE, and pGFP-P4M were sourced from the Sergio Grinstein Lab at University of Toronto (Toronto, Canada), pGFP-PHDx3 was sourced from the Bernard Payrastre Lab at the French National Insitute of Health and Medical Research (Touloum, France) and pRFP-CDH, pGFP-CDH, pMRFP, and pMGFP were sourced from the Guangwei Du Lab at University of Texas (Houston, TX). Plasmids were transformed into *E. coli* Top10 competent cells by heat shock method described above. Successful transformants were then used to inoculate LB liquid media and grown overnight at 37°C with 200 rpm shaking. Liquid cultures were processed with the EndoFree Plasmid Maxi Kit according to the manufacturer's instructions to purify large amounts of each plasmid. The EndoFree Plasmid Maxi Kit was purchased from Bio Basic (Markham, ON).

3.9.4. Transfections

To prepare for transfection, 2.0 μg of biosensor plasmid DNA of interest was diluted in Opti-MEM (Thermo) (2 μg/200 μL final concentration). This mixture was further added dropwise to a lipofectamine 2000 (Thermo) suspension in Opti-MEM (6 μg /200 μL) ensuring the DNA:lipofectamine ratio is 1:3-1:6. Solution was mixed gently and incubated at RT for 10 min. Media was aspirated and COS-7 or RAW 264.7 cells were washed with PBS followed by Opti-MEM. Equal volumes of Opti-MEM and the DNA-lipofectamine mixture were added and the cells were allowed to incubate for 4 h at 37°C + 5% CO_2. The transfection mixture was then removed and replaced with DMEM complete (without antibiotics) and cells were allowed to incubate for 16 h at 37°C + 5% CO_2. Samples used for live imaging were then taken for confocal

imaging. Samples used to prepare fixed slides proceed through fixation protocol prior to imaging.

3.9.5. Fixed Slide Preparation

The fixation process was performed at RT, shielded from light. DMEM was removed and cells were washed with PBS. The coverslip was then allowed to soak for 2 min intervals in fresh PBS, repeating the soak 3 times with fresh PBS. The coverslip was then soaked in 4% Paraformaldehyde in PBS for 15 min prior to washing with PBS and quenching in 0.1 M glycine in PBS for 5 min. The coverslip was finally washed in PBS and excess liquid was drained before mounting to a glass slide with ProLong Gold Antifade mounting media (Thermo). The slide was then cured for 24 h in the dark.

3.9.6. Confocal imaging

Slides or live cells were imaged using the Leica TCS SP8 confocal microscope using Leica Application Suite X software version 3.4.2.18368. Magnification was achieved using 63x oil objective with a numerical aperture of 1.40.

4. Results

4.1. Mycobacterial EspD sequence alignment

Analysis of the protein sequence of EspD did not indicate the presence of any known functional domains and did not demonstrate sequence homology to any well characterized proteins. Therefore, sequences of EspD from several mycobacterial species were aligned to determine which residues are highly conserved (Figure 9). Residues exhibiting a high degree of conservation can indicate importance for protein structure and function as mutations to these residues are accepted less frequently than mutations in other residue positions (Capra and Singh, 2007). CLUSTAL sequence alignment was performed using protein sequences of EspD from *M. tb*, BCG, *M. bovis*, *M. leprae*, and *M. marinum* (Figure 9).

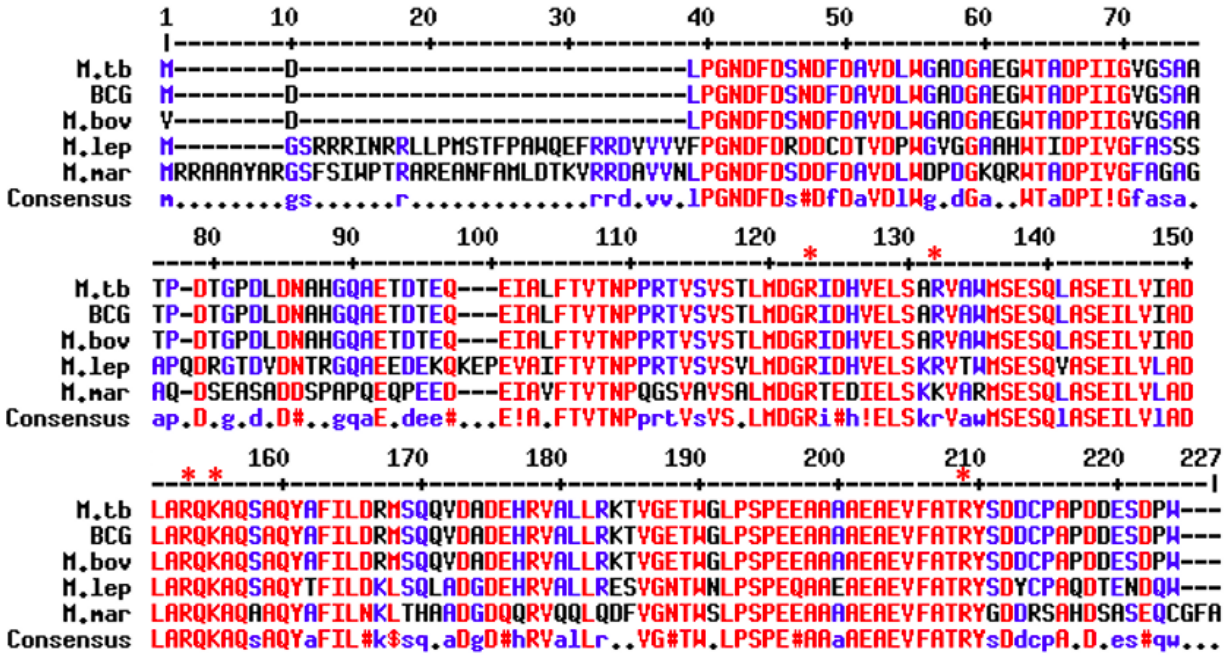

Figure 9: CLUSTAL omega multiple sequence alignment of EspD protein sequences from several Mycobacterial species using EMBL-EBI. Residues in red indicate a high level of conservation. Residues in blue indicate conservation to a lesser degree. Residues in black are not considered conserved. Red asterisks indicate residues targeted for mutation in this thesis.

Unpublished work on EspD indicated that the protein may be capable of binding eukaryotic phospholipids in a specific manner (Figure 8). To target residues of EspD that may be involved in phospholipid binding, basic residues from highly conserved regions of the protein were selected for mutation. The positively charged side chains of these residues could interact with the negative head group of the phospholipid molecules to facilitate binding. Five residues

on EspD were targeted, indicated by the red asterisks on Figure 9. Specifically, the Arginines at positions 83, 92, 113, and 169 as well as the Lysine at position 115 were all mutated into Alanine residues. These mutations were performed on the *espD* gene of the pMDespACD vector. The resultant plasmids were transformed into the *M. tb* Erdman *espA*::Tn strain to investigate the impact of these mutations in *M. tb*.

4.2. Characterization of *M. tb espA*::Tn strains expressing variant EspD proteins

EspD's function within the mycobacterial cell has previously been identified (Chen *et al.*, 2012). This work established several strains of *M. tb* expressing EspD with single point mutations. Some of these strains were chosen for further characterization here, specifically *M. tb espA*::Tn pMDespACD^{W19R}, *M. tb espA*::Tn pMDespACD^{W27R}, and *M. tb espA*::Tn pMDespACD^{P31A}. Additionally, the control strains *M. tb espA*::Tn pMD31, *M. tb espA*::Tn pMDespACD^{WT}, and *M. tb espA*::Tn pMDespACD^{STOP} were included. These strains were analyzed alongside the newly constructed strains expressing EspD with mutations on conserved basic residues. Together, all *M. tb* strains were analyzed for differences in growth rates and secretion profiles.

4.2.1. *M. tb* strains expressing variants of EspD demonstrate similar growth rates

Using *M. tb* strains expressing variant EspD proteins, several independent growth curves were performed in both complete and minimal media types to screen for any differences in growth. Figure 10 demonstrates a single independent growth curve from each media type, complete 7H9 media (Figure 10a) and Sautons minimal media (Figure 10b). Across all independent growth curves, there were no strains that consistently grew slower or faster than others. Additional growth curves (data not shown) demonstrated a similar spread of OD_{600} values due to unavoidable differences in culture preparations and OD_{600} measurements of the slow growing mycobacteria. Therefore, there appeared to be no differences in growth between these *M. tb* strains expressing variant EspD proteins.

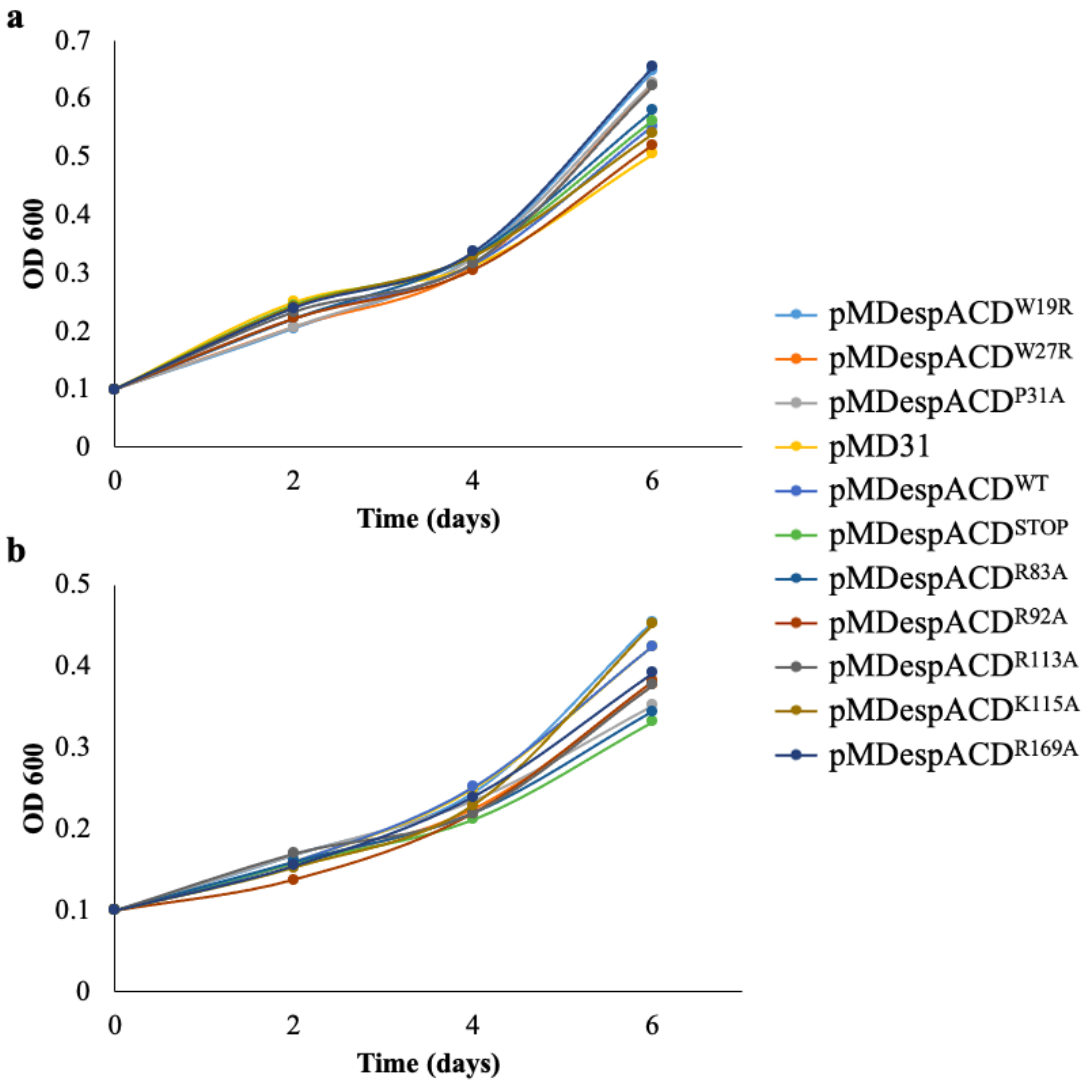

Figure 10: Growth curve analysis of *M. tb espA*::Tn strains in (a) 7H9 complete media and (b) Sautons minimal media.

4.2.2. *M. tb* strains expressing variants of EspD secrete EsxA at wild-type levels

Secretion profile analyses were performed on *M. tb espA*::Tn strains expressing variant EspD proteins to monitor the impact of point mutations of EspD on ESX-1 associated secretion. EsxA and EspD were monitored specifically, as well as control proteins Ag85 and GroEL2. Secretion of EsxA indicates that the mutation present does not appear to affect the secretion of other ESX-1 members. As Ag85 is secreted from *M. tb* through a non-ESX-1 system it should be constitutively present in all samples, while GroEL2 is a cell-associated protein and should only be visualized if cells were lysed. The culture filtrate (CF) represents which proteins are

successfully being secreted, while the cell lysate (CL) represents which proteins are being expressed and remain stable within the *M. tb* cell.

Results obtained in these experiments confirmed results of previously published data (Chen *et al.*, 2012). When EspD was not expressed, as with *M. tb espA*::Tn pMDespACD^{STOP} and *M. tb espA*::Tn pMD31, EsxA was not secreted and stayed trapped within the cell (Figure 11b). Analyses of *M. tb espA*::Tn pMDespACD^{W19R}, *M. tb espA*::Tn pMDespACD^{W27R}, and *M. tb espA*::Tn pMDespACD^{P31A} were also performed. It was confirmed that these three strains were able to secrete EsxA (Figure 11a). Additionally, it was confirmed that *M. tb espA*::Tn pMDespACD^{P31A} was secreting EspD^{P31A} similarly to the *M. tb espA*::Tn pMDespACD^{WT} strain, *M. tb espA*::Tn pMDespACD^{W27R} has reduced ability to secrete EspD^{W27R}, and *M. tb espA*::Tn pMDespACD^{W19R} was unable to secrete EspD^{W19R} (Figure 11a). This work confirms that the *M. tb espA*::Tn pMDespACD^{W19R} strain can be utilized as a negative control for EspD secretion as it appears to lack EspD secretion alone without disrupting the secretion of other ESX-1 members. The newly constructed strains, *M. tb espA*::Tn pMDespACD^{R83A}, *M. tb espA*::Tn pMDespACD^{R92A}, *M. tb espA*::Tn pMDespACD^{R113A}, *M. tb espA*::Tn pMDespACD^{K115A}, and *M. tb espA*::Tn pMDespACD^{R169A} were all capable of secreting both EsxA and EspD mutants (Figure 11a). *M. tb espA*::Tn pMDespACD^{R92A} was consistently found to be most comparable to the wild-type strain, *M. tb espA*::Tn pMDespACD^{WT}.

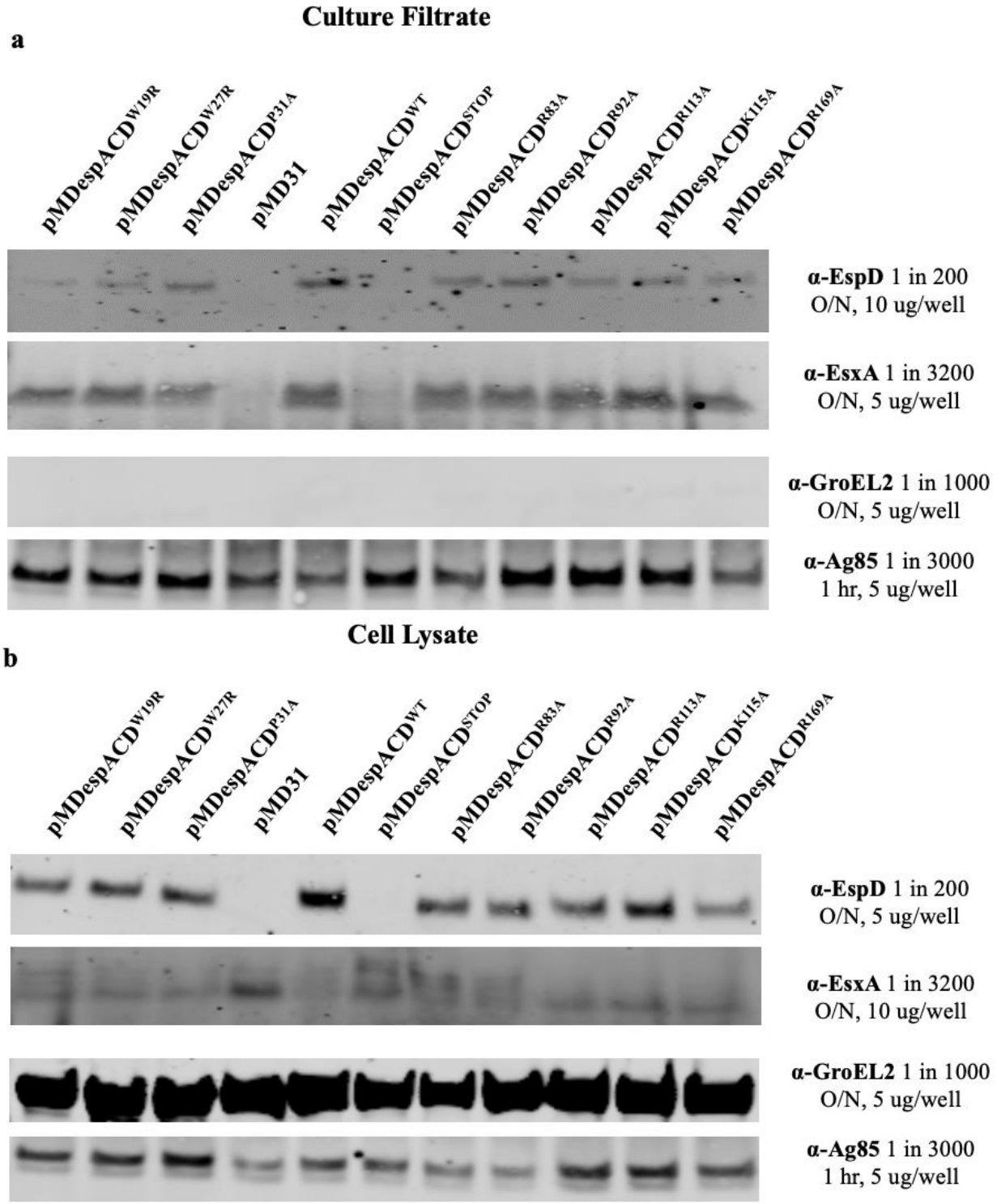

Figure 11: Western blotting analysis of (a) culture filtrates and (b) cell lysates from *M. tb espA::*Tn strains expressing variants of EspD using the indicated primary antibodies. Detection was performed using fluorescent secondary antibodies and visualized with the Li-Cor Odyssey CLx.

4.3. Cytotoxicity in THP-1 human macrophage cells

To monitor the impact of secreted EspD, several of these *M. tb* strains with varying secretion profiles were chosen for cytotoxicity experiments. Comparing these mutant strains for their ability to cause cell death during an infection determined whether these mutations led to a decrease in virulence. *M. tb espA*::Tn pMDespACD^{W19R} was observed to cause a reduction in bacterial load compared to *M. tb espA*::Tn pMDespACD^{WT} in the lungs and spleen of infected mice (Figure 6). This indicated that the *M. tb espA*::Tn pMDespACD^{W19R} strain, lacking in EspD secretion alone, may be less virulent. To investigate this, a methodology was developed for working with human THP-1 cells. These monocytic cells were differentiated into macrophages and were infected with *M. tb espA*::Tn pMD31, *M. tb espA*::Tn pMDespACD^{WT}, *M. tb espA*::Tn pMDespACD^{STOP}, *M. tb espA*::Tn pMDespACD^{W19R}, or *M. tb espA*::Tn pMDespACD^{R92A} and measured for their ability to cause cell death.

4.3.1. Establishment of conditions for effective THP-1 preparation for infections

To understand the impact of *M. tb* during early human infection, it is necessary to establish a relevant human macrophage cell line for in vitro experiments. THP-1 cells are human monocytes that can be terminally differentiated into macrophages with the use of a stimulant, PMA. Cells were treated with PMA and then allowed time to recover in media without PMA to establish differentiation into macrophages prior to infection. A methodology was developed here that established consistent results while working with THP-1 cells. To determine these parameters, several tests were performed establishing the appropriate cell density of THP-1s in the necessary plate format, the concentration of PMA required for differentiation, and the length of recovery time necessary prior to infection.

Initial tests began with a previously used method, $1x10^6$ THP-1 cells/well in a 24-well plate format or $5x10^5$ THP-1 cells/well in a 48-well plate format with exposure to 5 ng/mL PMA for three days followed by five additional days of recovery in media free of PMA. The desired phenotype of adherent, terminally differentiated cells was not observed. Cells appeared to remain as monocytes and were crowded and stacked on top of one another (data not shown). Effectively differentiated cells should demonstrate a mound-like appearance, losing the refractive edges expected of non-adherent monocytes and having space to adhere to the plate and expand as they

become macrophage-like. Therefore, cell number was ultimately lowered to $2x10^5$ THP-1 cells/well in 24-well plates and $1x10^5$ THP-1 cells/well in 48-well plates to avoid crowding.

Further tests were performed to determine an appropriate concentration of PMA by treating THP-1 cells with incrementally higher concentrations of PMA for a three-day period. A macrophage-like phenotype began to appear in several cells around 20 ng/mL PMA (Figure 12a), however the majority of cells appeared differentiated at a concentration of 80 ng/mL PMA (Figure 12b). At 100 ng/mL PMA (Figure 12c), THP-1 cells demonstrated the desired phenotype and ultimately showed less stacking during the recovery days following removal of PMA. The length of exposure to PMA was consistently kept at three days, as work done by other members of the lab demonstrated shorter time periods at similar concentrations were less effective.

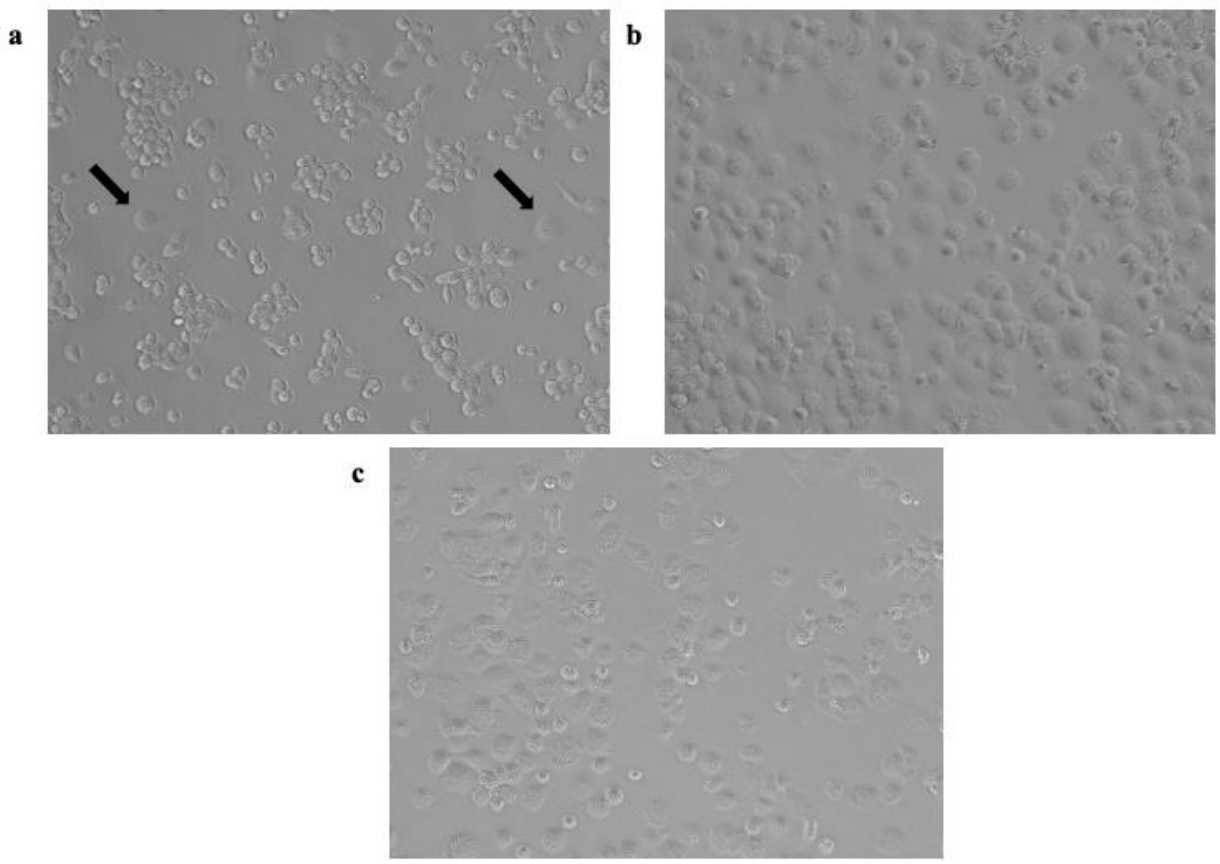

Figure 12: Seeded THP-1 cells after three-day exposure to variable concentrations of PMA: (a) 20 ng/mL, (b) 80 ng/mL, (c) 100 ng/mL. Cells were seeded at a density of $2x10^5$ cells/well in a 24-well plate format and imaged under 10x magnification. Arrows in (a) indicate THP-1 cells that appear differentiated after 20 ng/mL PMA treatment.

Lastly, an appropriate length of time for THP-1 recovery was determined. Throughout these tests, it was found that the overall age of the THP-1 cells contributed to how consistently the cells responded during infection experiments. Older THP-1 cells (>28 days since revival) were more likely to respond inconsistently to PMA treatment and therefore working with the cells within this timeline was kept a priority while determining the length of the recovery period. After treatment with 100 ng/mL PMA for three days, the majority of THP-1 cells displayed the desired phenotype. The previously used recovery time of five days led to cells stacking after remaining monocytes continued replicating (Figure 13a). Shortening the recovery time to two days, allowed the majority of THP-1 cells to remain in the desired phenotype (Figure 13b). This timeframe for recovery avoided expansion of any undifferentiated cells and also ensured that the THP-1s were infected prior to reaching 28-day post-revival age.

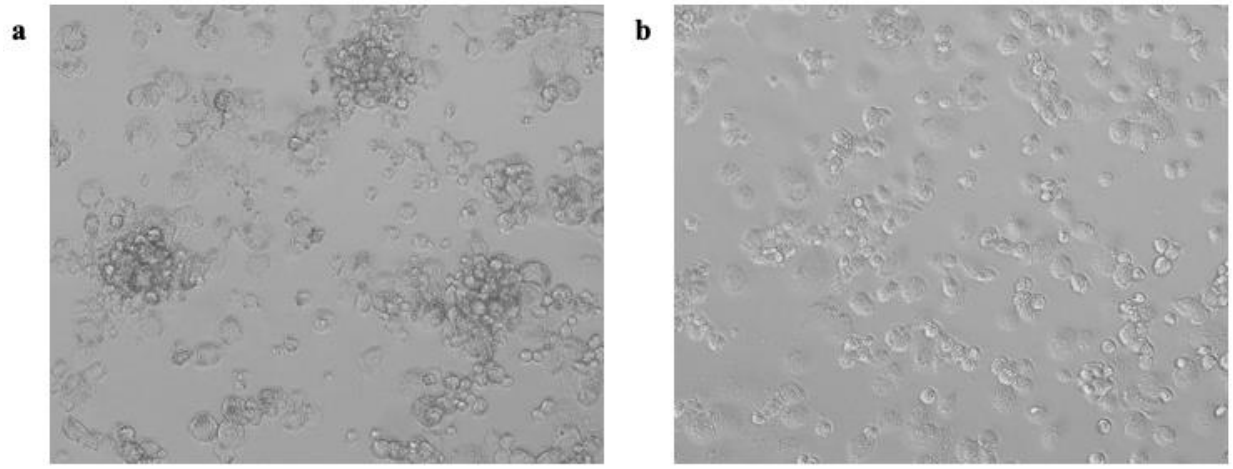

Figure 13: THP-1 cells differentiated with 100 ng/mL of PMA and allowed to recover in media without PMA for (a) five days and (b) two days. Cells were seeded at a density of $2x10^5$ cells/well in a 24-well plate format and imaged under 10x magnification.

4.3.2. PrestoBlue analysis reveals a consistent trend of reduced cytotoxicity with *M. tb espA*::Tn pMD*espACD*^{W19R} compared to *M. tb espA*::Tn pMD*espACD*^{WT}

THP-1 cells were infected with selected *M. tb* strains to examine their cytotoxic effect. Preliminary infection experiments were performed at varying MOIs (0.2, 1, 5, and 10) and in varying multi-well plate formats before confirming the final conditions used for these experiments. To characterize strains for their cytotoxic ability, infections were performed in 48-well plate formats at $1x10^5$ THP-1 cells/well at an MOI of 5 for 72 h. Using *M. tb espA*::Tn pMD31, *M. tb espA*::Tn pMDespACD^{WT}, *M. tb espA*::Tn pMDespACD^{STOP}, *M. tb espA*::Tn

pMDespACD^{W19R}, and *M. tb espA*::Tn pMDespACD^{R92A} cytotoxicity experiments were performed primarily by measuring cell viability using PrestoBlue reagent. This resazurin-based solution is converted into a fluorescent product by the reducing power of viable cells. The relative fluorescence output was quantified and compared between infected and uninfected groups of cells. These measurements were then converted into values of percent cytotoxicity.

The least cytotoxic strain was the strain missing the entire *espACD* operon, *M. tb espA*::Tn pMD31 (Figure 14). The highest level of cytotoxicity was exhibited by *M. tb espA*::Tn pMD-espACD^{WT} (Figure 14). *M. tb espA*::Tn pMDespACD^{STOP}, *M. tb espA*::Tn pMDespACD^{W19R}, and *M. tb espA*::Tn pMDespACD^{R92A} appeared less cytotoxic than *M. tb espA*::Tn pMDespACD^{WT} (Figure 14). The lower cytotoxicity observed with the *M. tb espA*::Tn pMDespACD^{W19R}, which unlike *M. tb espA*::Tn pMDespACD^{STOP} can secrete EspA, EspC, EsxA, and EsxB and is only missing EspD secretion, was observed repeatedly (Figure 14). Statistical analyses demonstrated no significant differences between *M. tb espA*::Tn pMDespACD^{W19R} and *M. tb espA*::Tn pMD-espACD^{WT}, however this phenotype remained consistent across three independent experiments.

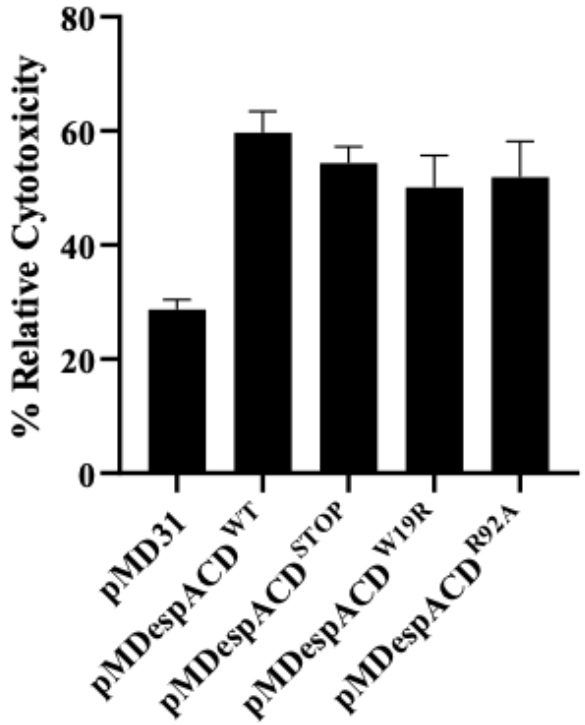

Figure 14: Percent relative cytotoxicity of *M. tb espA*::Tn strains expressing the indicated plasmid in PMA-differentiated THP-1 human macrophage cells analyzed through PrestoBlue. Infections were performed at an MOI of 5 for 72 h. Repeated measures one-way ANOVA ($p = 0.2978$) performed with GraphPad Prism Version 8.4.3. Values represent the mean of three independent experiments. Error bars represent standard error of means.

4.3.3. LDH analysis demonstrates a similar trend of reduced cytotoxicity with *M. tb espA*::Tn pMD*espACD*^{W19R} compared to *M. tb espA*::Tn pMD*espACD*^{WT}

A parallel approach to examine cytotoxicity was performed through measurement of LDH, a cytosolic enzyme released from cells when the plasma membrane is damaged. A single LDH experiment was performed on *M. tb* infected THP-1 macrophages to corroborate the results obtained through PrestoBlue analysis. Here, the trend demonstrated that *M. tb espA*::Tn pMDespACD^{W19R} was less cytotoxic than *M. tb espA*::Tn pMDespACD^{STOP} and *M. tb espA*::Tn pMDespACD^{WT} (Figure 15). However, despite confirming this trend, the LDH measurement technique appeared to give unrealistic values for relative percent cytotoxicity. Not all values fell within the 0-100% range and several were roughly double the values obtained through the PrestoBlue assay (Table 4). Additionally, the cytotoxicity measured with *M. tb espA*::Tn pMDespACD^{R92A} was unexpectedly low for a strain with a wildtype-like secretion profile and contradicted what was observed across several PrestoBlue experiments. As the values obtained through the LDH assay appeared less realistic, this methodology was forgoed in favour of PrestoBlue analysis. The phenotype exhibited by *M. tb espA*::Tn pMDespACD^{W19R} in the LDH, PrestoBlue, and the unpublished mouse infection analyses collectively suggest that this strain is less virulent than *M. tb espA*::Tn pMDespACD^{WT}.

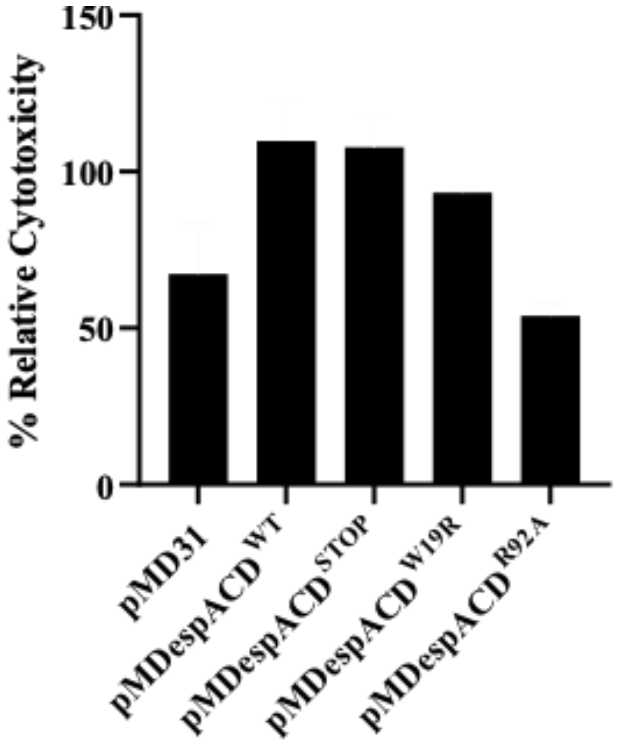

Figure 15: Percent relative cytotoxicity of *M. tb espA*::Tn strains expressing the indicated plasmid in PMA-differentiated THP-1 human macrophage cells analyzed through LHD assay. Infections were performed at an MOI of 5 for 3 days. Data points represent results after a single experiment, averaging only three replicates of each group.

Table 4: Summary of the percent cytotoxicity values obtained for THP-1 cells infected with selected *M. tb espA*::Tn strains and analyzed through PrestoBlue and LDH assays.

M. tb espA::Tn strain	Average % Cytotoxicity (PrestoBlue)	% Cytotoxicity (LDH)
pMD31	28.7	67.3
pMDespACD^{WT}	59.7	109.8
pMDespACD^{STOP}	54.3	107.8
pMDespACD^{W19R}	50.1	93.3
pMDespACD^{R92A}	51.9	53.9

4.4. IL1β and TNFα production is suppressed in *M. tb espA*::Tn pMDespACD^{W19R}

ESX-1 dependent cell death in *M. tb* infected macrophages has been shown to correspond with the induction of pro-inflammatory cytokines (Chen et al., 2013a). As *M. tb espA*::Tn pMDespACD^{W19R} appeared to cause a decrease in macrophage cell death compared to *M. tb espA*::Tn pMDespACD^{WT}, production of IL1β and TNFα was monitored to determine if this phenotype corresponds to pro-inflammatory cytokine production. THP-1 cells were infected with

M. tb espA::Tn pMD31, *M. tb espA*::Tn pMDespACD^{WT}, *M. tb espA*::Tn pMDespACD^{STOP}, *M. tb espA*::Tn pMDespACD^{W19R}, or *M. tb espA*::Tn pMDespACD^{R92A} and infection supernatants were measured 24 h post-infection through ELISA.

Pro-inflammatory cytokine production was reduced in the case of THP-1 infections with *M. tb espA*::Tn pMDespACD^{W19R} compared to *M. tb espA*::Tn pMDespACD^{WT} (Figure 16). This difference is statistically significant in the case of IL1β (Figure 16a). Results for IL1β and TNFα displayed a consistent trend across all strains. Both IL1β and TNFα production in THP-1 cells induced by *M. tb espA*::Tn pMD31 and *M. tb espA*::Tn pMDespACD^{R92A} were found to be similar to one another and were not significantly different from *M. tb espA*::Tn pMDespACD^{WT} (Figure 16). The *M. tb espA*::Tn pMDespACD^{STOP} strain induced a higher production of pro-inflammatory cytokines in THP-1 cells than *M. tb espA*::Tn pMDespACD^{WT} (Figure 16). These results demonstrate that ESX-1 dependent cell death does not necessarily correspond with an increase in pro-inflammatory cytokine production.

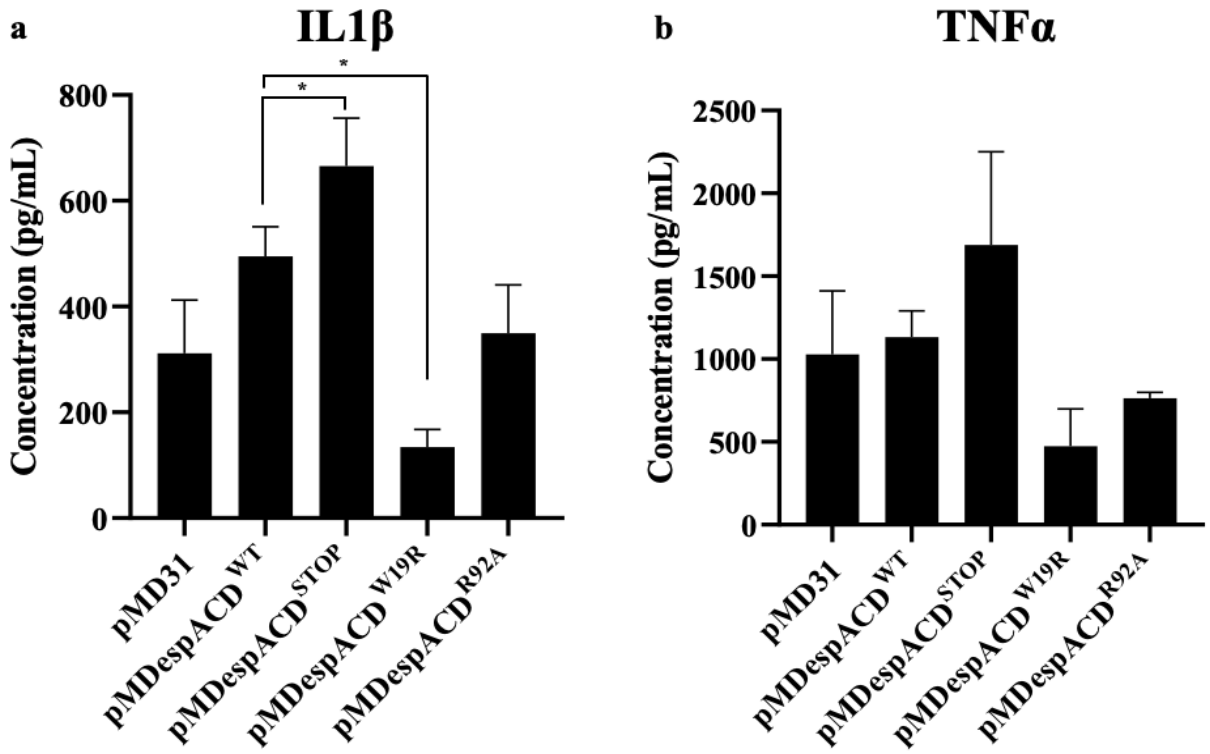

Figure 16: *M. tb espA*::Tn strains expressing the indicated plasmids infected PMA-differentiated THP-1 human macrophages for 24 h at an MOI of 10 before supernatants were collected for ELISA analysis for (a) IL1β concentration and (b) TNFα concentration. Repeated measures one-way ANOVA (IL1β: $p = 0.0362$, TNFα: $p = 0.2960$) performed with GraphPad Prism Version 8.4.3. Statistically significant differences with $p < 0.05$ indicated with (*). Values represent the mean of three independent experiments. Error bars represent standard error of means.

4.5. Monitoring expression levels of proteins of pro-inflammatory pathways

To further investigate the differences observed in the production of pro-inflammatory cytokines, *M. tb* infected THP-1 cell lysates were analyzed through Western blot. Several proteins involved in the pathways leading to pro-inflammatory cytokine production were detected in the infection lysates collected 24 h post-infection. To investigate the differences seen in IL1β production, NLRP3 and cleaved caspase-1 were monitored to observe activation of the NLRP3 inflammasome (Broz and Dixit, 2016). Additionally, the presence of total NF-κB and phosphorylated NF-κB were observed as the NF-κB signaling pathway is highly interconnected with TNFα signaling (Hayden and Ghosh, 2014).

4.5.1. NLRP3 and cleaved caspase-1

Western blots detecting NLRP3 and cleaved caspase-1 were loaded with 15 μg protein/well of the lysates of THP-1 cells infected with the selected *M. tb* strains. The detected levels of NLRP3 were similar across all infected lysates, including the uninfected group (Figure 17). Attempts were made to optimize the signal by increasing the amount of sample. However, blots with more than 15 μg of total protein/well did not display improved NLRP3 signal. Cleaved caspase-1 was not detected at any protein concentration. Additional tests may be needed to confirm the functionality of the α-cleaved caspase-1 primary antibody. Western blots were performed using each of these primary antibodies (NLRP3, cleaved caspase-1, total NF-κB, pNF-κB, and β-actin) on multiple sets of infected THP-1 cell lysates. Blots are representative of the results observed across all samples, however any minor signal differences observed in these blots were not consistently seen across other sample sets and should not be considered conclusive.

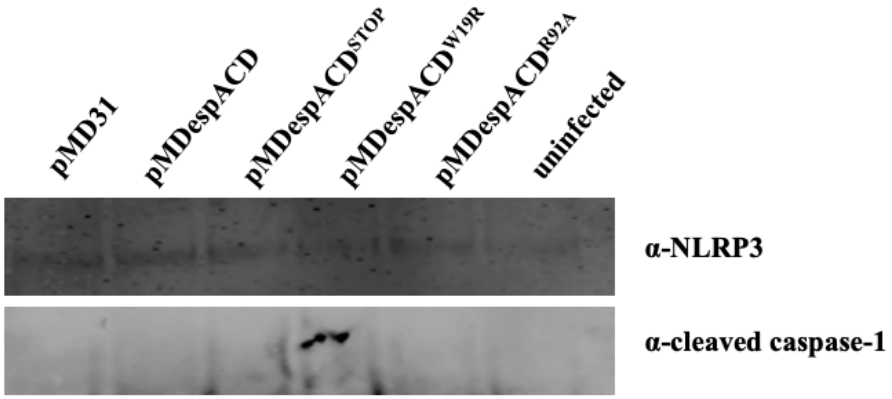

Figure 17: *M. tb espA*::Tn strains expressing the indicated plasmids infected PMA-differentiated THP-1 human macrophages for 24 h at an MOI of 10. Cell lysates were collected for Western blotting to identify the presence of NLRP3 and cleaved caspase-1. Primary antibodies were used at a 1:1000 dilution incubated overnight before detection with fluorescent secondary antibody.

4.5.2. NF-κB phosphorylation

Western blots detecting total NF-κB, pNF-κB, and β-actin were performed with 10 μg of total protein/well from the infected THP-1 lysate samples. Similar to the signal observed with NLRP3, there were no detectable differences in NF-κB phosphorylation in THP-1 cells infected with the different *M. tb* strains (Figure 18). If there were any differences in phosphorylation of NF-κB caused by any of the selected *M. tb* strains, they were missed at the single timepoint of 24 h post-infection. The signal visualized here appears to be the basal level of NF-κB and pNF-κB, indicated by the similarity of signals in all infected lysates to the signal of the uninfected lysate.

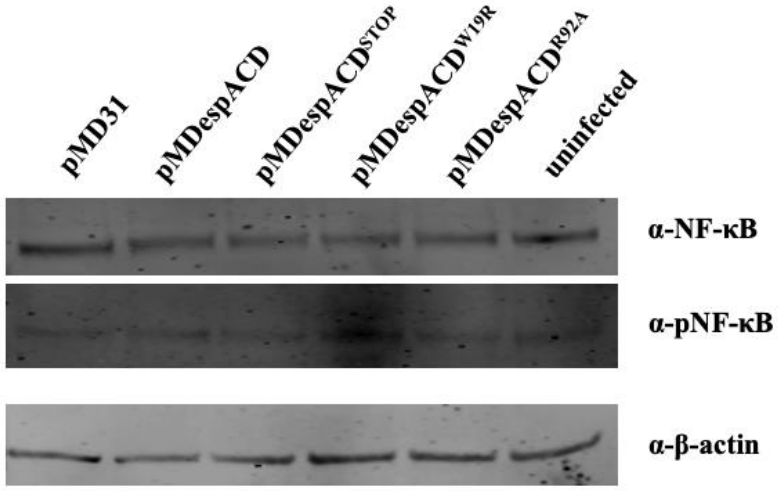

Figure 18: *M. tb espA*::Tn strains expressing the indicated plasmids infected PMA-differentiated THP-1 human macrophages for 24 h at an MOI of 10. Cell lysates were collected for Western blotting to identify the presence of total NF-κB and pNF-κB. β-actin was used as a loading control. Primary antibodies were used at a 1:1000 dilution incubated overnight before detection with fluorescent secondary antibody.

4.6. Production of recombinant EspD protein

Through the investigation of *M. tb espA*::Tn pMDespACD^{W19R}, which is unable to secrete EspD, it is clear this protein has a function contributing to the *M. tb* infection in macrophages. To understand the role of secreted EspD, efforts to express and purify the protein from *E. coli* were made to facilitate investigation of its biochemical properties. Purification of this protein was attempted under both non-denaturing (native) conditions as well as denaturing conditions.

4.6.1. Non-denaturing purification of EspD

Many attempts were made to purify recombinantly expressed EspD from *E. coli* in its native form. A native purification approach that provides high purity and yield has not yet been developed for EspD and is necessary in order to perform further biophysical analyses including circular dichroism (CD) and dynamic light scattering (DLS). Through these purification trials, a proposed protocol was developed, however it was only partially successful (Figure 19). This proposed protocol includes three levels of purification: His-tag purification, anion-exchange chromatography (AEC), and SEC. Here, this protocol will be discussed and recommendations for future work on development of a native protocol for the purification of EspD are provided.

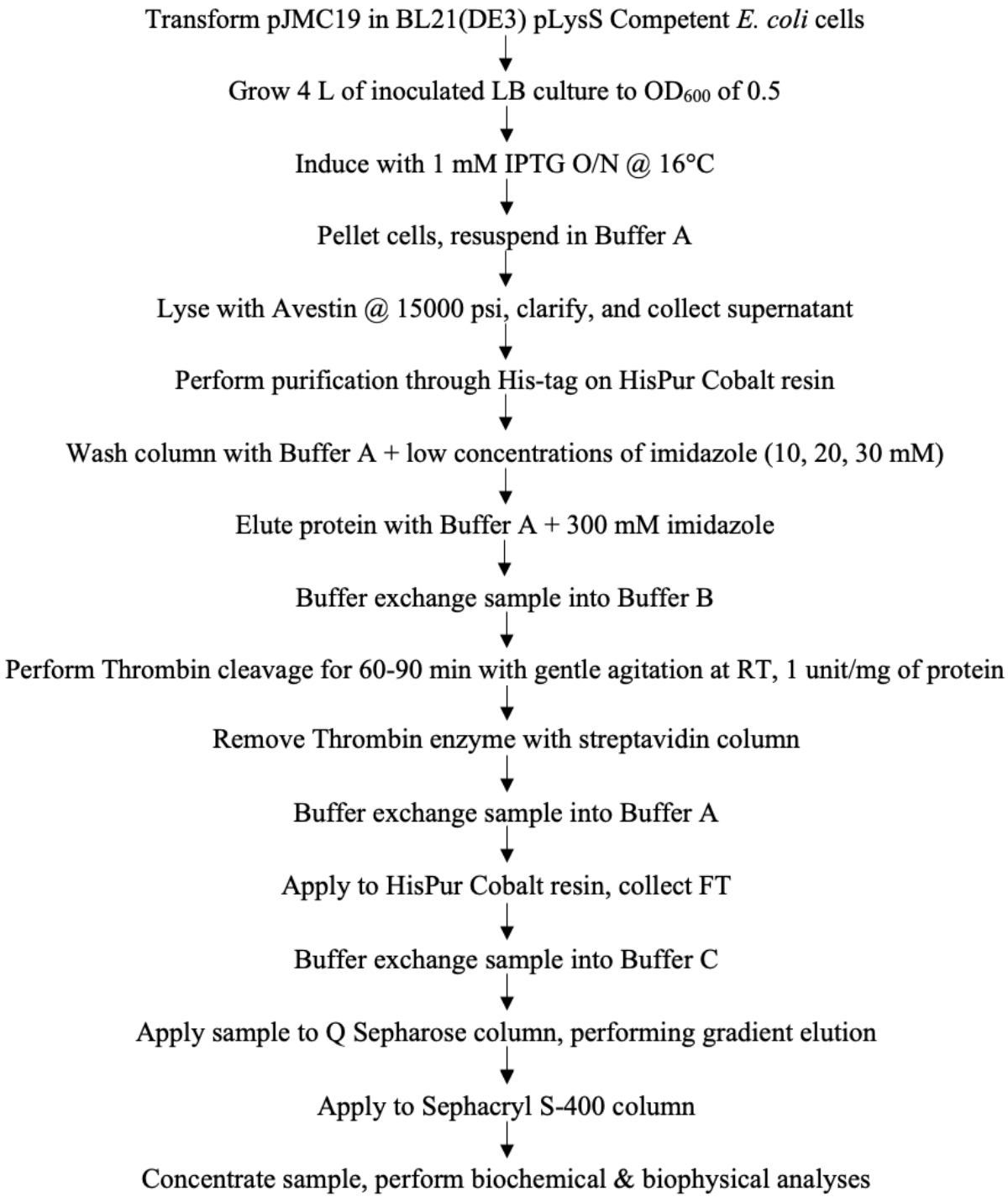

Figure 19: Tentative non-denaturing purification protocol for recombinantly produced EspD from *E. coli*. Buffer A: 50 mM NaH_2PO_4, 300 mM NaCl, 10 mM imidazole, pH 7.4. Buffer B :20 mM Tris-HCl, 150 mM NaCl, 2.5 mM $CaCl_2$; pH 8.4. Buffer C: 20 mM Tri-HCl, pH 8.0, eluting with 1M NaCl, pH 8.0. All column buffers should be degassed and filtered prior to use. Total protein concentration of the sample to be monitored through BCA Assay and purity observed through LDS-PAGE. Samples can be concentrated when necessary with appropriate MWCO Sartorius Vivaspin 20 Centrifugal Concentrators.

Expression in E. coli:

The protein of interest was encoded in the pET28a-based vector, pJMC19, and transformed into *E. coli* BL21(DE3) pLysS. The His-tag was encoded on the N-terminus of EspD with a Thrombin cleavage site located between the encoded tag and the protein itself. Expression was controlled under the lac operon and therefore induced by the addition of IPTG once the *E. coli* pJMC19 cultures reached mid-log phase of growth in LB media. Induction was allowed to proceed overnight before collecting the cell pellets.

Induction conditions were established after observing protein expression at varying temperatures. Culture samples were taken prior to the addition of IPTG (pre-induction) and after induction was allowed to proceed in full (post-induction). After the addition of IPTG, several cultures were allowed to incubate at 37°C for 4 h, while others were incubated overnight at 16°C. Samples were then diluted relative to the OD_{600} of the culture at the time the sample was taken. Evaluation of pre-induction and post-induction samples from all cultures was performed through LDS-PAGE and Coomassie blue staining. The target protein was visualized at ~25 kDa in size and induction was observed in samples across both temperatures (Figure 20). Consistently, more of the target protein was present relative to the contaminating proteins in the post-induction samples of cultures induced overnight at 16°C than was observed with cultures induced at 37°C for 4 h. These conditions were selected moving forward.

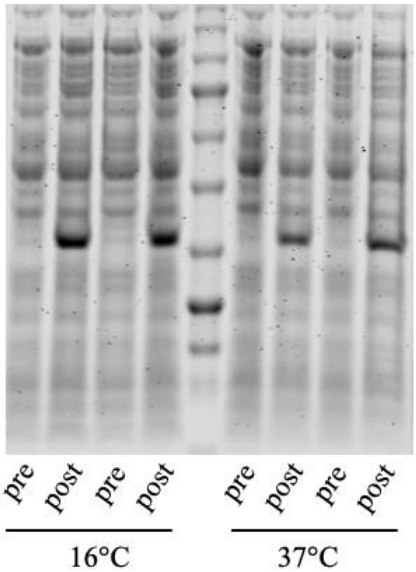

Figure 20: EspD protein expression tests of *E. coli* pJMC19 cultures. Samples taken before (pre) and after (post) induction with IPTG at 16°C overnight or 37°C for 4 h. Samples were analyzed through LDS-PAGE and Coomassie blue staining.

Buffer tests and lysis:

Preliminary buffer tests established that buffers of lower ionic strength (< 200 mM NaCl) lead to greater EspD aggregation than buffers of higher ionic strength (300-500 mM NaCl). Eventually, a buffer containing 50 mM sodium phosphate, 300 mM sodium chloride, 10 mM imidazole; pH 7.4 was established as the base formula for EspD's purification buffer (Buffer A). This buffer was used for lysis, equilibrium, and wash steps throughout the His-tag purification and SEC steps. Buffer A is used to resuspend the centrifuged bacterial cell pellets collected after induction. Lysis was then performed using an Avestin French press. Pressure was allowed to reach > 15000 psi for two full passages to ensure effective lysis. Additional passages can be damaging to the protein and should be avoided when possible.

His-tag purification:

The clarified lysate was applied to HisPur Cobalt resin, capturing the protein through its His-tag. Resin was washed with Buffer A, followed by washes with gradual increases in imidazole concentrations (10-30 mM imidazole). Elutions were performed using Buffer A containing 300 mM imidazole (elution buffer). Samples were taken from the flow through (FT) of each stage of the column purification. Monitoring through LDS-PAGE allowed observation of the relative concentration of EspD present in each stage (Figure 21). Total lysate samples demonstrated the impurity of the starting sample and the high concentration of protein at the target size. Initial passage through the HisPur column and washes removed much of the contaminating protein, but also lead to loss of target protein. A much larger volume of HisPur resin was required in the purification demonstrated by Figure 21 to capture an appropriate amount of target protein from the lysate. After the addition of elution buffer, typically the first and second column volumes (CV) of buffer contained the highest concentration of target protein. Volumes of elution buffer beyond three CVs were found to be redundant and did not release any further bound protein. There remained a significant amount of target protein loss that occurred during His-tag purification. EspD remained bound to the resin after elution attempts were performed. Attempts to increase the imidazole concentration in the elution buffer were unsuccessful at releasing more protein from the resin. Optimization of these steps is still needed to provide higher concentrations of EspD going into subsequent purification steps.

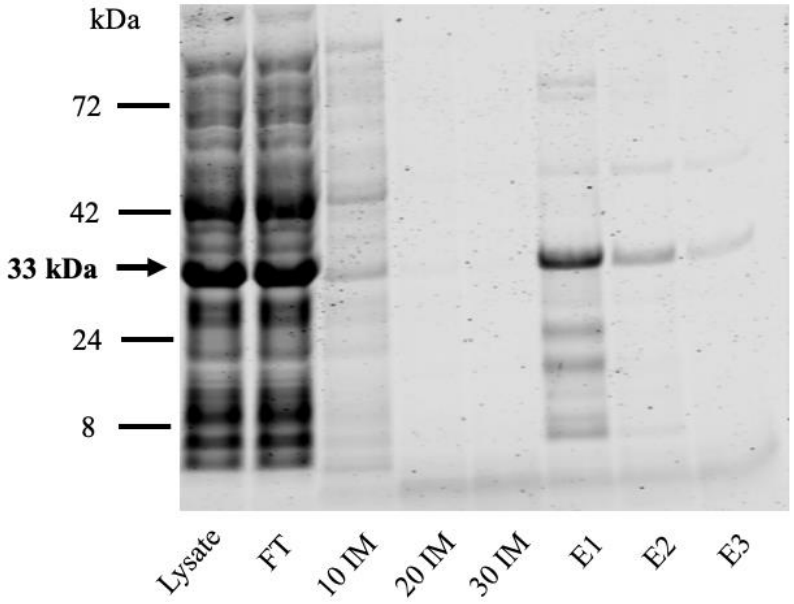

Figure 21: LDS-PAGE electrophoresis of samples from the stages of small scale His-tag purification of recombinant EspD through HisPur cobalt resin. Protein was visualized with Coomassie blue staining. FT = flow through, IM = mM concentration of imidazole present in wash buffer (50 mM NaH_2PO_4, 300 mM NaCl, pH 7.4), E1 = elution fraction 1, E2 = elution fraction 2, E3 = elution fraction 3.

Buffer exchange and His-tag cleavage:

High concentrations of imidazole should be immediately dialyzed out of elution fractions containing EspD. Buffer exchange was performed into Thrombin activity-friendly Buffer B (20 mM Tris-HCl, 150 mM NaCl, 2.5 mM $CaCl_2$; pH 8.4). Biotinylated Thrombin enzyme was added to the protein sample to remove the His-tag. LDS-PAGE evaluation confirmed the cleavage success (Figure 22). A streptavidin column was used to remove the enzyme from the protein sample before dialyzing the sample back into Buffer A. Further application to fresh HisPur Cobalt resin binds EspD protein that remains linked to its His-tag. The flow through from this column contained the target EspD protein with the His-tag removed.

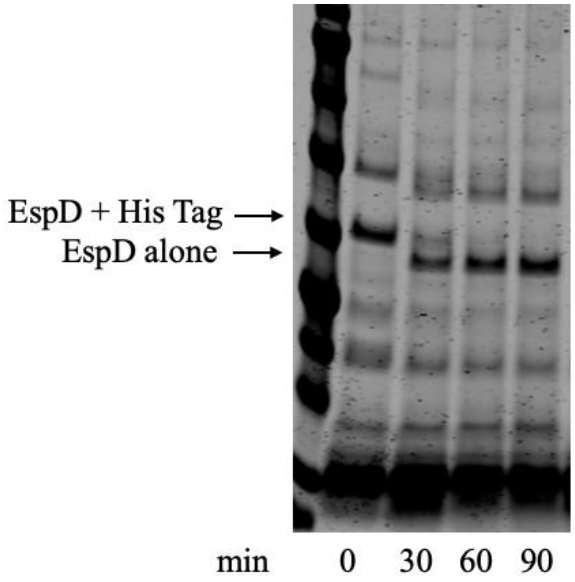

Figure 22: Thrombin cleavage analysis of recombinant EspD protein from 0 min to 90 mins. Samples were electrophoresed through LDS-PAGE and gel was stained with Coomassie blue.

Anion exchange and size exclusion chromatography:

The remaining purification steps were not completed in their proposed order from Figure 19. It has been advised that AEC be performed with the sample following His-tag removal. This process can release contaminating proteins that may remain bound to EspD itself prior to application to SEC as the final step of purification. Due to EspD's low predicted isoelectric point of 4.1, anion exchange will be performed using the available Q Sepharose column. Trials of this purification stage should begin with Buffer C (20 mM Tri-HCl, pH 8.0, eluting with 1M NaCl, pH 8.0) and may require further optimization.

Attempts using SEC were previously performed immediately after His-tag removal. Higher concentrations of protein were necessary, therefore the procedure should be scaled upwards, as indicated in the proposed protocol. Buffer A was used through SEC tests and no EspD aggregation was observed at this stage. Moving forward, SEC should be performed using a Sephacryl S-400 column to effectively purify EspD in its large oligomeric state. Each of these chromatography steps will require confirmation that an effective elution peak is observed indicating high concentration of fractionated EspD from the column. Once a high yield and pure sample of EspD has been achieved further biochemical and biophysical analyses can be completed.

Other insights into the purification of recombinant EspD under non-denaturing conditions:

Several practices were found to promote the aggregation of EspD in solution and should be avoided while further establishing purification methodology. Prior to selecting the current three stages of purification as His-tag purification, AEC, and SEC, salting out methods were attempted as well. Ammonium sulfate treatment led to the formation of insoluble precipitates made up predominantly of EspD protein. Additionally, it was not found to be an effective purification technique as EspD did not appear to precipitate at any specific salt concentrations. It is recommended that this method of purification not be attempted in the future for EspD.

Initial thermostability tests with His-tag purified EspD samples revealed that aggregation occurred over a brief period of time at any temperature. As well, the protein was sensitive to freeze-thawing. Due to these issues, purification is recommended to proceed uninterrupted until the protein sample has proceeded through His-tag cleavage, enzyme removal, and buffer exchange into Buffer A. Failure to remove the His-tag enzymatically led to aggregation of the EspD samples during storage. Protein samples appeared to remain stably stored for a longer period of time (> several weeks at 4°C) after His-tag removal than protein samples that remain His-tag linked (no longer than a few days).

Initial purification trials were performed using a Nickel-IDA silica-based resin for His-tag purification. This dried silica resin was a major cause of EspD aggregation. After many attempts to find a buffer that allowed for use of this resin with EspD, it was finally concluded that the resin itself instigated the protein insolubility. Additionally, His-tag resins using Nickel, opposed to Cobalt, led to higher amounts of protein loss during His-tag purification due to the higher strength of Nickel-His binding. As effective elutions of EspD from the His-tag purification column were a consistent issue, Nickel based resins are expected to only amplify this issue further.

4.6.2. Denaturing purification of recombinant EspD

Denaturing conditions were used to purify recombinant EspD protein from inclusion bodies of *E. coli* cultures. Protein expression was induced, and bacterial cells were collected and lysed, as mentioned in the non-denaturing protocol. Inclusion bodies were collected, washed, and solubilized in Denaturing Buffer (50 mM sodium phosphate, 300 mM sodium chloride, 8M urea, pH 8.0) before mixing with Nickle-IDA silica resin for His-tag purification. This mixture was washed with Denaturing Buffer containing low concentrations of imidazole (10-30 mM

imidazole) to remove nonspecifically bound proteins and eluted with Denaturing Buffer containing 300 mM imidazole. Purity was determined by observation through LDS-PAGE and Coomassie blue staining (Figure 23). The elution fraction containing the target protein was then dialyzed in a stepwise fashion to remove all urea and imidazole leaving the protein in the Assay Buffer (50 mM sodium phosphate, 300 mM sodium chloride, pH 8.0). Dialysis was the most practical methodology available to promote refolding of the purified EspD sample, however, it is worth noting that these samples may contain a considerable portion of unfolded or misfolded protein. Protein concentration was determined by BCA assay. Under denaturing conditions, purification of recombinant EspD yielded 1-5 mg of total protein with reasonable purity (Figure 23). This was a large improvement relative to the purification trials performed previously. Due to aggregation issues, the EspD purifications performed under non-denaturing conditions led to final protein yields of < 250 μg in total and contained more contamination (Figure 21).

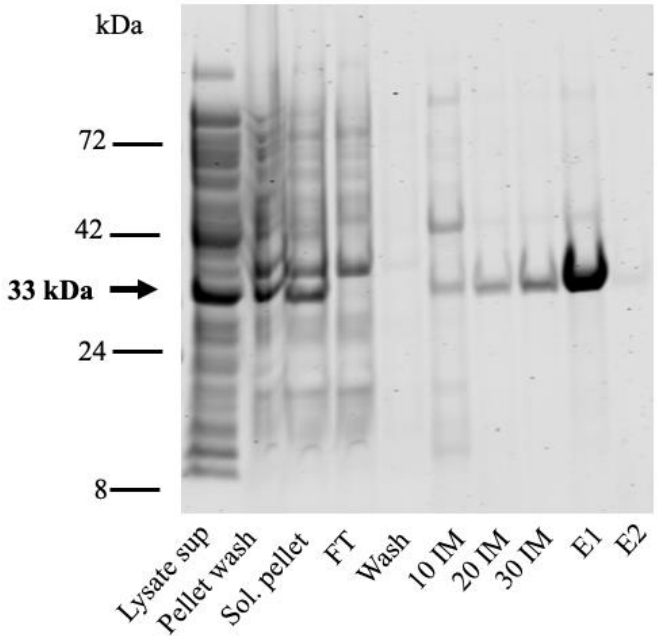

Figure 23: LDS-PAGE analysis of His-tag purification of EspD performed under denaturing conditions. FT = flow through, IM = concentration of imidazole (mM) present in wash buffer (50 mM NaH_2PO_4, 300 mM NaCl, 8M urea, pH 8.0), E1 = elution fraction 1, E2 = elution fraction 2.

4.7. Analysis of purified recombinant EspD protein

Unpublished work performed on recombinant EspD protein produced through small-scale non-denaturing purification displayed that EspD may form large oligomers and may bind eukaryotic phospholipids (Figures 7 & 8). To investigate if these features might also be seen with

recombinant EspD purified from *E. coli* under denaturing conditions, protein samples were dialyzed to remove denaturing agents in the buffer and then analyzed through Native-PAGE, TEM, and phospholipid binding assays.

4.7.1. Structural analysis with Native-PAGE and TEM

EspD was analyzed through Native-PAGE and TEM to observe oligomerization of the purified protein. Native-PAGE was performed on decreasing concentrations of EspD and visualized through Western blot using α-EspD primary antibody (Figure 24). Native-PAGE demonstrated that EspD appears to exist predominantly in oligomeric forms in sizes upwards of 400 kDa in size, similar to what was seen with the unpublished SEC data (Figure 7a). The observed smear may imply there is not one static size of the EspD oligomer and instead the protein may bind with itself in a non-specific manner, allowing for oligomers of various sizes. There did not appear to be any banding pattern that could represent a monomer or dimer, etc. However, the oligomeric smear in the well loaded with 5 μg of EspD appeared to extend to lower sizes (60-80 kDa), which may imply that EspD can exist in these smaller oligomers to a lesser degree. This could also be evidence of contaminating proteins binding non-specifically to the α-EspD antibody during Western blotting.

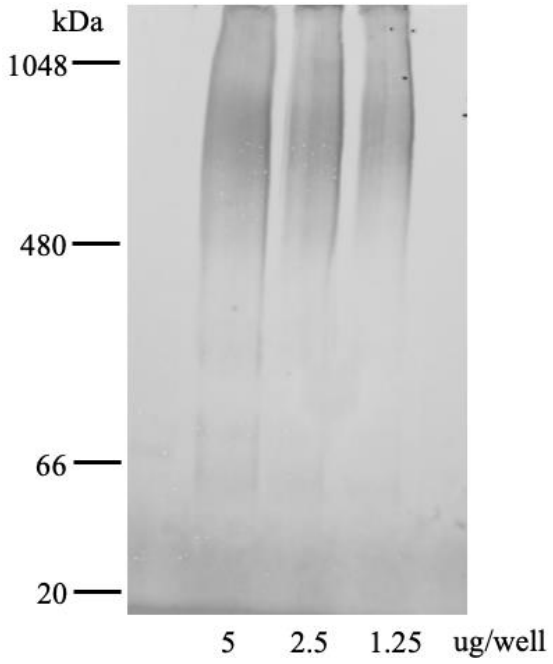

Figure 24: Native-PAGE of purified and refolded EspD protein detected through Western blotting with α-EspD primary antibody and fluorescent secondary antibody.

EspD samples were diluted to a 1000 nM concentration in the Assay Buffer and were absorbed onto 400 mesh TEM grids, stained with a tungsten negative stain, and imaged at 50k magnification using the Hitachi HT7700 microscope (Figure 25). EspD protein prepared here was unable to be imaged through this methodology without causing the protein to aggregate. Previous unpublished data visualized recombinant EspD protein in an unaggregated state displaying chain-like oligomeric structure (Figure 7b).

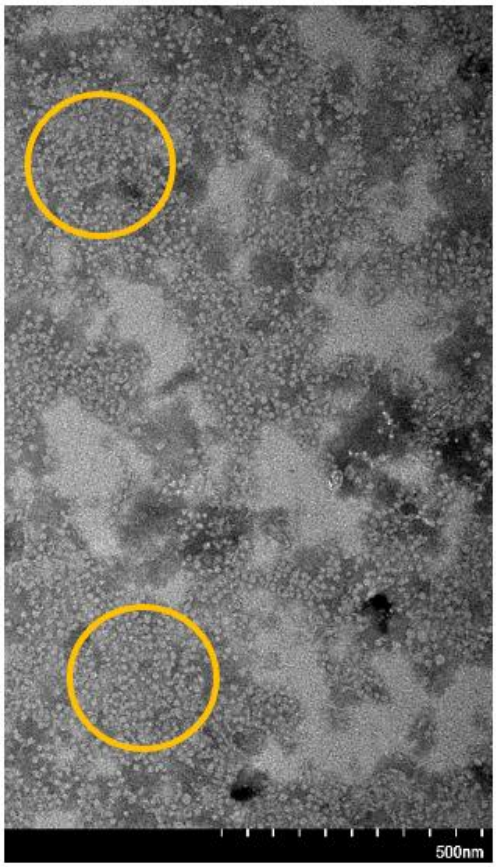

Figure 25: TEM images taken at 50k magnification of purified and refolded EspD protein. Images were obtained at the Western College of Veterinary Medicine Image Centre on the Hitachi HT7700 TEM. Yellow circles indicate some large areas of aggregated protein.

4.7.2. Phospholipid-EspD binding assays

Unpublished work on recombinant EspD uncovered that the protein appears to bind specifically to several eukaryotic phospholipids (Figure 8). The protein's ability to bind eukaryotic phospholipids may contribute to the impact secreted EspD appears to have during *M. tb* infections of macrophages. Here, recombinant protein samples purified from *E. coli* under

denaturing conditions were refolded and binding tests were performed using commercially available phospholipid membranes and beads.

Membranes embedded with eukaryotic phospholipids were incubated with 100 nM purified EspD protein. PIP Strips include fifteen different phospholipids at 100 pmol/spot, while PIP Arrays include eight different phosphoinositides at concentrations from 100 pmol/spot decreasing to 1.56 pmol/spot. Membranes were further probed with α-EspD antibody to assess which of the phospholipids bind EspD. The PIP Strips identified that EspD was predominantly bound to PA and the phosphatidylinositol monophosphates, including PI3P, PI4P, PI5P (Figure 26a). The PIP Arrays further investigated EspD's ability to bind phosphoinositides. EspD again demonstrated binding to phosphatidylinositol monophosphates (Figure 26b). Taken together, EspD appeared to consistently bind strongly to PI4P.

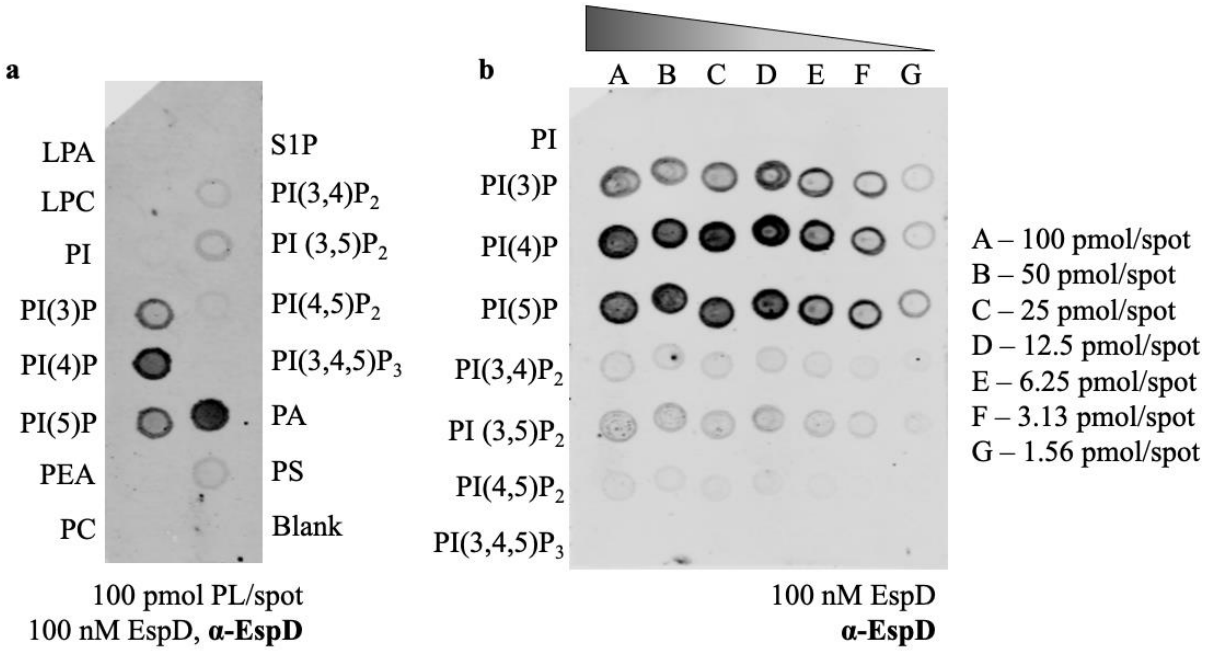

Figure 26: Commercially available membrane (a) PIP Strip (b) PIP Array incubated with 100 nM purified and refolded EspD protein and detected through Western blotting with α-EspD primary antibody and fluorescent secondary antibody. LPA = lysophosphatidic acid, LPC = lysophosphocholine, PI = phosphatidylinositol, PIP = phosphorylated phosphatidylinositol species, PEA = phosphatidyl-ethanolamine, PC = phosphatidylcholine, S1P = sphingosine 1-phosphate, PA = phosphatidic acid, PS = phosphatidylserine.

Additional phospholipid binding tests were performed using commercially available agarose beads coated in phospholipids of interest. Beads were incubated with 500 nM purified protein and washed to remove non-specifically bound protein. Beads were boiled to release the remaining bound protein and samples were evaluated through LDS-PAGE and α-EspD probing. Signal observed from pull-downs with control beads indicate non-specifically bound protein as these beads are comprised of blocked agarose and are not coated in phospholipids. EspD demonstrated binding towards PA and PI4P (Figure 27). This phenotype further corroborates the results observed using PIP Strips and PIP Arrays from Figures 8 & 26.

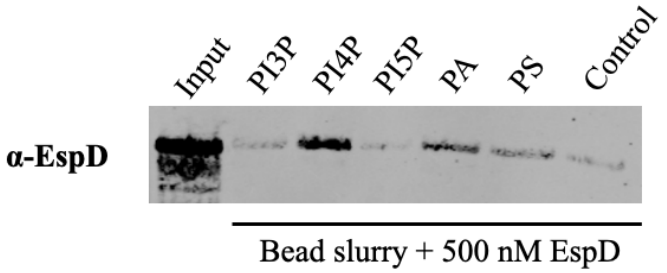

Figure 27: Commercially available beads coated in the indicated phospholipids were incubated with 500 nM purified and refolded EspD protein. Bound protein was detected through Western blotting with α-EspD primary antibody and fluorescent secondary antibody. PIP = phosphorylated phosphatidylinositol species, PA = phosphatidic acid, PS = phosphatidylserine.

4.8. Phospholipid bead pull-down with *M. tb* produced EspD

To further investigate EspD's ability to bind PI4P, samples of *M. tb* cultures were utilized in pull-down experiments using phospholipid coated beads. Original attempts were made using cell lysate samples of *M. tb espA*::Tn pMDespACD^{WT} and *M. tb espA*::Tn pMDespACD^{STOP} to determine whether a pull-down experiment could be successful using a mixture of proteins as opposed to a purified protein sample. EspD was able to be pulled down from the *M. tb espA*::Tn pMDespACD^{WT} cell lysates, with a stronger signal for EspD in the case of the PI4P beads than with the control beads (Figure 28). Bead washing was not rigorous enough to effectively remove the non-specifically bound protein, therefore true binding to PI4P beads may be weaker than observed. Nonetheless, this assay stands as a proof of concept that specific proteins may be able to be pulled down and detected through this method.

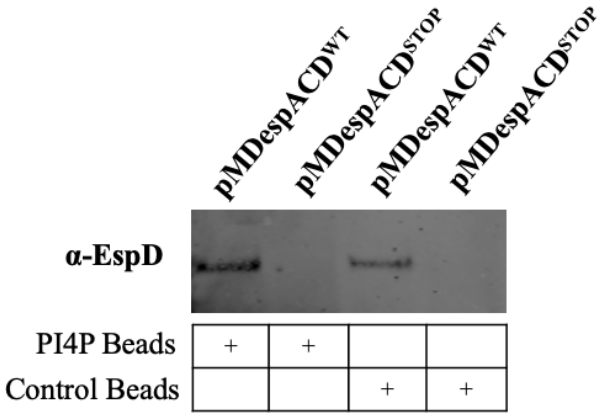

Figure 28: Cell lysate samples (expressed proteins) of the *M. tb espA*::Tn strains indicated were used to perform phospholipid-coated bead pulldowns with PI4P and control beads.

To attempt to confirm that secreted EspD is capable of this binding, culture filtrate samples for *M. tb espA*::Tn pMDespACD^{WT} and *M. tb espA*::Tn pMDespACD^{STOP} were made. Due to the low relative concentration of EspD in culture filtrates, large volumes (6 x that of standards culture filtrate Western blots) were prepared. Each culture filtrate sample was confirmed for the presence of Ag85 and absence of GroEL2 to ensure the bacteria was not lysed during sample preparation. These filtrates were concentrated, and pull-downs were performed using PI4P and control beads. This assay displayed a high amount of background signal, however, Figure 29 demonstrated that secreted EspD was pulled down from *M. tb espA*::Tn pMDespACD^{WT} culture filtrate sample using PI4P beads. Despite the faint signal, this result corroborates the PI4P binding phenotype observed in recombinant EspD purified under both non-denaturing (Figure 8) and denaturing conditions (Figures 26 & 27).

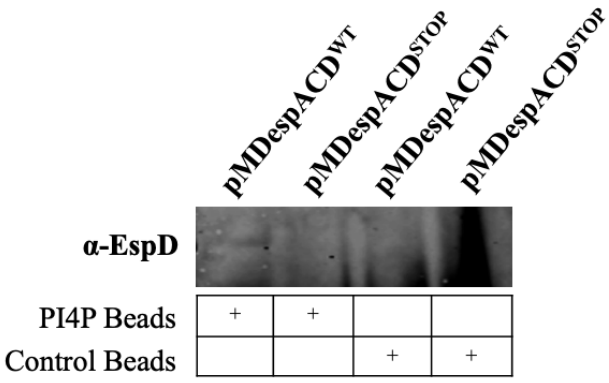

Figure 29: Culture filtrate samples (secreted proteins) of the *M. tb espA*::Tn strains indicated were used to perform phospholipid-coated bead pull-downs with PI4P and control beads.

4.9. Generation of mammalian cells expressing phospholipid biosensors

Establishing the binding of secreted EspD to eukaryotic phospholipids, especially PI4P, leads to interest in exploring this phenotype within the host cell during infection. To begin monitoring the potential impact to the eukaryotic host, a collection of fluorescent biosensor plasmids was established for the purposes of monitoring phospholipids of interest within eukaryotic cells (Table 5). These plasmids encode probes which bind specifically to the target phospholipid. Probes are expressed attached to either green fluorescent protein (GFP) or red fluorescent protein (RFP) to allow visualization through confocal microscopy.

Table 5: Fluorescent biosensor plasmid library for the sensing of eukaryotic phospholipids.

Biosensor Name	Phospholipid Target	Source
pGFP-LactC2	PS	Sergio Grinstein at the University of Toronto
pEGFP-2FYVE	PI3P	Sergio Grinstein at the University of Toronto
pGFP-P4M	PI4P	Sergio Grinstein at the University of Toronto
pGFP-PHDx3	PI5P	Bernard Payrastre at the French National Institute of Health and Medical Research
pRFP-CDH	PA	Guangwei Du at the University of Texas
pGFP-CDH	PA	Guangwei Du at the University of Texas
pMRFP	PA	Guangwei Du at the University of Texas
pMGFP	PA	Guangwei Du at the University of Texas

Plasmids were first evaluated for their functionality and ability to produce fluorescent signal. Transfections were performed with a lipofectamine method using an easily transfectable cell line, COS-7 fibroblast-like monkey kidney cells. Using confocal microscopy, it was determined that all plasmid biosensors were functional (Figures 30 & 31). All biosensors demonstrated strong fluorescent signal and displayed localization patterns that appeared distinct between the different phospholipids of interest, indicating effective localization.

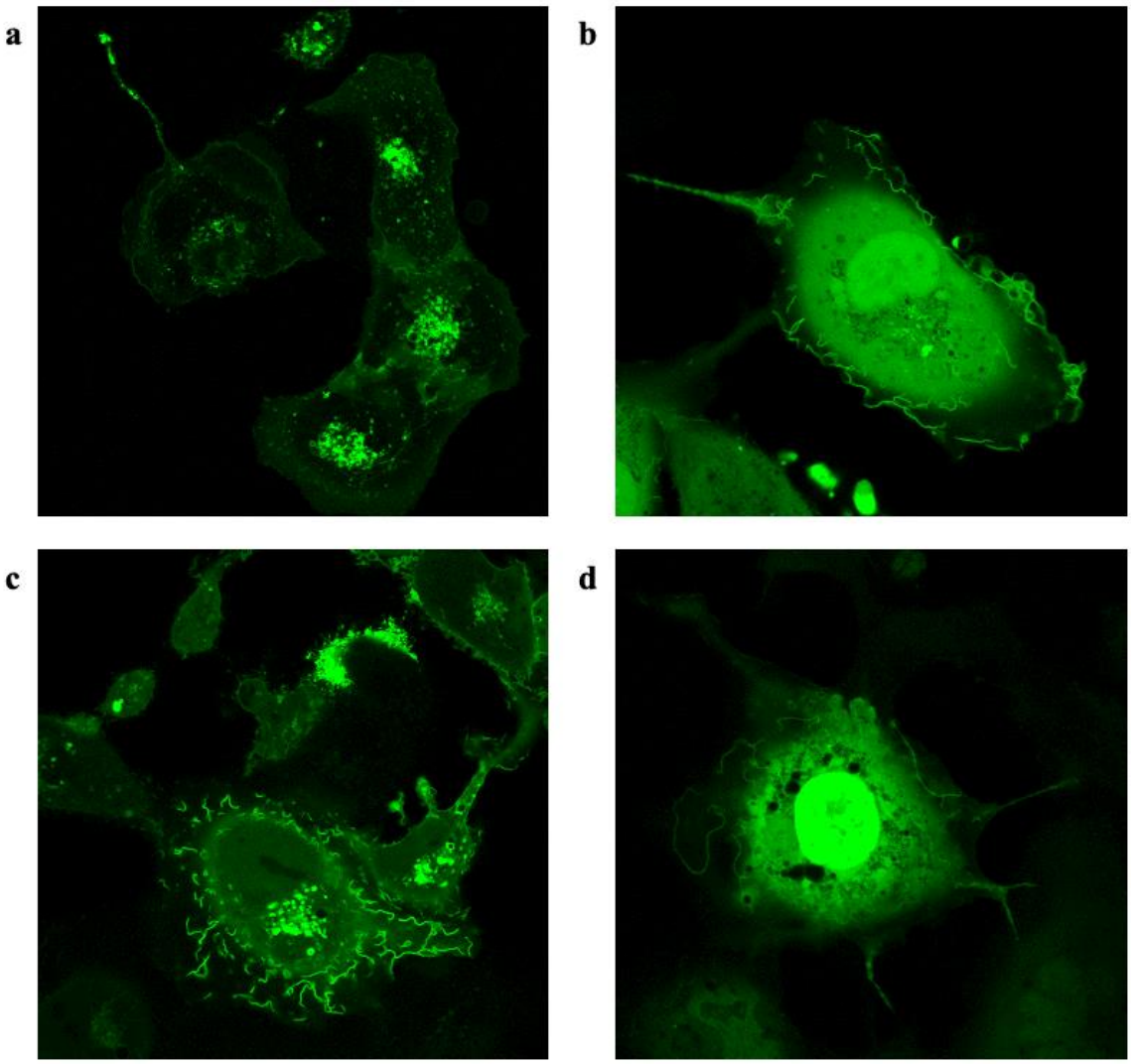

Figure 30: COS-7 monkey kidney fibroblast cells transfected with (a) pGFP-LactC2, sensing PS (b) pEGFP-2FYVE, sensing PI3P (c) pGFP-P4M, sensing PI4P (d) pGFP-PHDx3, sensing PI5P. Live cell imaging was performed 16 h post-transfection on the Leica TCS SP8 confocal microscope using Leica Application Suite X software version 3.4.2.18368. Magnification was achieved using 63x oil objective with a numerical aperture of 1.40.

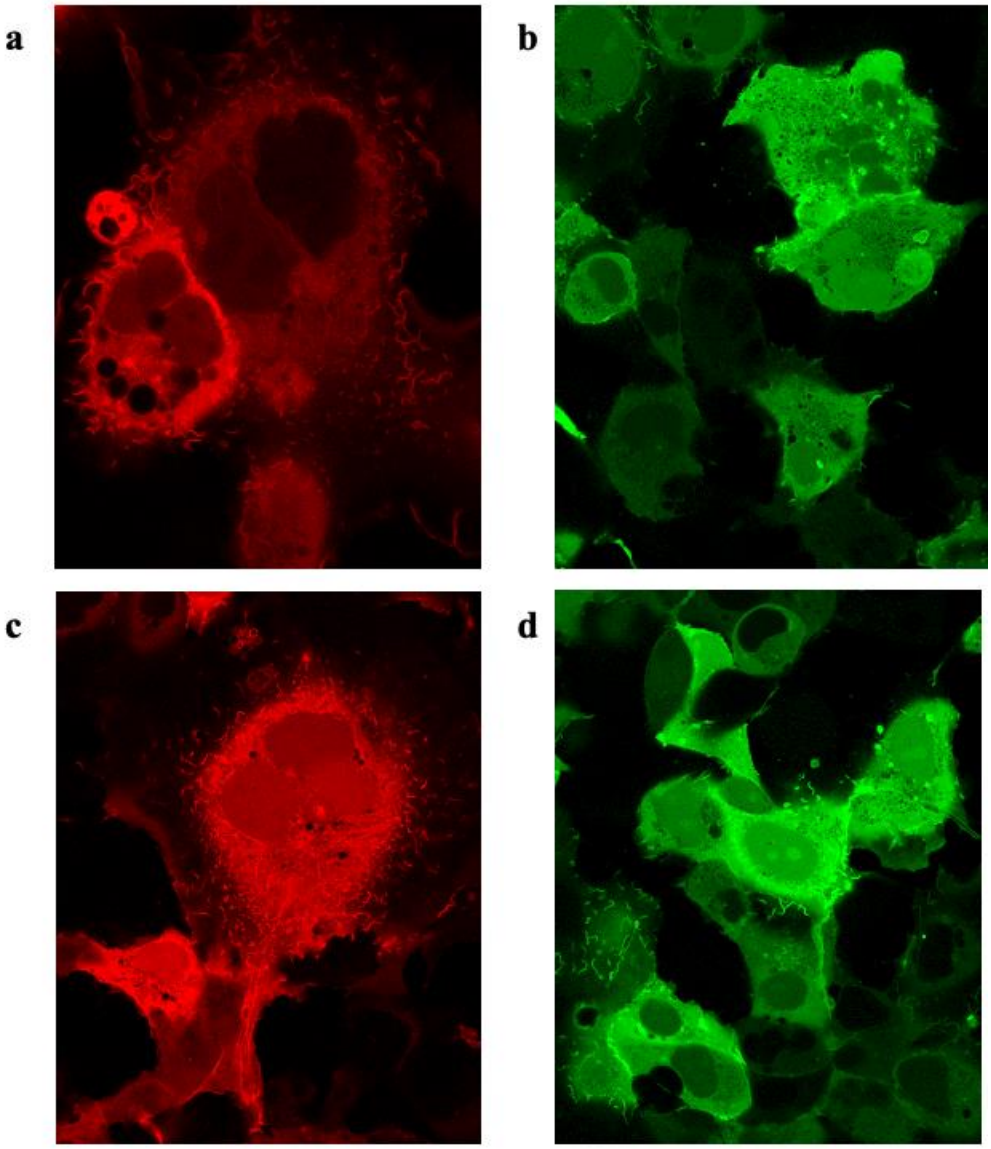

Figure 31: COS-7 monkey kidney fibroblast cells transfected with (a) pCDH-RFP (b) GFP-PASS (c) pM-RFP (d) GFP-PASS. These plasmids were all constructed to sense PA. Live cell imaging was performed 16 h post-transfection on the Leica TCS SP8 confocal microscope using Leica Application Suite X software version 3.4.2.18368. Magnification was achieved using 63x oil objective with a numerical aperture of 1.40.

After confirming functionality of the biosensor plasmids, the next necessary step was to develop a way to utilize these plasmids in a relevant macrophage cell line. Ideally, human macrophage cells could be used to most accurately represent human *M. tb* infections. However, transfections were unable to be performed in THP-1 cells using a lipofectamine-based method. Additionally, attempts were made using a THP-1 specific nucleofection kit, but ultimately this cell line was not able to be transfected effectively with the biosensor plasmids. The next available relevant cell line was RAW 264.7 cells, a murine macrophage cell line. Unlike THP-1 cells, RAW 264.7 cells are not terminally differentiated and replicate with a doubling time of ~11 hours (Sakagami *et al.*, 2009). Without terminal macrophages, the transfection protocol requires temporal restrictions in order to be successful.

A protocol was established for transfecting RAW 264.7 cells with these fluorescent biosensor plasmids using lipofectamine. This method was optimized to keep the transfection rate of the macrophages around 60-80%. Additional tests were performed to image transfected cells both live and fixed to coverslips with similar results. All biosensors tested, including GFP-PASS (sensing PA), GFP-LactC2 (sensing PS), GFP-2FYVE (sensing PI3P), GFP-P4M (sensing PI4P), and GFP-PHDx3 (sensing PI5P) were able to display fluorescent signal (Figure 32). The signal displayed by these transfected macrophages was not as obviously distinct as the signal seen previously in COS-7 cells. The small size of the macrophages and the lower cell density made imaging at high resolution more challenging. Several of the transfected macrophages, across all transfection groups, displayed a few common signal issues. Firstly, discrepancies in the type of signal produced by the same biosensor were observed depending on the time of imaging post-transfection. Additionally, some cells appeared entirely fluorescent, potentially due to overexpression of the biosensor, and did not allow for any discrimination of localization patterns. Lastly, several cells appeared to be dead or dying and displayed highly fragmented signals. These signal issues were reiterated by time course imaging experiments performed by other members of the lab using these same biosensors. Moving forward, the frequency at which transfected cells display these types of signals should continue to be monitored. Advancing into *M. tb* infections of the transfected macrophages will require further optimization of RAW 264.7 cell density, appropriate MOI, and ideal imaging time post-infection. Overall, the establishment of these biosensor expressing cells positions this work to begin exploring EspD's phospholipid binding within the cell.

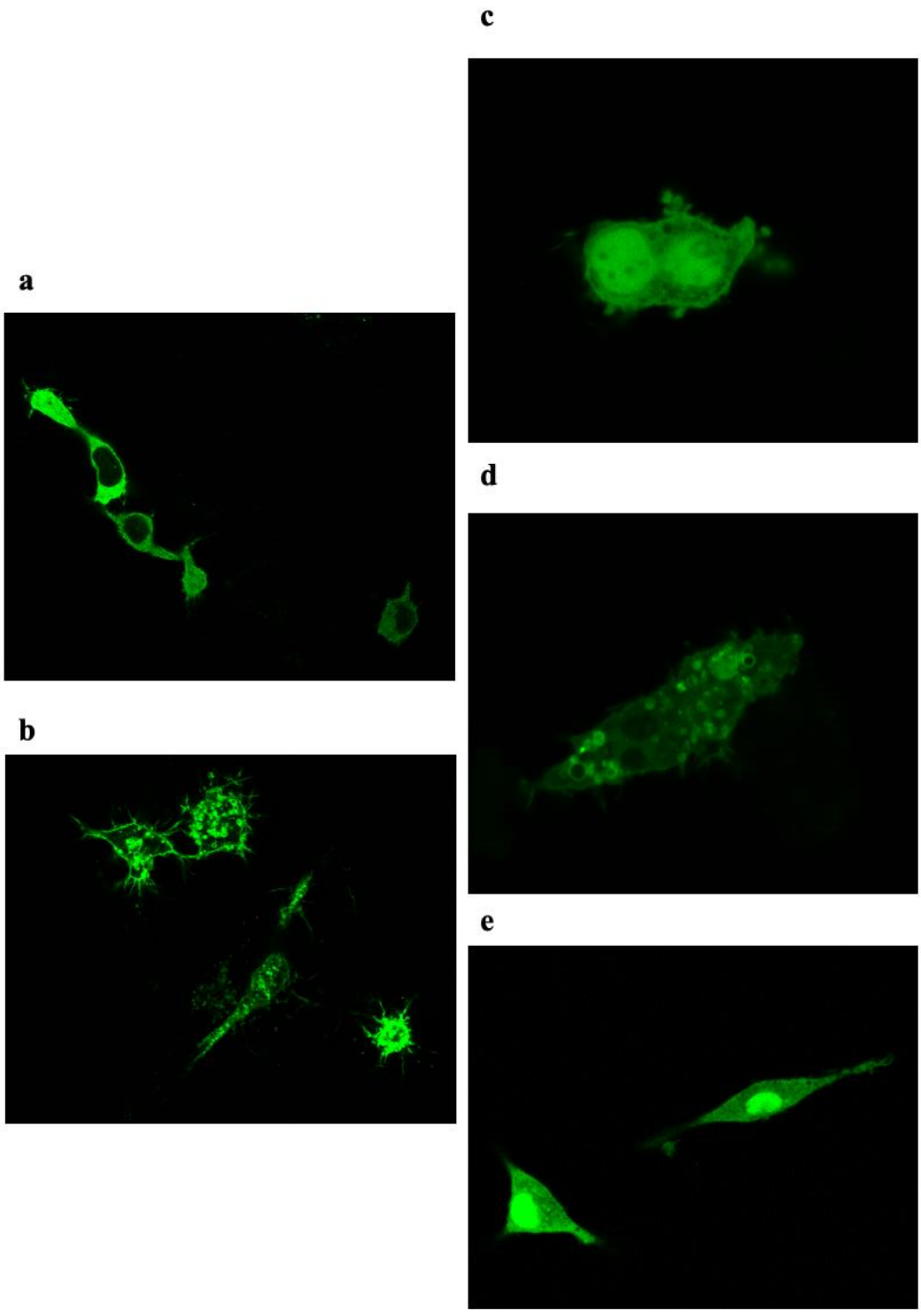

Figure 32: RAW 264.7 murine macrophage cells transfected with (a) GFP-PASS plasmid, sensing PA (b) GFP-LactC2 plasmid, sensing PS (c) GFP-2FYVE plasmid, sensing PI3P (d) GFP-P4M plasmid, sensing PI4P (e) GFP-PHDx3 plasmid, sensing PI5P. Live cell imaging was performed 16 h post-transfection on the Leica TCS SP8 confocal microscope using Leica Application Suite X software version 3.4.2.18368. Magnification was achieved using 63x oil objective with a numerical aperture of 1.40.

5. Discussion

In this work, we sought to better characterize the *M. tb* secreted protein, EspD. Unpublished work on this protein demonstrated that secreted EspD may contribute to *M. tb* replication in mice (Figure 6). Additionally, unpublished work uncovered that purified recombinant EspD may be capable of binding to eukaryotic phospholipids (Figure 8). This led to the hypothesis that secreted EspD interacts with eukaryotic phospholipids and disrupts host-cell processes to potentiate ESX-1 mediated *M. tb* virulence. We have attempted to address this through the characterization of *M. tb* strains that express variants of EspD, analyzing these strains in their interactions with macrophages, and studying purified recombinant EspD protein.

5.1. Characterization of *M. tb espA*::Tn strains expressing EspD variants

There is very little known about EspD, its structure or its function. Analysis of EspD's protein sequence did not reveal any known functional domains or previously characterized structural regions. Therefore, to begin studying this protein, mutations were made to the EspD protein expressed in *M. tb* in the hopes of identifying new phenotypes. The mutations made to EspD were targeted to highly conserved areas of the protein on residues with basic, positively charged side chains (Figure 9). These residues may be involved in the binding to eukaryotic phospholipids observed in the unpublished data (Figure 8). The basic side chains could form favorable electrostatic interactions with the negatively charged head group of the phospholipid. Mutating these basic residues resulted in the construction of five new strains of *M. tb* which express EspD with alanine substitutions of arginine or lysine residues.

In addition to the newly constructed strains, several strains for which secretion profiles were previously published were used in this study. The secretion profiles for the published strains were confirmed here, identifying *M. tb espA*::Tn pMDespACD^{W19R} as a key strain, which can be utilized as a negative control for EspD secretion without interrupting the secretion of other ESX-1 proteins. The newly constructed strains, with EspD mutated on conserved basic residues, did not establish any new growth or secretion phenotypes as all new strains demonstrated the ability to secrete EsxA and their mutated EspD proteins (Figures 10 & 11). Interestingly, the level of EspD mutant secretion appeared to differ subtly between these strains (Figure 11). As EspD is secreted at quite low concentrations relative to other secreted proteins, this variability will be interesting to interrogate more deeply in the future. These strains will be utilized in monitoring

phospholipid localization and signal changes during *M. tb* infections of macrophages expressing fluorescent phospholipid biosensors. However, for further investigation into the impact to cytotoxicity and inflammation, *M. tb espA*::Tn pMDespACD^{R92A} was selected for further characterization here as this strain was found to consistently secrete a similar level of EspD^{R92A} to that of *M. tb espA*::Tn pMDespACD^{WT}. Additionally, *M. tb espA*::Tn pMDespACD^{W19R} and the control strains: *M. tb espA*::Tn pMD31, *M. tb espA*::Tn pMDespACD^{WT}, and *M. tb espA*::Tn pMDespACD^{STOP} were used for these experiments.

These selected *M. tb* strains were evaluated for their cytotoxic effect on THP-1 human macrophages through PrestoBlue and LDH assays. Firstly, an effective protocol was developed for maintaining, differentiating, and infecting THP-1 cells (Figures 12 &13). These cells were then infected with *M. tb* at an MOI of 5 for three days at which time the infection supernatants were evaluated for the presence of LDH, an enzyme released from dying cells as the plasma membrane is damaged. The LDH assay was found to require further optimization as several values for percent relative cytotoxicity were calculated to be outside of the 0-100% range (Figure 15). Additionally, LDH analysis of *M. tb espA*::Tn pMDespACD^{R92A} infection supernatants displayed unrealistically low values for percent cytotoxicity. As *M. tb espA*::Tn pMD-espACD^{R92A} has a similar secretion profile to *M. tb espA*::Tn pMDespACD^{WT}, the similar cytotoxicity observed with these strains through PrestoBlue analysis appears more consistent with current understandings of this strain. However, the trend observed for the remaining selected strains from the LDH experiment corresponded with what was observed with PresoBlue analysis (Table 4). The infected THP-1 cells were monitored for their ability to respirate through the conversion of PrestoBlue into a fluorescent product. The PrestoBlue results demonstrated that *M. tb espA*::Tn pMDespACD^{W19R}, a strain unable to secrete EspD alone, appeared to have a similar level of cytotoxicity in THP-1 cells to a strain unable to secrete several ESX-1 proteins, *M. tb espA*::Tn pMDespACD^{STOP} (Figure 14). Both of these strains appeared less cytotoxic to THP-1 cells than *M. tb espA*::Tn pMDespACD^{WT} (Figure 14). These differences were not statistically significant; however, this trend was consistent across three independent experiments. Taken together with the evidence of *M. tb espA*::Tn pMDespACD^{W19R} causing a reduced bacterial load in infected mice compared to *M. tb espA*::Tn pMDespACD^{WT}, it appears that secreted EspD indeed has an impact on virulence during *M. tb* infections (Figures 6, 14, &15).

There are several pathways involved in eukaryotic cell death during *M. tb* infections (Zhang et al., 2021). The subtle phenotype observed with the PrestoBlue cytotoxicity experiments between the selected *M. tb* strains may indicate that overall cell death is not the best measurement for the impact of secreted EspD. This assay is only representative of the overall cell death observed after three days of infection. Continued investigation into these phenotypes could benefit from performing infections for 24 h or 48 h with higher MOIs. Perhaps the phenotype is more evident during very early stages of infection, as was observed with investigations into the pro-inflammatory response induced in these infected THP-1 cells.

5.2. Analysis of the impact of secreted EspD during *M. tb* infections of macrophages

Secreted EspD appears to contribute to the virulence of *M. tb* as evidenced by the reduced cytotoxicity in THP-1 cells infected with *M. tb espA*::Tn pMDespACD^{W19R} compared to *M. tb espA*::Tn pMDespACD^{WT}. To further explore the role of secreted EspD, the selected *M. tb* strains were used to infect THP-1 cells at an MOI of 10 for 24 h to observe differences in cytokine production. Interestingly, the production of IL1β and TNFα was largely reduced in the case of THP-1 cell infections with *M. tb espA*::Tn pMDespACD^{W19R} compared to *M. tb espA*::Tn pMDespACD^{WT} (Figure 16). This suggests that secreted EspD is involved in the production of pro-inflammatory cytokines. *M. tb espA*::Tn pMDespACD^{R92A} and *M. tb espA*::Tn pMD-espACD^{WT} induced similar levels of IL1β and TNFα production in THP-1 cells, which is expected due to their similar secretion profiles (Figure 16). However, an interesting phenotype was uncovered for *M. tb espA*::Tn pMDespACD^{STOP}. This strain does not express EspD, which leads to the loss of secretion of EspA, EspC, EsxA, and EsxB. *M. tb espA*::Tn pMDespACD^{STOP} was shown to consistently display a lower cytotoxic effect towards THP-1 cells relative to *M. tb espA*::Tn pMDespACD^{WT} (Figures 14 & 15). While observing the induction of IL1β and TNFα, it was found that *M. tb espA*::Tn pMDespACD^{STOP} induced an increased amount of pro-inflammatory cytokine compared to *M. tb espA*::Tn pMDespACD^{WT} (Figure 16). Previously, it was thought that ESX-1 mediated cytotoxicity in macrophages correlates with an increased pro-inflammatory response in host-cells (Chen et al., 2013a). Here, the *M. tb espA*::Tn pMDespACD^{STOP} strain provides evidence that ESX-1 dependent cell death does not necessarily correspond with increased production of pro-inflammatory cytokines.

Having discovered that secreted EspD is somehow involved in the pro-inflammatory response in *M. tb* infected macrophages, further investigation was done into the host-cell pathways involved. As the EspD protein has demonstrated an ability to bind eukaryotic phospholipids (Figures 8, 16, & 27), it could be speculated that this binding may be involved in the secreted protein's role in the host-cell's inflammatory response. PI4P is a very abundant phospholipid in eukaryotic cells and is a key component of the Golgi apparatus (Del Campo *et al*., 2014). This phospholipid is involved in membrane trafficking at the Golgi as well as being the scaffold for the formation of the NLRP3 inflammasome complex (Chen and Chen, 2018; De Matteis *et al*., 2013). NLRP3 is recruited to the Golgi and binds to PI4P in order to further bind the adapter protein, ASC, and caspase-1 to form the NLRP3 inflammasome complex (Broz and Dixit, 2016; Rathinam and Fitzgerald, 2016). If secreted EspD is able to target PI4P during an infection, it is possible that this binding could induce or stabilize the formation of the NLRP3 inflammasome (Figure 32). The presence of secreted EspD may thereby contribute to the activation of caspase-1 and lead to the cleavage of Pro-IL1β into IL1β.

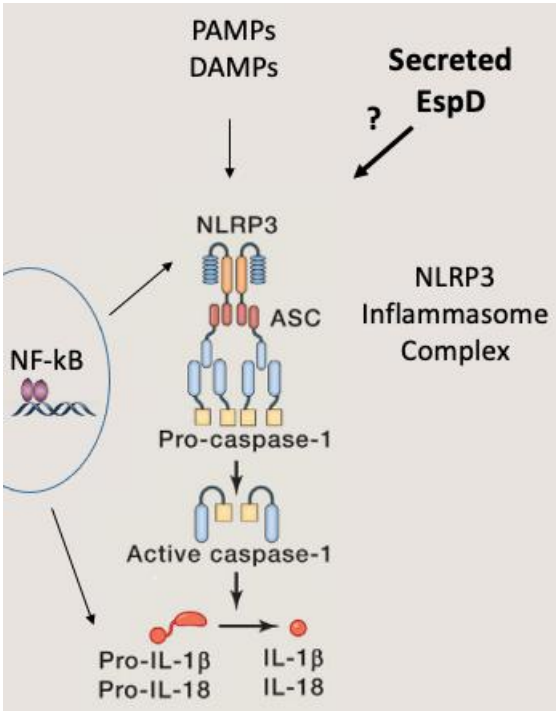

Figure 33: Potential inflammatory pathways that could be impacted by the presence of secreted EspD produced by *M. tb* during macrophage infection. Figure adapted from Rathinam and Fitzgerald, 2016.

The presence of secreted EspD during *M. tb* infections could also influence NF-κB signaling. NF-κB is an important transcription factor involved in several aspects of the inflammatory response and its signaling pathway is highly interconnected with that of TNFα (Hayden and Ghosh, 2014; Liu et al., 2017b). Additionally, NF-κB has been shown to be influenced by PI4P treatment. Macrophages infected with mycobacteria have exhibited enhanced NF-κB activation when treated with exogenous PI4P (Gutierrez et al., 2009). Here, we show that secreted EspD contributes to the production of TNFα (Figure 16b) and that EspD appears to bind PI4P (Figures 8, 16, & 27). Therefore, it is of interest to monitor NF-κB and its phosphorylation in addition to the activation of the NLRP3 inflammasome in *M. tb* infected macrophages. To begin exploring whether changes in these host-cell responses are occurring, we observed the presence of several proteins in THP-1 cell lysates after infection with the selected *M. tb* strains. Infections were performed at an MOI of 10 for 24 h and lysates were harvested for analysis through immunoblot to observe NLRP3, cleaved caspase-1, and pNF-κB. Results did not demonstrate any difference between lysates of THP-1 cells infected with *M. tb espA*::Tn pMDespACD^{W19R} and *M. tb espA*::Tn pMDespACD^{WT} (Figures 17 & 18). Similarly, the infected lysates did not differ from the uninfected lysates for the presence of any of the targeted proteins. It is likely that the signals observed for these proteins represent their basal levels within the cell and are not indicative of any activation of the inflammatory pathways (Figure 17 & 18).

Lysates used in these Western blot experiments were harvested at 24 h post-infection. This single time point did not demonstrate any differences between *M. tb espA*::Tn pMDespACD^{WT} infected and uninfected cells and therefore could not identify any differences with the EspD secretion control strain, *M. tb espA*::Tn pMDespACD^{W19R}. A time course, harvesting infected cell lysates over several shorter time periods would be the next necessary step for investigating this phenotype. Additionally, due to the inability to detect strong signal from cleaved caspase-1 across several protein concentrations analyzed through Western blot, tests should be performed to ensure this antibody is functional. All antibodies used in these experiments were obtained commercially and were prepared as recommended by the manufacturer, however, attempts should be made to optimize antibody signal, especially in the case of cleaved caspase-1 and pNF-κB with the use of titrations, positive control samples, and varying primary antibody concentrations.

In addition to investigating changes in the inflammatory response, we wanted to examine if there are changes in phospholipid localization of macrophages in response to infections with *M. tb* strains expressing variant EspD proteins. EspD's potential to bind eukaryotic phospholipids during infection could contribute to *M. tb*'s ability to hijack and manipulate host-defense mechanisms. Many pathogenic bacteria, including *M. tb*, are known to target phospholipids and therefore interfere with their functions in cell-signaling, maintenance of cytoskeletal dynamics, membrane composition, and more (Walpole *et al.,* 2018). Monitoring changes to the localization patterns of several key phospholipids during infections with these *M. tb* strains could allow for visual evidence of the role EspD is playing. To observe these changes a collection of fluorescent biosensor plasmids, encoding phospholipid-specific probes linked to GFP or RFP, was made. These biosensors were tested in both COS-7 and RAW 264.7 cell lines and were found to be functional. This work established a methodology for using these phospholipid biosensors and will enable future infections of these cells to observe strain to strain differences.

5.3. Purification and analysis of recombinant EspD protein from *E. coli*

Purification trials were performed on recombinant EspD from *E. coli* for the purposes of further evaluating the structure and function of EspD. Ideally, purification would be performed under non-denaturing conditions. This allows for a higher quality protein sample as the protein remains properly folded throughout the purification. Protein refolding can occur for samples purified under denaturing conditions; however, this is more likely to produce unfolded or misfolded protein, which can yield inaccurate biophysical and biochemical information. Here, a proposed protocol for purification of recombinant EspD from *E. coli* under non-denaturing conditions was created. The trials attempted for non-denaturing EspD purification were met with consistent aggregation issues despite testing numerous buffer conditions. Ultimately, a major source of the aggregation was found to be the dried Nickel-IDA silica-based resin originally used for His-tag purification. Replacing this resin, which had been previously used in the small-scale purifications performed for EspD in the unpublished data, allowed for EspD purification to proceed and allowed for enhanced stability of the protein in solution. Further optimization of the later purification steps to enhance purity may be required moving forward. Once successful purification of EspD under non-denaturing conditions is completed it will be of key importance to identify and purify variants of EspD to begin to investigate the key residues of this protein.

Sequence analysis of EspD indicates that there may be an intrinsically unfolded region located on the N-terminal portion of the protein. Truncations performed in this region may help to gain insights into the structure of EspD's C-terminal region and could provide information regarding how this disordered region may contribute to EspD's function. Additionally, large scale non-denatured purifications of EspD will allow for biophysical analysis of the protein through CD and DLS to gather more insight into the structure and oligomerization of the protein. Furthermore, this protein can be used to confirm the phospholipid binding analyses that were performed here using EspD samples purified under denaturing conditions.

Although not ideal or preferred, a relatively pure sample of recombinant EspD was obtained under denaturing conditions and used to confirm the phospholipid binding phenotype demonstrated in the unpublished data (Figure 8). Here, we were able to repeat this phenotype, showing that recombinant EspD was able to bind to PA, PI3P, PI4P, and PI5P using phospholipid embedded membranes (Figure 26). Similarly, recombinant EspD demonstrated binding to PA and PI4P during pulldowns with phospholipid coated beads (Figure 27). In the case of both the phospholipid embedded membranes and the phospholipid coated beads EspD demonstrated strong binding to PI4P. To further confirm this binding to PI4P, pulldown experiments were performed using *M. tb* expressed EspD. Initial pulldowns were performed using lysates of *M. tb espA*::Tn pMDespACD^{WT} and *M. tb espA*::Tn pMDespACD^{STOP}. Cell lysates contain a much higher relative concentration of EspD and were able to serve as a proof-of-concept to determine if EspD could be pulled down from a mixture of proteins using this method. Indeed, EspD protein was able to be pulled down by the PI4P-coated beads from the *M. tb espA*::Tn pMDespACD^{WT} cell lysate (Figure 28). Despite the need for stronger washing in this experiment to remove all non-specific binding to the control beads, the stronger signal from the PI4P-coated beads seems to imply EspD and PI4P are binding. Lastly, to observe PI4P binding to secreted EspD, culture filtrate samples of *M. tb espA*::Tn pMDespACD^{WT} and *M. tb espA*::Tn pMDespACD^{STOP} were used in a similar pulldown. Again, EspD can be visualized in the PI4P-coated bead pulldown from *M. tb espA*::Tn pMDespACD^{WT} (Figure 29). Optimization of this methodology may be necessary to amplify the faint signal. It is likely that the high concentration of other secreted proteins in the sample causes interference with the binding or with the Western blot analysis itself. Overall, EspD consistently appears to demonstrate phospholipid binding. The recombinant EspD protein produced under non-denaturing conditions from the unpublished data (Figure 8), the

recombinant EspD protein produced under denaturing conditions (Figures 26 & 27), and the *M. tb* secreted EspD used in pulldowns (Figure 29) were all able to provide evidence of EspD's ability to bind eukaryotic phospholipids, especially PI4P.

5.4. Conclusions

This work has established a better understanding of the role EspD plays during *M. tb* infections of macrophages. Several new strains of *M. tb* expressing single point variants of EspD were constructed. These strains were found to possess no growth defects and were all capable of secreting the ESX-1 proteins, EsxA and EspD. Secretion profiles of several previously published variant *M. tb* strains were additionally confirmed here (Chen *et al.*, 2012). A strain incapable of secreting EspD alone, *M. tb espA*::Tn pMDespACD^{W19R}, appeared to be less cytotoxic to THP-1 macrophages and induced a significantly lower concentration of pro-inflammatory cytokine compared to *M. tb espA*::Tn pMDespACD^{WT}. This indicates that secreted EspD appears to be involved in the virulence of *M. tb* during infections of macrophages and contributes to the pro-inflammatory response of the host-cells. This work also demonstrated that both recombinantly produced EspD protein and *M. tb* secreted EspD protein are capable of binding eukaryotic phospholipids, including PI4P. Overall, this work provides a foundation for further investigation into the *M. tb* secreted protein, EspD.

6. References

Aguiló, N., Marinova, D., Martín, C., and Pardo, J. (2013). ESX-1-induced apoptosis during mycobacterial infection: To be or not to be, that is the question. Front. Cell. Infect. Microbiol. *3*, 1–7.

Anderson, P., and Doherty, T.M. (2005). The success and failure of BCG - implications for a novel tuberculosis vaccine. Nat. Rev. Microbiol. *3*, 656–662.

Beeckman, D.S.A., and Vanrompay, D.C.G. (2010). Bacterial secretion systems with an emphasis on the chlamydial Type III secretion system. Curr. Issues Mol. Biol. *12*, 17–41.

Berghe, T. Vanden, Linkermann, A., Jouan-Lanhouet, S., Walczak, H., and Vandenabeele, P. (2014). Regulated necrosis: The expanding network of non-apoptotic cell death pathways. Nat. Rev. Mol. Cell Biol. *15*, 135–147.

Blasco, B., Chen, J.M., Hartkoorn, R., Sala, C., Uplekar, S., Rougemont, J., Pojer, F., and Cole, S.T. (2012). Virulence regulator EspR of mycobacterium tuberculosis is a nucleoid-associated protein. PLoS Pathog. *8*, 1-12.

Bottai, D., di Luca, M., Majlessi, L., Frigui, W., Simeone, R., Sayes, F., Bitter, W., Brennan, M.J., Leclerc, C., Batoni, G., et al. (2012). Disruption of the ESX-5 system of Mycobacterium tuberculosis causes loss of PPE protein secretion, reduction of cell wall integrity and strong attenuation. Mol. Microbiol. *83*, 1195–1209.

Bottai, D., Gröschel, M.I., and Brosch, R. (2017). Type VII Secretion Systems in Gram-Positive Bacteria. Curr. Top. Microbiol. Immunol. *404*, 1-42.

Broz, P., and Dixit, V.M. (2016). Inflammasomes: Mechanism of assembly, regulation and signalling. Nat. Rev. Immunol. *16*, 407–420.

Bunduc, C.M., Bitter, W., and Houben, E.N.G. (2020). Structure and Function of the Mycobacterial Type VII Secretion Systems. Annu. Rev. Microbiol. *74*, 315–335.

Del Campo, C.M., Mishra, A.K., Wang, Y.H., Roy, C.R., Janmey, P.A., and Lambright, D.G. (2014). Structural basis for PI(4)P-specific membrane recruitment of the legionella pneumophila effector DrrA/SidM. Structure *22*, 397–408.

Capra, J.A., and Singh, M. (2007). Predicting functionally important residues from sequence conservation. Bioinformatics *23*, 1875–1882.

Chen, J.M. (2016). Mycosins of the mycobacterial type VII ESX secretion system: The glue that holds the party together. MBio *7*, 6–8.

Chen, J., and Chen, Z.J. (2018). PtdIns4P on dispersed trans-Golgi network mediates NLRP3 inflammasome activation. Nature *564*, 71–76.
Chen, J.M., Boy-Röttger, S., Dhar, N., Sweeney, N., Buxton, R.S., Pojer, F., Rosenkrands, I., and Cole, S.T. (2012). EspD is critical for the virulence-mediating ESX-1 secretion system in Mycobacterium tuberculosis. J. Bacteriol. *194*, 884–893.
Chen, J.M., Zhang, M., Rybniker, J., Boy-Röttger, S., Dhar, N., Pojer, F., and Cole, S.T. (2013a). Mycobacterium tuberculosisEspB binds phospholipids and mediates EsxA-independent virulence. Mol. Microbiol. *89*, 1154–1166.
Chen, J.M., Zhang, M., Rybniker, J., Basterra, L., Dhar, N., Tischler, A.D., Pojer, F., and Cole, S.T. (2013b). Phenotypic profiling of mycobacterium tuberculosis espa point mutants reveals that blockage of ESAT-6 and CFP-10 secretion in vitro does not always correlate with attenuation of virulence. J. Bacteriol. *195*, 5421–5430.
Chen, K.W., Boucher, D., and Broz, P. (2019). Divide to conquer: NLRP3 is activated on dispersed trans-Golgi network. Cell Res. *29*, 181–182.
Conrad, W.H., Osman, M.M., Shanahan, J.K., Chu, F., Takaki, K.K., Cameron, J., Hopkinson-Woolley, D., Brosch, R., and Ramakrishnan, L. (2017). Mycobacterial ESX-1 secretion system mediates host cell lysis through bacterium contact-dependent gross membrane disruptions. Proc. Natl. Acad. Sci. U. S. A. *114*, 1371–1376.
Deretic, V. (2008). Autophagy, an immunologic magic bullet: Mycobacterium tuberculosis phagosome maturation block and how to bypass it. Future Microbiol. *3*, 517–524.
Divangahi, M., Chen, M., Gan, H., Desjardins, D., Hickman, T.T., Lee, D.M., Fortune, S., Behar, S.M., and Remold, H.G. (2009). Mycobacterium tuberculosis evades macrophage defenses by inhibiting plasma membrane repair. Nat. Immunol. *10*, 899–906.
Dorhoi, A., Nouailles, G., Jörg, S., Hagens, K., Heinemann, E., Pradl, L., Oberbeck-Müller, D., Duque-Correa, M.A., Reece, S.T., Ruland, J., et al. (2012). Activation of the NLRP3 inflammasome by Mycobacterium tuberculosis is uncoupled from susceptibility to active tuberculosis. Eur. J. Immunol. *42*, 374–384.
Ejeh, E.F., Raji, M.A., Bello, M., Lawan, F.A., Francis, M.I., Kudi, A.C., and Cadmus, S.I.B. (2014). Prevalence and direct economic losses from bovine tuberculosis in Makurdi, nigeria. Vet. Med. Int. *2014*, 1-6.
Ernst, J.D. (2012). The immunological life cycle of tuberculosis. Nat. Rev. Immunol. *12*, 581–

591.
Forrellad, M.A., Klepp, L.I., Gioffré, A., García, J.S., Morbidoni, H.R., de la Paz Santangelo, M., Cataldi, A.A., and Bigi, F. (2013). Virulence factors of the mycobacterium tuberculosis complex. Virulence *4*, 3–66.
Fortune, S.M., Jaeger, A., Sarracino, D.A., Chase, M.R., Sassetti, C.M., Sherman, D.R., Bloom, B.R., and Rubin, E.J. (2005). Mutually dependent secretion of proteins required for mycobacterial virulence. Proc. Natl. Acad. Sci. *102*, 10676–10681.
Gröschel, M.I., Sayes, F., Simeone, R., Majlessi, L., and Brosch, R. (2016). ESX secretion systems: Mycobacterial evolution to counter host immunity. Nat. Rev. Microbiol. *14*, 677–691.
Guo, Q., Bi, J., Wang, H., and Zhang, X. (2021). Mycobacterium tuberculosis ESX-1-secreted substrate protein EspC promotes mycobacterial survival through endoplasmic reticulum stress-mediated apoptosis. Emerg. Microbes Infect. *10*, 19–36.
Gutierrez, M.G., Master, S.S., Singh, S.B., Taylor, G.A., Colombo, M.I., and Deretic, V. (2004). Autophagy is a defense mechanism inhibiting BCG and Mycobacterium tuberculosis survival in infected macrophages. Cell *119*, 753–766.
Gutierrez, M.G., Gonzalez, A.P., Anes, E., and Griffiths, G. (2009). Role of lipids in killing mycobacteria by macrophages: Evidence for NF-κB-dependent and -independent killing induced by different lipids. Cell. Microbiol. *11*, 406–420.
Ham, H., Sreelatha, A., and Orth, K. (2011). Manipulation of host membranes by bacterial effectors. Nat. Rev. Microbiol. *9*, 635–646.
Harris, J., Lang, T., Thomas, J.P.W., Sukkar, M.B., Nabar, N.R., and Kehrl, J.H. (2017). Autophagy and inflammasomes. Mol. Immunol. *86*, 10–15.
Hayden, M., and Ghosh, S. (2014). Regulation of NF-κB by TNF Family Cytokines. Semin. Immunol. *26*, 1–7.
Houben, E.N.G., Bestebroer, J., Ummels, R., Wilson, L., Piersma, S.R., Jiménez, C.R., Ottenhoff, T.H.M., Luirink, J., and Bitter, W. (2012). Composition of the type VII secretion system membrane complex. Mol. Microbiol. *86*, 472–484.
Hu, D., Wu, J., Wang, W., Mu, M., Zhao, R., Xu, X., Chen, Z., Xiao, J., Hu, F., Yang, Y., et al. (2015). Autophagy regulation revealed by SapM-induced block of autophagosome-lysosome fusion via binding RAB7. Biochem. Biophys. Res. Commun. *461*, 401–407.
Huang, D.D., and Bao, L. (2016). Mycobacterium tuberculosis EspB protein suppresses

interferon-γ-induced autophagy in murine macrophages. J. Microbiol. Immunol. Infect. *49*, 859–865.

De Jonge, M.I., Pehau-Arnaudet, G., Fretz, M.M., Romain, F., Bottai, D., Brodin, P., Honoré, N., Marchal, G., Jiskoot, W., England, P., et al. (2007). ESAT-6 from Mycobacterium tuberculosis dissociates from its putative chaperone CFP-10 under acidic conditions and exhibits membrane-lysing activity. J. Bacteriol. *189*, 6028–6034.

Keane, J., Balcewicz-Sablinska, M.K., Remold, H.G., Chupp, G.L., Meek, B.B., Fenton, M.J., and Kornfeld, H. (1997). Infection by Mycobacterium tuberculosis promotes human alveolar macrophage apoptosis. Infect. Immun. *65*, 298–304.

Keane, J., Remold, H.G., and Kornfeld, H. (2000). Virulent Mycobacterium tuberculosis Strains Evade Apoptosis of Infected Alveolar Macrophages . J. Immunol. *164*, 2016–2020.

Lee, J., Repasy, T., Papavinasasundaram, K., Sassetti, C., and Kornfeld, H. (2011). Mycobacterium tuberculosis induces an atypical cell death mode to escape from infected macrophages. PLoS One *6*, 1–13.

Lerner, T.R., Borel, S., and Gutierrez, M.G. (2015). The innate immune response in human tuberculosis. Cell. Microbiol. *17*, 1277–1285.

Liu, C.H., Liu, H., and Ge, B. (2017a). Innate immunity in tuberculosis: Host defense vs pathogen evasion. Cell. Mol. Immunol. *14*, 963–975.

Liu, T., Zhang, L., Joo, D., and Sun, S.C. (2017b). NF-κB signaling in inflammation. Signal Transduct. Target. Ther. *2*, 1-9.

Lou, Y., Rybniker, J., Sala, C., and Cole, S.T. (2017). EspC forms a filamentous structure in the cell envelope of Mycobacterium tuberculosis and impacts ESX-1 secretion. Mol. Microbiol. *103*, 26–38.

De Matteis, M.A., Wilson, C., and D'Angelo, G. (2013). Phosphatidylinositol-4-phosphate: The Golgi and beyond. BioEssays *35*, 612–622.

Mehra, A., Zahra, A., Thompson, V., Sirisaengtaksin, N., Wells, A., Porto, M., Köster, S., Penberthy, K., Kubota, Y., Dricot, A., et al. (2013). Mycobacterium tuberculosis Type VII Secreted Effector EsxH Targets Host ESCRT to Impair Trafficking. PLoS Pathog. *9*, 1-13.

Mishra, B.B., Moura-Alves, P., Sonawane, A., Hacohen, N., Griffiths, G., Moita, L.F., and Anes, E. (2010). Mycobacterium tuberculosis protein ESAT-6 is a potent activator of the NLRP3/ASC inflammasome. Cell. Microbiol. *12*, 1046–1063.

Miyoshi-Akiyam, T., Matsumura, K., Iwai, H., Funatogawa, K., and Kirikae, T. (2012). Complete annotated genome sequence of Mycobacterium tuberculosis Erdman. J. Bacteriol. *194*, 2770.

Nagata, S. (2018). Apoptosis and Clearance of Apoptotic Cells. Annu. Rev. Immunol. *36*, 489–517.

Ohol, Y.M., Goetz, D.H., Chan, K., Shiloh, M.U., Craik, C.S., and Cox, J.S. (2010). Mycobacterium tuberculosis MycP1 protease plays a dual role in regulation of ESX-1 secretion and virulence. Cell Host Microbe *7*, 210–220.

Pai, M., Behr, M.A., Dowdy, D., Dheda, K., Divangahi, M., Boehme, C.C., Ginsberg, A., Swaminathan, S., Spigelman, M., Getahun, H., et al. (2016). Tuberculosis. Nat. Rev. Dis. Prim. *2*, 1-23.

Pérez-Morote, R., Pontones-Rosa, C., Gortázar-Schmidt, C., and Muñoz-Cardona, Á.I. (2020). Quantifying the economic impact of bovine tuberculosis on livestock farms in south-western spain. Animals *10*, 1–25.

Philips, J.A., and Ernst, J.D. (2012). Tuberculosis Pathogenesis and Immunity. Annu. Rev. Pathol. Mech. Dis. *7*, 353–384.

Poirier, V., and Av-Gay, Y. (2012). Mycobacterium tuberculosis modulators of the macrophage's cellular events. Microbes Infect. *14*, 1211–1219.

Public Health Agency of Canada (2014). Canadian Tuberculosis Standards 7th Edition.

Puri, R.V., Reddy, P.V., and Tyagi, A.K. (2013). Secreted Acid Phosphatase (SapM) of Mycobacterium tuberculosis Is Indispensable for Arresting Phagosomal Maturation and Growth of the Pathogen in Guinea Pig Tissues. PLoS One *8*, 1-12.

Rathinam, V.A.K., and Fitzgerald, K.A. (2016). Inflammasome Complexes: Emerging Mechanisms and Effector Functions. Cell *165*, 792–800.

Romagnoli, A., Etna, M.P., Giacomini, E., Pardini, M., Remoli, M.E., Corazzari, M., Falasca, L., Goletti, D., Gafa, V., Simeone, R., et al. (2012). ESX-1 dependent impairment of autophagic flux by Mycobacterium tuberculosis in human dendritic cells. Autophagy *8*, 1357–1370.

Romao, S., Gasser, N., Becker, A.C., Guhl, B., Bajagic, M., Vanoaica, D., Ziegler, U., Roesler, J., Dengjel, J., Reichenbach, J., et al. (2013). Autophagy proteins stabilize pathogen-containing phagosomes for prolonged MHC II antigen processing. J. Cell Biol. *203*, 757–766.

Di Russo Case, E., and Samuel, J.E. (2016). Contrasting Lifestyles Within the Host Cell.

Microbiol Spectr. *4*, 1-31.
Saini, N.K., Baena, A., Ng, T.W., Venkataswamy, M.M., Kennedy, S.C., Kunnath-Velayudhan, S., Carreño, L.J., Xu, J., Chan, J., Larsen, M.H., et al. (2016). Suppression of autophagy and antigen presentation by Mycobacterium tuberculosis PE-PGRS47. Nat. Microbiol. *1*, 1–12.
Sakagami, H., Kishino, K., Amano, O., Kanda, Y., Kunii, S., Yokote, Y., Oizumi, H., and Oizumi, T. (2009). Cell death induced by nutritional starvation in mouse macrophage-like RAW264.7 cells. Anticancer Res. *29*, 343–347.
Schroder, K., and Tschopp, J. (2010). The Inflammasomes. Cell *140*, 821–832.
Shah, S., Bohsali, A., Ahlbrand, S.E., Srinivasan, L., Rathinam, V.A.K., Vogel, S.N., Fitzgerald, K.A., Sutterwala, F.S., and Briken, V. (2013). Cutting Edge: Mycobacterium tuberculosis but Not Nonvirulent Mycobacteria Inhibits IFN-β and AIM2 Inflammasome–Dependent IL-1β Production via Its ESX-1 Secretion System . J. Immunol. *191*, 3514–3518.
Sia, J.K., and Rengarajan, J. (2019). Immunology of Mycobacterium tuberculosis Infections. Microbiol. Spectr. *7*, 3–22.
Stutz, M.D., Clark, M.P., Doerflinger, M., and Pellegrini, M. (2018). Mycobacterium tuberculosis: Rewiring host cell signaling to promote infection. J. Leukoc. Biol. *103*, 259–268.
Swanson, K. V., Deng, M., and Ting, J.P.Y. (2019). The NLRP3 inflammasome: molecular activation and regulation to therapeutics. Nat. Rev. Immunol. *19*, 477–489.
Tran, V., Liu, J.U.N., and Behr, M.A. (2014). BCG Vaccines. 1–11.
Tufariello, J.A.M., Chapman, J.R., Kerantzas, C.A., Wong, K.W., Vilchèze, C., Jones, C.M., Cole, L.E., Tinaztepe, E., Thompson, V., Fenyö, D., et al. (2016). Separable roles for Mycobacterium tuberculosis ESX-3 effectors in iron acquisition and virulence. Proc. Natl. Acad. Sci. U. S. A. *113*, E348–E357.
Vergne, I., Chua, J., Lee, H.H., Lucas, M., Belisle, J., and Deretic, V. (2005). Mechanism of phagolysosome biogenesis block by viable Mycobacterium tuberculosis. Proc. Natl. Acad. Sci. U. S. A. *102*, 4033–4038.
Vieira, O. V., Botelho, R.J., Rameh, L., Brachmann, S.M., Matsuo, T., Davidson, H.W., Schreiber, A., Backer, J.M., Cantley, L.C., and Grinstein, S. (2001). Distinct roles of class I and class III phosphatidylinositol 3-kinases in phagosome formation and maturation. J. Cell Biol. *155*, 19–25.
Walpole, G.F.W., Grinstein, S., and Westman, J. (2018). The role of lipids in host-pathogen

interactions. IUBMB Life 384–392.
Wong, K.W., and Jacobs, W.R. (2011). Critical role for NLRP3 in necrotic death triggered by Mycobacterium tuberculosis. Cell. Microbiol. *13*, 1371–1384.
Xu, G., Wang, J., Gao, G.F., and Liu, C.H. (2014). Insights into battles between Mycobacterium tuberculosis and macrophages. Protein Cell *5*, 728–736.
Yang, Y., Wang, H., Kouadir, M., Song, H., and Shi, F. (2019). Recent advances in the mechanisms of NLRP3 inflammasome activation and its inhibitors. Cell Death Dis. *10,* 1-11.
Yeung, T., Heit, B., Dubuisson, J.F., Fairn, G.D., Chiu, B., Inman, R., Kapus, A., Swanson, M., and Grinstein, S. (2009). Contribution of phosphatidylserine to membrane surface charge and protein targeting during phagosome maturation. J. Cell Biol. *185*, 917–928.
Zhai, W., Wu, F., Zhang, Y., Fu, Y., and Liu, Z. (2019). The immune escape mechanisms of Mycobacterium Tuberculosis. Int. J. Mol. Sci. *20,* 1-18.
Zhang, L., Jiang, X., Pfau, D., Ling, Y., and Nathan, C.F. (2021). Type I interferon signaling mediates Mycobacterium tuberculosis–induced macrophage death. J. Exp. Med. *218,* 1-12.
Zhao, X., Khan, N., Gan, H., Tzelepis, F., Nishimura, T., Park, S.Y., Divangahi, M., and Remold, H.G. (2017). Bcl-x L mediates RIPK3-dependent necrosis in M. tuberculosis-infected macrophages. Mucosal Immunol. *10,* 1553–1568.
Global Tuberculosis Report (2019). Geneva: World Health Organization; 2019. Licence: CCBY-NC-5A3.0IGO.